# COMPENSATION AND AMBIPOLAR CONDUCTION IN SEMI-INSULATING GaAs BULK CRYSTALS

Ru-Shyah Tang

B.S., National Tsing-Hua University, Taiwan, 1977
M.S., National Tsing-Hua University, Taiwan, 1979

A dissertation submitted to the faculty of the

Oregon Graduate Institute
of
Science and Technology

in partial fulfillment of the
requirements for the degree
Doctor of Philosophy
in
Electrical Engineering

August, 1990

The dissertation "Compensation and Ambipolar Conduction in Semi-insulating GaAs Bulk Crystals" by Ru-Shyah Tang has been examined and approved by the following Examination Committee:

John S. Blakemore, Thesis Advisor
Professor

James Parsons
Associate Professor

Rajendra Solanki
Associate Professor

Dae Mann Kim
Adjunct Professor

## ACKNOWLEDGMENTS

I would like to express my deepest gratitude to my advisor Professor John S. Blakemore for his constant support, encouragement and direction throughout this work. I also wish to express my sincere thanks to Mrs. Blakemore for her love and kindness both to me and to my family.

Much credit is due to Lisa Sargent for her optical absorption measurements which yielded a number of the carbon and EL2 concentrations in this work.

This work has been supported by the National Science Foundation through Grant DMR-8700432.

I wish to thank many friends in OGI and in the Beaverton area, those who helped me three years ago when I had a severe burn accident. My special thanks go to my neighbors as well as best friends Sin-Jing Chen and Ed Chang. They spent a lot of time in helping me to travel from hospital, school and home during the period of my recovery.

In addition, I am most grateful to my wife for her understanding and assistance in preparing this dissertation, and to my mother for her continual encouragement in my life time. Without their love and support, this dissertation would never be possible.

Finally, I thank God for His faithfulness and goodness in my new life.

TABLE OF CONTENTS

Page

ACKNOWLEDGMENTS ........................................ iii

LIST OF TABLES ........................................ vi

LIST OF FIGURES........................................ vii

ABSTRACT........................................ x

Chapter

1. INTRODUCTION

1.1 History of GaAs Crystal Growth from the Melt ............. 1
1.2 Some Modern Melt-Growth Methods ..................... 3
1.3 Dopant Effects in GaAs.............................. 5
1.4 Defect Species in Melt-grown GaAs...................... 7
1.5 Models and Their Controversies for EL2 .................. 8
1.6 Origins and Development of Semi-insulating (SI) GaAs....... 9
1.7 Compensation Models for SI GaAs....................... 12
1.8 Possible Characterization Methods for SI GaAs............. 14
References.......................................... 18

2. EXPERIMENTAL SYSTEMS USED IN THE PRESENT STUDY

2.1 Difficulties of Hall/Resistivity Measurement in SI GaAs..... 25
2.2 System Developed for Such Measurements Versus Temperature ................................ 31
2.3 Local Vibrational Mode (LVM) Absorption for Impurity Detection.......................................... 34
2.4 Near and Mid-Infrared Measurements for EL2 Absorption, Impurity Photoionization, and Free Carrier Absorption .... 43
References.......................................... 48

3. COMPENSATION AND AMBIPOLAR CONDUCTION IN SI GaAs

3.1 The "Three-Level" Model for Undoped SI GaAs.............50
3.2 Ambipolar Conduction Complications for Near-Intrinsic GaAs.............52
3.3 Usefulness of Temperature-Dependent Electrical Transport Data.............65
References.............70

4. RESULTS FOR "UNDOPED" GaAs CRYSTALS GROWN BY VARIOUS METHODS

4.1 Rationale for the Results Described Here.............72
4.2 Electrical Data for a Range of Samples from Near-Intrinsic to "Failed SI".............76
4.3 Electrical Data for Undoped VB-Grown Crystals.............88
4.4 Brief Comment on Undoped VGF Crystals.............93
4.5 Data for VZM and Zone-Refined GaAs.............96
4.6 Data for More Recent VZM GaAs.............121
References.............128

5. RESULTS FOR DOPED GaAs CRYSTALS

5.1 Dopants for High-Resistivity GaAs.............130
5.2 Electrical and Optical Data for Doped High-Resistivity GaAs. 135
5.3 Conducting GaAs.............144
References.............163

6. CONCLUSIONS CONCERNING SEMI-INSULATING GaAs.............165

APPENDIX.............169

VITA.............171

## LIST OF TABLES


| Table | | page |
|---|---|---|
| 2-1 | Prominent two-phonon absorption peaks in GaAs, and a set of possible assignments. | 38 |
| 2-2 | Spectral Locations of LVM Absorption Bands in GaAs | 39 |
| 4-1 | 300 K properties for six various "undoped" samples | 79 |
| 4-2 | Parameters for a fit of the resistivity and electron density data for six "undoped" samples | 79 |
| 4-3 | 300 K properties of the five VB-grown SI samples | 90 |
| 4-4 | 300 K electrical properties for vertical zone melt and zone refined crystals | 100 |
| 4-5 | 300 K properties for samples from VZM-grown Crystals 25-66N and 25-69N | 122 |
| 5-1 | The absorption coefficient and related parameters for sample Si-I | 160 |

## LIST OF FIGURES


| Figure | | page |
|---|---|---|
| 1-1 | GaAs carrier densities and conductivity vs Fermi energy | 13 |
| 2-1 | A triaxial guarding arrangement | 27 |
| 2-2 | Hall measurement system | 33 |
| 2-3 | GaAs Reststrahlen absorption | 36 |
| 2-4 | GaAs multiphonon lattice absorption | 37 |
| 2-5 | Carbon LVM absorption in GaAs | 41 |
| 2-6 | Near-IR EL2-related absorption | 45 |
| 3-1 | Ambipolar conduction region in GaAs | 54 |
| 3-2 | Near-intrinsic conduction: the factor F(y) | 58 |
| 3-3 | Weak-field Hall factor $r_H$ vs temperature | 61 |
| 3-4 | Hall factors for holes in GaAs, vs temperature | 62 |
| 3-5 | Ambipolar correction factors F(y) and f(z) | 66 |
| 4-1 | Resistivity vs (1000/T) for SI and failed-SI samples | 80 |
| 4-2 | Hall mobility vs temperature for these samples | 81 |
| 4-3 | Electron concentration vs (1000/T) for these samples | 83 |
| 4-4 | Fermi energy vs temperature for the same samples | 84 |
| 4-5 | EL2 ionized fraction $P_i$ derived for these samples | 87 |

4-6 Electron concentration vs. T for VB-grown samples 91

4-7 Fermi energy vs. T for the VB samples 92

4-8 EL2 ionized fraction $P_i$ for the VB samples 94

4-9 Near-IR absorption for VGF-grown SI GaAs sample 97

4-10 Cross-sectional views of VZM and zone-refined crystals 99

4-11 Electron concentration vs. (1000/T) for VZM samples 102

4-12 Resistivity vs. (1000/T) for the VZM samples 103

4-13 Fermi energy vs. temperature for the VZM samples 104

4-14 EL2 ionized fraction $P_i$ for VZM samples 105

4-15 Hall mobility vs. temperature for VZM samples 106

4-16 Carbon LVM absorption for VZM samples 107

4-17 Near-IR EL2-related absorption of a VZM sample 109

4-18 Near-IR "EL2 map" for a VZM wafer 111

4-19 Similar map for another VZM wafer 112

4-20 Electron concentration vs. (1000/T) for zone-refined GaAs 114

4-21 Resistivity vs. (1000/T) for the zone-refined GaAs 115

4-22 Fermi energy vs. T for the zone-refined GaAs 116

4-23 EL2 ionized fraction $P_i$ for the zone-refined GaAs 117

4-24 Carbon LVM absorption for the zone-refined GaAs 119

4-25 Summary for zone-refined GaAs of carbon and EL2 distributions 120

4-26 Near-IR absorption spectrum for a VZM-grown sample 125

4-27 That near-IR absorption compared with EL2 photoionization 126

5-1 Hole density and resistivity vs. (1000/T) for Fe-doped high resistivity P-type GaAs 136

5-2 Hole mobility vs. T for this P-type GaAs:Fe 138

5-3 Fermi energy vs. T for this P-type GaAs:Fe 139

5-4 Near-IR absorption for the P-type GaAs:Fe 141

5-5 Resistivity vs. (1000/T) for Cr-doped and Fe-doped SI GaAs 145

5-6 Electron concentration vs. (1000/T) for these doped SI samples 146

5-7 Fermi energy vs. T for these doped SI samples 147

5-8 Hall mobility vs. T for these doped SI samples 148

5-9 Electron concentration for Si-doped N-type samples 150

5-10 Mobility vs. T for these N-type samples 151

5-11 Photoluminescence spectra for strongly N-type (Si-doped) and P-type (Zn-doped) samples 154

5-12 PL spectra for a less strongly Si-doped N-type sample 156

5-13 Near-IR transmittance for strongly Si-doped sample 158

5-14 Near-IR absorption for the less strongly Si-doped sample 161

## ABSTRACT


Compensation and Ambipolar Conduction in

Semi-insulating GaAs Bulk Crystals

Ru-Shyah Tang, Ph. D.

Oregon Graduate Institute of Science and Technology, 1990

Supervising Professor: John S. Blakemore

Melt-grown semi-insulating (SI) GaAs is a material of technological importance. Although SI status can arise from chromium doping, there is much interest in "undoped" GaAs, with SI behavior derived from compensation of a small shallow acceptor concentration (notably $C_{As}$) by the midgap native donor defect EL2. The work described in this dissertation was directed towards determination of these various concentrations and of the electronic consequences. The GaAs characterization involved both electrical and optical measurements.

A versatile Hall and conductivity measurement system was developed, for data over a wide temperature range: to above 400 K for SI material, to cryogenic temperatures for conducting samples. The value of such temperature-dependent analysis, for SI samples especially, has been demonstrated. The system provides valid numbers for a sample with

conductance exceeding $10^3$ S, and also for one with resistance approaching $10^{10}$ Ω. The measured Hall coefficient and conductance for a near-intrinsic SI sample are affected by ambipolar conduction, and a simple way to correct for the hole conduction contribution was evolved, and incorporated into the data analysis program. It was thereby possible to study Fermi energy vs. temperature, thus learning whether EL2 or some other level was in control.

Several optical measurement methods were used to complement electrical observations. Mid-IR local vibrational mode (LVM) absorption was used to measure $C_{As}$ acceptor concentrations, while near-IR absorption was used to measure the neutral and ionized EL2 concentrations. Near-IR absorption could also measure Fe-related absorption in a crystal known to contain iron. Photoluminescence was used for Si-doped GaAs in showing that part of the silicon contributed to deep-level complexes.

A major contribution in this work has been a comparison of SI GaAs grown by several methods, not just the conventional liquid encapsulated Czochralski (LEC) technique. Material studied included SI crystals grown by the vertical Bridgman (VB) and vertical gradient freeze (VGF) methods, and by vertical zone melt (VZM) including vertical zone refining; all showing considerable promise.

# CHAPTER 1

# INTRODUCTION

## 1.1 History of GaAs Crystal Growth from the Melt

Gallium arsenide, a III-V compound semiconductor, has the zinc-blende structure consisting of two interpenetrating f.c.c. sublattices. One sublattice consists of Ga atoms, the other consists of As atoms and is displaced one quarter of the way along the main diagonal of the other. This material was first created by Goldschmidt [1] in 1929.

The technology involved in the growth of GaAs is considerably more complicated than silicon, since one is dealing with more complicated binary phase equilibria and a highly volatile arsenic component. A lot of effort has been put into control of the stoichiometry ratio, during GaAs crystal growth.

Traditionally GaAs bulk crystal growth from the melt can be classified in terms of Bridgman (nonpulling) methods and Czochralski (pulling) methods. A typical system for a nonpulling method was described by Cunnell *et al* [2], called the Horizontal Bridgman (HB) method. In this, one has a three-zone furnace with the GaAs charge, and excess arsenic in a separate boat, all placed in a sealed ampoule. During the growth process,

the charge was heated up to its melting point (>1240° C) and the arsenic reservoir was kept at around 600° C to supply the required As partial pressure. When molten GaAs moved into a zone slightly lower than its melting point GaAs was solidified and crystallized hopefully with an orientation provided by a seed.

A successful pulling technique was developed by Mullin [3] for volatile materials, called the Liquid-Encapsulated Czochralski (LEC) method, using a nonreactive material boric oxide ($B_2O_3$) as an encapsulation layer to cover the molten charge in a crucible typically (at first) of quartz. To initiate growth, a seed crystal was dipped through the boric oxide layer into the melt. When the temperature was lowered until a small amount of crystalline material solidified onto the seed, then a crystal could be slowly withdrawn from the melt .

In both HB and LEC methods, the GaAs melt is directly contacted by the container which traditionally was quartz. Some reaction between melt and quartz container makes silicon a major impurity in GaAs [4,5]. This is not a problem for a N-type conductive crystal, since silicon is a preferred dopant with not far from unity segregation coefficient [6]. But for systematic growth of semi-insulating (SI) GaAs in the early days, a deep level acceptor impurity, chromium, had to be added to approximately $10^{17}$ $cm^{-3}$ [7,8] to compensate the shallow level donor silicon. This highly compensated material not only shows poor mobility, but also causes some difficulty in IC fabrication [9,10] due to Cr redistribution [11] and anomalous conversion. The use of a pyrolytic boron nitride (PBN) crucible or container

was reported by Swiggard *et al*[12,13] as greatly reducing the level of silicon contamination, for both high purity GaAs synthesis and crystal growth. Since then PBN has become an essential part in designing a system for melt-growth of undoped semi-insulating (SI) GaAs.

In the early years, optoelectronics was the only obvious application of GaAs. Since a Bridgman crystal has lower dislocation density [14] and a lower cost than a Czochralski crystal, the HB technique has been successfully used for a long time in production of high quality and large volume conducting GaAs single crystals. More recently, microelectronics (high speed digital devices and microwave integrated circuits) has become a significant factor in the GaAs industry. Since most of the standard semiconductor processing equipment for ICs requires round circular wafers, the HB method with its typical "D-shaped" wafers has lost favor, with respect to the growth methods now to be listed.

## 1.2 Some Modern Melt-Growth Methods

LEC growth with PBN crucible has recently been enjoying supremacy over other growth technologies for SI GaAs, because of its circular wafer shape, large wafer area, homogeneity over a wafer, and the high purity due to the possibility of direct synthesis. Besides those advantages there is a serious drawback: a high dislocation density (typically 50,000 $cm^{-2}$) due to the thermal stresses generated in the crystal during and after growth.

Ingenious possible improvements have been reported, one called the LEK [15], LEF [16], or FEC [17] techniques in which one uses thick $B_2O_3$ to reduce the temperature gradient during growth, and another called MLEC [18], or VMLEC [19] techniques in which a magnetic field is applied to the growth chamber in order to reduce temperature fluctuations. Addition of up to ~0.5% of InAs to the melt, to "harden" the crystal lattice, also enjoyed a vogue in SI GaAs LEC growth during about the period 1984-88. However, high thermal stress because of the large temperature gradient still is the Atlas heel of all LEC methods.

In response to the above-noted problems of LEC growth, some other promising technologies have been developed in recent years, as now listed:

(i) Vertical Gradient Freeze (VGF) method. This is a kind of nonpulling method, related to Horizontal Gradient Freeze (HGF). It was developed by Gault *et al*[20] using a vertical PBN crucible with a stoichiometry controlled As reservoir, and a carefully designed heating environment. It can produce 75 mm diameter undoped SI GaAs single crystals [21]. Since the temperature gradient is low, less than 1000 $cm^{-2}$ dislocation density can be achieved in VGF crystals [20,22].

(ii) Vertical Bridgman (VB) method. Also a kind of nonpulling method, the difference from VGF being that VGF relies on an electrically adjusted furnace profile to move the melt/solid interface, whereas in VB the PBN crucible is physically transported with respect to the furnace assembly. Semi-insulating VB GaAs single crystals with low dislocation density and 75 mm diameter have been reported [23,24]. In this method $B_2O_3$ may be used

as encapsulant to suppress decomposition of GaAs, and a vertical PBN round boat is held in a sealed quartz ampoule. During the growth process, the boat-ampoule assembly moves versus the furnace [23] or vice versa [24].

(iii) Vertical Zone Melt (VZM) method. This is a new zone melt method recently developed by Swiggard [25], utilizing $B_2O_3$ liquid encapsulant and a PBN crucible with a seed compartment at the base in a vertical configuration. A special furnace with a thermal spike creates a molten zone in a rod of GaAs. In this design the length of molten zone and thermal gradient can be adjusted, and undoped semi-insulating GaAs single crystals of some 28 mm diameter have been grown to this time (1990). A special feature of the VZM method is that the crystal can be refined by multiple passes of the molten zone. A very nearly intrinsic condition has been obtained in some parts of GaAs crystals grown by VZM [26].

## 1.3 Dopant Effects in GaAs

As in other semiconductors, GaAs can be doped with various impurities. A foreign atom can sit on a Ga or As site, or interstitially.

(i) Group II elements : If a group II element is incorporated and any such atom sits on a Ga site, it needs to accept an extra electron to complete its tetrahedral bonds. Therefore it acts as an acceptor in GaAs. Elements such as Be, Mg, Zn, Cd, and Hg produce acceptor levels which are P-type dopants. Among them Zn and Cd are most commonly used as P-type

dopants, due to their high solid solubilities.

(ii) Group VI elements : In contrast to a group II element, if a group VI element substitutes for an As atom in GaAs, it will have an extra electron, surplus to its bonding requirements. Therefore it behaves as a donor. S, Se, as well as Te are shallow donors, and are frequently used as N-type dopants in GaAs.

(iii) Group IV elements : There are several possible substitutions for a group IV element in GaAs. Such atoms can occupy Ga sites acting as donors, or occupy As sites acting as acceptors. They can occupy two neighboring sites as pairs and remain electrically neutral, or they may substitute both sub-lattices in unequal numbers and can be either donors or acceptors[27]. Usually Si and Ge substitute the Ga site as shallow donors, but carbon substitutes the As site as a shallow acceptor in normal melt growth crystals.

(iv) Transition elements : Most 3d transition element dopants are deep levels in III-V semiconductors, since the electronic state of them cannot be described by hydrogenic or effective mass theory[28]. Ni, Co, Fe, Mn, Cr, and even V are deep acceptors in GaAs [28-30]. So also is Cu, which while not a transition element (having a filled 3d shell) lies adjacent to that group of elements in the Periodic Table. Cr was extensively studied during the period 1964-1982, since it was the most important deep acceptor for making high resistivity SI GaAs. $Cr_{Ga}$ generates a level at $\varepsilon_v + 0.79$ eV which is quite close to the center of the intrinsic energy gap, permits a 300 K resistivity as high as $10^9$ Ω-cm, and has a solid solubility of some $5 \times 10^{17}$ $cm^{-3}$ [31]. Due to the high diffusivity of Cr, V has been proposed as a

replacement for Cr in making SI GaAs [29,32]. Iron also has been used for making semi-insulating GaAs, but the highest 300K resistivity obtained is about $10^5$ Ω-cm. The reason for this is that the deep levels produced by Fe are not close enough to mid gap, only ~0.5 eV above $\varepsilon_v$ [31].

## 1.4 Defect Species in Melt-grown GaAs

The families of defect species in GaAs are quite complicated. From a thermodynamic point of view, in 1975 Van Vechten [33,34] predicted that there should be some single vacancies ($V_{Ga}$, $V_{As}$), and that also isolated antisite defects ($As_{Ga}$, $Ga_{As}$) could form in III-V compound semiconductors. Later Baraff and Schluter [35] used a self-consistent Green's function technique to deduce the electronic structure as well as energies of eight dominant defects for As-rich and Ga-rich GaAs, including also two kinds each of Ga and As interstitials. They predicted that native defects should be abundant in doped or undoped GaAs. Recently Bourgoin *et al* [36] commented that not only simple intrinsic defects (As and Ga interstitials, vacancies and antisites) but also some complexes, could be formed by the interaction of these defects among themselves or with impurities.

A listing of electron traps and hole traps in GaAs materials had been summarized and reported by Martin's group [37,38] in 1977. At least fifteen electron levels (EL) and twelve hole levels (HL) had been found by them, with activation energies varying from 0.15 to 0.90 eV. They noted

some defects as existing in melt-grown and epitaxial GaAs, but some other defects only can be found in ion implantated or in electron irradiated samples [39].

Among those families of defects, the members with an energy level near midgap are most important for the semi-insulating property. The most famous defect, named EL2 by Martin's group, is a donor with an energy level at $\varepsilon_g$ - 0.8 eV (the enthalpy or "activation energy"). Its concentration is typically in the range 0.2-3 x $10^{16}$ $cm^{-3}$ in "undoped" SI GaAs grown under moderately As-rich conditions. Thus the EL2 concentration is 10 to 1,000 times larger than for various other subsidiary defect species [36].

## 1.5 Models and Their Controversies for EL2

Since EL2 was named by Martin *et al.* in 1977, a large number of papers have been published because of its unique important property in semi-insulating GaAs. Among those papers the identification of EL2 was the most controversial topic. It has been characterized as a "stoichiometric defect" or "intrinsic defect", but an actual microscopic model of EL2 is still an unsettled subject [40].

EPR is a powerful technique to give information on the microstructural composition of defects. In 1980 Wagner *et al.* [41] first investigated an EPR 4 line spectrum in SI GaAs, which was attributed to the $As_{Ga}$ antisite defect. Later the same EPR signal was also found in fast neutron irradiated GaAs

[42] and in plastically deformed samples [43]. When optical or electronic properties of EL2, and EPR signals of defects, were compared later, many models or hypotheses were proposed. One significant feature of EL2, apparent only for low temperatures, is a photo-quenching phenomenon requiring a metastable version of the electron-filled (neutral) charge condition [44].

Not only the photoquenching behaviour of EL2 cannot be understood if one assumes EL2 to be composed exclusively of the isolated $As_{Ga}$ defect, but also an EPR experiment cannot exclude more complex structures if $As_{Ga}$ is associated with some second-neighbor defects [44]. Because of this, some other suggestions about the formation of EL2 have included $As_{Ga}$-$V_{As}$ by Walukiewicz *et al* [45], As-aggregates by Ikoma *et al* [46] as well as $As_{Ga}$-$As_i$ by Meyer *et al* [47] and von Bardeleben *et al* [48]. Also, each of these models leaves some problems. A even more complex ternary model $As_{Ga}V_{Ga}V_{As}$ was suggested by Wang and Zou *et al* [49] and Wager and van Vechten [50], in trying to fit better all kinds of properties which are evidenced by EL2.

## 1.6 Origins and Development of Semi-insulating (SI) GaAs

The first semi-insulating GaAs has been known since the 1950's, when it was obtained as an accident of the crystal growth conditions [51]. People didn't know why, and high resistivity was not reproducible at that

time.

At the beginning of the 1960's, Hilsum and Rose-Innes [52] reported that high resistivity GaAs could be obtained by adding oxygen. People then learned how to make high resistivity GaAs more consistently. It was believed that oxygen could be used to compensate residual shallow acceptors in GaAs in making high resistivity material. Actually, very high resistivity and even SI GaAs were obtained later using the HB technique, by introducing an oxygen partial pressure into the ampoule[53-55] or by adding $Ga_2O_3$ to the melt [55-57]. Nevertheless, some later studies showed that the presence of oxygen is in reality to suppress the $Si_{Ga}$ donor contamination from a quartz boat/crucible by gettering it from the melt [58,59]. Further study even suggested that oxygen relates to a deep level EL0, which essentially has the same activation energy (825±4 meV) as EL2 but is perhaps not directly involved in electrically active centers [60]. Therefore, "O" doped SI GaAs may be just an early stage of EL2 dominated "undoped" SI GaAs.

Not only oxygen has been used to encourage SI GaAs. People found that doping with transition elements could also generate high resistivity. Many elements including Co, Cr, Fe, Mn, Ni, and Ti had been tried to produce SI GaAs [7]. Among them, Cr doping was a standard method for making semi-insulating GaAs since 1964 [7]. The Cr deep acceptor was (and still is) added to HB or LEC crystals to compensate the residual shallow donor Si which comes from a quartz boat or crucible. Chromium can produce a very high resistivity SI GaAs, but because of Cr redistribution during a

device fabrication process, many device fabrication houses prefer "undoped" SI GaAs. That is to say, SI GaAs not intentionally doped, and thus controlled by the EL2 defect.

EL2 is a mid-gap deep level native defect in As-rich melt grown GaAs. Of course it has a problem similar to Cr in device processing in that locations of EL2 *move* during process steps, but EL2 is not an extrinsic impurity so it cannot be avoided. The amount of EL2 present is dependent on the stoichiometry ratio of the melt, and the thermal history during and after growth. When Si contamination in crystal growth can be reduced by use of a PBN boat or crucible, residual acceptors such as carbon will tend to be in excess, for a P-type tendency. If one can have enough EL2 to compensate the excess shallow acceptors, one can get EL2 controlled semi-insulating GaAs.

Nonetheless, chromium and EL2 are not the only solutions for making SI GaAs. There were reports by Ulrici *et al*[29] and Katayama-Yoshida *et al* [61] of using the less mobile transition element vanadium to produce semi-insulating GaAs. They claimed that this might avoid the redistribution problem present with Cr and the concentration uncertainty problem for EL2. Despite this and other impurity-related work, EL2-dominated SI GaAs remains the central focus in this dissertation, a substrate material of choice for direct-implant MESFET ICs, and for various optoelectronic applications where an impurity intervention from the substrate would be disastrous.

## 1.7 Compensation Models for SI GaAs

A room temperature (300 K) conductivity of SI GaAs in the range $10^{-6}$ - $10^{-9}$ S/cm corresponds to an electron concentration of $10^{9}$ - $10^{6}$ $cm^{-3}$ (Fig.1-1). This low electron and hole concentration, close to intrinsic, cannot be achieved by purification with any current technology. The only possibility is that the material has been properly compensated, so that the Fermi level $\varepsilon_F$ is pinned close to its intrinsic level $\psi$ by an extrinsic (impurity/ defect) level of suitable energy.

Residual impurities in bulk GaAs have been analyzed by Krauskopf *et al* [62] using charged particle activation analysis (CPAA), nuclear reaction analysis (NRA), and spark source mass spectrography (SSMS). Their result shows twenty different detectable elements, all with concentration in sub-ppm or ppb order. It includes shallow donors (Si, S), shallow acceptors (C, Zn, Mg, Cd), and deep level transition elements (Cr, Mn, Fe, Ni, Co, Cu). One can thus see that, when GaAs is synthesized from "6N" Ga and As, the "6N" label is legitimate.

For such a material, let the total shallow acceptor concentration be $N_a$, total shallow donor concentration $N_d$, total deep donor concentration $N_{DD}$, and total deep acceptor concentration be $N_{DA}$. Then several combinations can happen, as follows :

(i) When $N_a > N_d$ and $N_{DA} > N_{DD}$, the material is simply P-type.

(ii) When $N_a > N_d$ yet $N_{DD} > N_{DA}$, but $(N_a - N_d) > (N_{DD} - N_{DA})$, the material still is p-type.

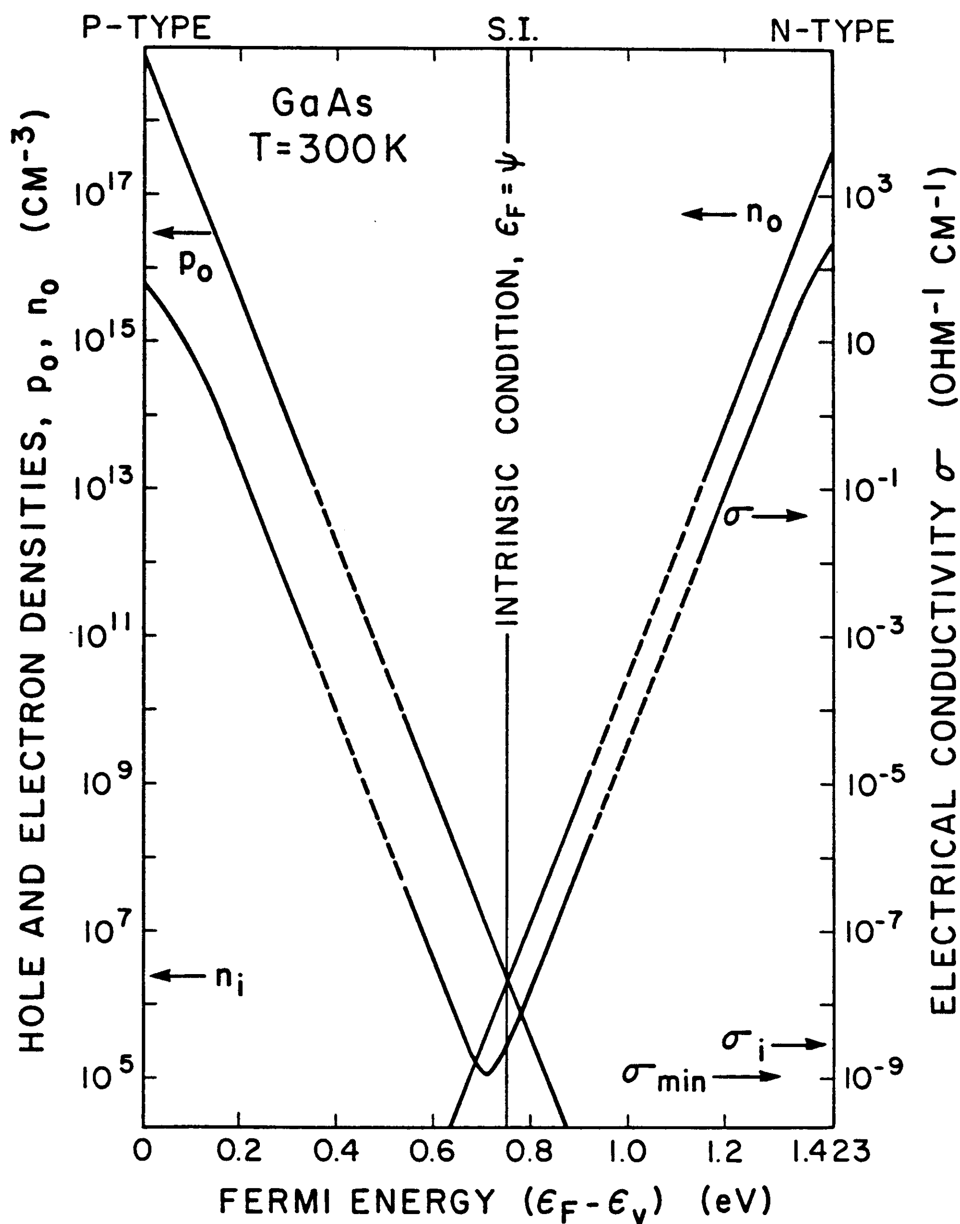


**Figure 1-1** A variation of the 300 K thermal carrier densities ($n_o$ and $p_o$) and the resulting conductivity as a function of the Fermi level position, with the assumed values $n_i = 2.25 \times 10^6$ cm$^{-3}$, $\epsilon_i = 1.423$ eV, and $\mu_n = 25\ \mu_p = 8000$ cm$^2$/V-s.

(iii) When $N_a > N_d$ yet $N_{DD} > N_{DA}$, and now $(N_a - N_d) < (N_{DD} - N_{DA})$, the material will be high resistivity with $\varepsilon_F$ locked to one of the deep donor levels. This could be the case of "oxygen" doped or EL2 dominant undoped SI GaAs.

(iv) When $N_d > N_a$ and $N_{DD} > N_{DA}$ the material is N-type.

(v) When $N_d > N_a$ and $N_{DA} > N_{DD}$, but also $(N_d - N_a) > (N_{DA} - N_{DD})$, the material is still N-type.

(vi) When $N_d > N_a$ and $N_{DA} > N_{DD}$, but $(N_d - N_a) < (N_{DA} - N_{DD})$ the material is high resistivity due to $\varepsilon_F$ locked to one of the deep acceptor levels. This is the case of Cr, V, or Fe doped SI GaAs.

## 1.8 Possible Characterization Methods for SI GaAs

The semi-insulating property is not due to some special chemical composition or different structure of GaAs, but is due to the electronic compensation of shallow and deep levels in a crystal. Comparable, but complicated, compensation schemes exist in numerous wide-gap compounds. Let us focus on the electrical and optical characterization methods then compare their capabilities for SI GaAs evaluation.

(i) Hall/resistivity : In this method we can get equilibrium electron concentration $n_0$ (or hole concentration $p_0$), mobility $\mu_n$ (or $\mu_p$ ), resistivity $\rho$, and conduction type of samples. From those basic parameters, one can also deduce the Fermi level $\varepsilon_F$ of the sample, and the ionization fraction $P_i$ of

any level whose energy level is known and located in the forbidden gap.

(ii) Absorption/transmission : This mechanism includes electronic transitions among both bands and discrete levels themselves, or between bands and discrete levels. From the near-IR absorption spectrum, we can deduce $N_{EL2^0}$ and $N_{EL2^+}$ by calibrated absorption cross section $\sigma_n$ and $\sigma_p$ [63,64]. From $N_{EL2^0}$ and $N_{EL2^+}$ one also can deduce $\varepsilon_F$, then estimate $n_0$ [64,65]. (This is an estimate, since any uncertainty of $\varepsilon_F$ will exponentially amplify in $n_0$). Besides electronic transitions, there can be an interaction between an impurity and incoming light which can be detected by local vibrational mode (LVM) absorption (vibronic not electronic) in the mid-IR range ( few tens of meV). Theoretically, one can monitor any desired impurity in GaAs, if one has enough resolution with good S/N ratio and a correct calibration factor. Unfortunately this is not true in the real world. Only carbon LVM data has been used in the SI GaAs community, and still causes a lot of argument about the calibration factor f which should be used [66-68].

(iii) Photoluminescence : The mechanism of photoluminescence (PL) is the inverse process of optical absorption, but is more complicated due to the competition of different recombination paths, of which only radiative transitions are detected. According to the Shockley-Read-Hall (SRH) model of recombination, the transitions will be dominated by deep levels in semi-insulating GaAs. A important problem is that PL is a semi-quantitative method. It is hard to determine concentrations because the measured intensity will vary with surface preparation and optical collection efficiency.

Thus information obtained from photoluminescence for SI GaAs [69,70] must be interpreted with care and expertise.

(iv) Photoconductivity : The extrinsic photoconductive spectrum can used to evaluate ionization energies of deep levels (near-IR) and shallow levels (mid to far-IR region) for SI GaAs. From a photoconductive decay process we also can study recombination, to get carrier life-time and capture cross section information of deep levels. Sometimes the analysis is quite complicated due to ambipolar conduction by electrons and holes since both may be created during the activation process [71]. For SI GaAs, another complication of a transient phenomenon such as photoconductive decay is provided by the rather long dielectric relaxation time, which may be in the μs time range.

(v) DLTS : Deep Level Transient Spectroscopy is a powerful method developed by Lang [72] for deep level characterization. From it one can determine activation energies, concentrations, capture cross-sections, even the type (electron or hole) of trap for different levels in semiconductors. Unfortunately, unlike other methods mentioned above, where some information can be obtained directly from a SI GaAs sample; DLTS has to extract its information from a pn-junction or Schottky barrier. A semi-insulating sample must be converted to N-type or P-type by ion implantation or other process. This is not only inconvenient, it also loses fidelity due to the extra processes in preparing a sample. Because of this, the powerful DLTS method is invalid for direct use in SI GaAs.

(vi) PITS : Photo Induced Transient Spectroscopy is a method similar

to DLTS. It also uses the rate window technique, but PITS measures current change instead of capacitance change. Since a PITS sample doesn't require a p-n junction or Schottky barrier, PITS can be done directly on semi-insulating materials [73]. PITS has the capability to obtain information including activation energies and capture cross-sections for deep level states involved in semiconductors, just as DLTS. However, PITS is not able to distinguish hole from electron traps [74]. It is also not easy to get quantitative analysis, due to the complex spatial distribution of light penetration.

(vi) EPR (or ESR) : Electron Paramagnetic Resonance or Electron Spin Resonance is a powerful tool, very frequently used by physicists to gain detailed information about defects in semiconductors. EPR or ESR is a form of Zeeman spectroscopy, which can detect the direct transition between the Zeeman-split electronic levels in a magnetic field. To observe an EPR signal, there must be an unpaired spin, i. e., a non-zero paramagnetism, such as may be due to electrons in the conduction band or a suitably charged point-, line-, or surface-defect state [75]. For GaAs or any of the III-V compounds, there are experimental difficulties which arise from the nuclear spins of the constituent atoms in a crystal lattice. This leads to broadening of spectral lines, resulting in no or poor resolution of the hyperfine splittings [76] in some case.

One could go on to list even exotic characterization methods, but the above notes the approaches used most commonly. The scene is thus set for describing the specific methods used in the present study.

REFERENCES: CH.1


1. V. M. Goldschmidt, Trans. Faraday Soc. **25**, 253 (1929).
2. F. A. Cunnell, J. T. Edmond, and W. R. Harding, Solid State Electron. **1**, 97 (1960)
3. J. B. Mullin, B. W. Straughan, and W. S. Brickell, J. Phys. Chem. Solids **26**, 782 (1965)
4. L. Ekstrom and L. R. Weisberg, J. Electrochem. Sec. **109**, 321 (1962)
5. M. E. Weiner, D. T. Lassota, and B. Schwartz, J. Electrochem. Soc. **118**, 301 (1971)
6. G. S. Kamath, Solid State Technology 173 (1984)
7. G. R. Cronin and R. W. Haisty, J. Electrochem. Soc. **111**, 874 (1964)
8. R. N. Thomas, H. M. Hobgood, G. W. Eldridge, D. L. Barrett, T. T. Braggins, L. B. Ta, and S. K. Wang, in *Semiconductors and Semimetals Vol. **20***, 4 (1984)
9. D. R. Chen, D. R. Decker, W. C. Peterson, and A. K. Gupta, Microwave J. March, 39 (1981)
10. C. G. Kirkpatrick, R. T. Chen, D. E. Holmes, P. M. Asbeck, K. R. Elliott, R. D. Fairman, and J. R. Oliver, in *Semiconductors and Semimetals Vol. **20***, 161 (1984)
11. T. Udagawa, M. Higashiura, and T. Nakanisi, in *Semi-Insulating III-V Materials: Nottingham 1980*, edited by G. J. Rees, (Shiva, Orpington, UK, 1980), p. 108

12. E. M. Swiggard, S. H. Lee, and F. W. Von Batchelder, Inst. Phys. Conf. Ser. No. **33b**, 23 (1977)

13. R. L. Henry, and E. M. Swiggard, Inst. Phys. Conf. Ser. No. **33b**, 28 (1977)

14. J. M. Parsey, Jr, in *Semi-Insulating III-V Materials: Malmo 1988*, edited by G. Grossmann and L. Ledebo, (Adam Hilger, Bristol, 1988), p.405

15. G. Jacob, J. Cryst. Growth **58**, 455 (1982)

16. P. Mo, J. Wu, Y. Zou, J. Yang, and S. Li, in *Semi-Insulating III-V Materials: Kah-nee-ta 1984*, edited by D. C. Look and J. S. Blakemore, (Shiva, Nantwich, UK, 1984), p. 134

17. H. Nakanishi, K. Yamada, and K. Hoshikawa, : *7th International Conf. on "Crystal Growth"* p. 12 (Stuttgart, Germany, 1983)

18. K. Terashima, T. Katsumata, F. Orito, T. Kikuta, and T. Fukuda, Jap. J. Appl. Phys. **22**, L325 (1983)

19. J. Osaka and K. Hoshikawa, in *Semi-Insulating III-V Materials: Kah-nee-ta 1984*, edited by D. C. Look and J. S. Blakemore , (Shiva, Nantwich, UK, 1984), p. 126

20. W. A. Gault, E. M. Monberg, and J. E. Clemans, J. Cryst. Growth **74**, 491 (1986)

21. J. E. Clemans and J. H. Conway, in *Semi-Insulating III-V Materials: Malmo 1988*, edited by G. Grossmann and L. Ledebo, (Adam Hilger, Bristol, 1988) , p.423.

22. C. R. Abernathy, A. P. Kinsella, A. S. Jordan, R. Caruso, S. J. Pearton, H. Temkin, and H. Wade, J. Cryst. Growth **85**, 106 (1987)

23. K. Hoshikawa, H. Nakanishi, H. Kohda, and M. Sasaura, J. Cryst. Growth **94**, 643 (1989)

24. R. E. Kremer, D. Francomano, G. H. Beckhart, and K. M. Burke, in *1989 Colorado Microelectronics Conference, Colorado Springs*, (March 1989)

25. E. M. Swiggard, J. Cryst. Growth **94**, 556 (1989)

26. R-S. Tang, L. Sargent, J. S. Blakemore, and E. M. Swiggard, J. Cryst. Growth (Proc. DRIP-III Conference, Tokyo, 1989)

27. C. H. Gooch, *Gallium Arsenide Lasers*, (John Wiley & Sons, New York 1969), p. 169

28. H-J Queisser, in *Festkorperprobleme XI (1971)*, edited by O. Madelung Pergamon/Vieweg (Braunschwieg, 1971), p. 45

29. W. Ulrici, K. Friedland, L. Eaves, and D. P. Halliday, Phys. Stat. Sol. (b) **131**, 719 (1985)

30. U. Kaufmann, H. Ennen, J. Schneider, R. Worner, J. Weber, F. Kohl, Phys. Rev. B **25**, 5598 (1982)

31. A. G. Milnes, in *Advances in Electronics and Electron Physics*, Vol. **61**, (Academic Press, 1983), p. 91, p. 100

32. W. Kutt, D. Bimberg, M. Maier, H. Krautle, F. Kohl, E. Bauser, Appl. Phys. Lett. **44**, 1078 (1984)

33. J. A. Van Vechten, J. Electrochem. Soc. **122**, 419 (1975)

34. J. A. Van Vechten, J. Electrochem. Soc. **122**, 423 (1975)

35. G. A. Baraff and M. Schluter, Phys. Rev. Lett. **55**, 1327 (1985)

36. J. C. Bourgoin and H. J. von Bardeleben, J. Appl. Phys. **64**, R65 (1988)

37. G. M. Martin, A. Mitonneau, and A. Mircea, Electronics Letters **13**, 191 (1977)

38. A. Mitonneau, G. M. Martin, and A. Mircea, Electronics Letters **13**, 666 (1977)

39. G. M. Martin and S. Makram-Ebeid, Physica **116B**, 371 (1983)

40. R. A. Morrow, J. Mater. Res. **2**, 681 (1987)

41. R. J. Wagner, J. J. Krebs, G. H. Strauss, and A. M. White, Solid State Commun. **36**, 15 (1980)

42. R. Worner, U. Kaufmann, and J. Schneider, Appl. Phys. Lett. **40**, 141 (1982)

43. E. R. Weber, H. Ennen, U. Kaufmann, J. Windscheif, J. Schneider, and T. Wosinski, J. Appl. Phys. **53**, 6140 (1982)

44. G. M. Martin and S. Makram-Ebeid, in *Deep centers in Semiconductors. A State of the Art Approach*, edited by S. T. Pantelides, (Gordon and Breach Science Publishers, New York, 1986), p. 443

45. W. Walukiewicz, J. Lagowski, and H. C. Gatos, Appl. Phys. Lett. **43**, 112 (1983)

46. T. Ikoma and Y. Mochizuki, Jpn. J. Appl. Phys. **24**, L 935 (1985)

47. B. K. Meyer, D. M. Hofman, J. R. Niklas, and J. M. Spaeth, Phys. Rev. B **36**, 1332 (1987)

48. H. J. von Bardeleben, D. Stievenard, J. C. Bourgin, and A. Huber, in *Semi-Insulating III-V Materials: Hakone 1986*, edited by H. Kukimoto and S. Miyazawa, ( Ohmsha, Tokyo, 1986), p. 355

49. G. Wang, Y. Zou, S. Benakki, A. Goltzene, and C. Schwab, J. Appl. Phys. **63**, 2595 (1988)

50. J. F. Wager and J. A. van Vechten, Phys. Rev. B **35**, 2330 (1987)

51. J. W. Whelan and G. H. Wheatley, J. Phys. Chem. Solids **6**, 169 (1958)

52. C. Hilsum and A. C. Rose-Innes, Semiconducting III-V Compounds, Pergamon Press, (1961), p. 142

53. N. G. Ainslie, S. E. Blum, and J. F. Woods, J. Appl. Phys. **33**, 2392 (1962)

54. J. F. Woods and N. G. Ainslie, J. Appl. Phys. **34**, 1469 (1963)

55. J. L. Fertin, J. Lebailly, and E. Deyris, Inst. Phys. Conf. Ser. **3**, 46 (1967)

56. J. M. Woodall and J. F. Woods, Solid State Commun. **4**, 33 (1966)

57. T. Shimoda and S. Akai, Jpn. J. Appl. Phys. **8**, 1352 (1969)

58. M. Kaminska, J. Lagowski, J. Parsey, K. Wada, and H. C. Gatos, Inst. Phys. Conf. Ser. **63**, 197 (1981)

59. G. M. Martin, G. Jacob, J. P. Hallais, F. Grainger, J. A. Roberts, J. B. Clegg, P. Blood, and G. Poiblaud, J. Phys. C **15**, 1841 (1982)

60. J. Lagowski, D. G. Lin, T. Aoyama, and H. C. Gatos, in *Semi-Insulating III-V Materials: Kah-nee-ta1984*, edited by D. C. Look and J. S. Blakemore, (Shiva, Nantwich, UK, 1984), p. 222

61. H. Katayama-Yoshida and A. Zunger, in *Semi-Insulating III-V Materials: Hakone 1986*, edited by H. Kukimoto and S. Miyazawa, (Ohmsha, Toyko, Japan, 1986), p. 459
62. J. Krauskopf, J. D. Meyer, B. Wiedemann, M. Waldschmidt, K. Bethge, G. Wolf, and W. Schutze, in *Semi-Insulating III-V Materials: Malmo 1988*, edited by G. Grossmann and L. Ledebo, ( Adam Hilger, Bristol, 1988), p. 165
63. P. Silverberg, P. Omling, and L. Samuelson, Appl. Phys. Lett. **52**, 1689 (1988)
64. J. S. Blakemore, L. Sargent, R-S. Tang, and E. M. Swiggard, Appl. Phys. Lett. **54** (21), 2106 (1989)
65. S. K. Brierley and D. S. Lehr, Appl. Phys. Lett. **55** (23), 2426 (1989)
66. L. Sargent and J. S. Blakemore, Appl. Phys. Lett. **54** (11), 1013 (1989)
67. T. Arai, T. Nozaki, J. Osaka, and M. Tajima, in *Semi-Insulating III-V Materials: Malmo 1988*, edited by G. Grossmann and L. Ledebo, (Adam Hilger, Bristol, 1988), p.201
68. M. R. Brozel, E. J. Foulkes, R. W. Series, and D. J. T. Hurle, Appl. Phys. Lett. **49**, 337 (1986)
69. M. Tajima, Appl. Phys. Lett. **53** (11), 959 (1988)
70. S. Kuma and Y. Otoki, in *Defect Recognition and Image Processing in III-V Compounds ; Monterey, 1987*, edited by E. R. Weber (Elsevier, Amsterdam, Netherlands, 1987), p.1

71. S. Rahimi, S. G. Johnson, W. B. Leigh, C-K. Chau and J. S. Blakemore, in *Semi-Insulating III-V Materials: Kah-nee-ta1984*, edited by D. C. Look and J. S. Blakemore, (Shiva, Nantwich, UK, 1984), p. 273

72. D. V. Lang, J. Appl. Phys. **45**, 3023 (1974)

73. C. Hurtes, M. Boulou, A. Mitonneau, and D. Bois, Appl. Phys. Lett. **32**, 821 (1978)

74. D. C. Look, *Electrical Characterization of GaAs Materials and Devices*, p.211 (John Wiley & sons, New York, 1989)

75. J. W. Corbett, R. L. Kleinhene, and N. D. Wilsey, in *Defects in Semiconductors*, edited by J. Narayan and T. Y. Tan, (Materials Research Society Symposia Proceedings, Vol. **2**, 1980), p. 1

76. N. D. Wilsey and T. A. Kennedy, in *Microscopic Identification of Electronic Defects in Semiconductors*, (Materials Research Society Symposia Proceedings, Vol. **46**, 1985), p. 309

# CHAPTER 2

# EXPERIMENTAL SYSTEMS USED IN THE PRESENT STUDY

## 2.1 Difficulties of Hall/Resistivity Measurement in SI GaAs

The resistivity of GaAs single crystal from $N^+$ conducting to semi-insulating can spread over the range from $10^{-4}$ to $10^{9}$ Ω-cm at room temperature [1]. Therefore, a typical 0.1 cm thick and 1 x 1 $cm^2$ sample can have a resistance ranging from $10^{-3}$ to $10^{10}$ Ω between any two contacts. When using as a measuring unit a commercial Digital Voltage Meter (DVM), such as HP-3478 or Keithley-196, the input impedance is about $10^{10}$ Ω. This impedance is good enough for many semiconductors, but will induce a tremendous loading error when measuring SI GaAs.

The solution for measuring a semi-insulating high resistivity sample is use of a high input impedance electrometer. However, due to the high impedance nature some difficulties will arise. The first problem is that it is very easy to pick-up interference noise and leakage signal from near by sources. Therefore, connection leads from the electrometer, as well as the sample itself, must be well shielded. A second problem is a very long RC time constant, produced from the stray capacitance of a shielded cable, and

the large specimen resistance. A typical coaxial cable may have a capacitance of 300 pf/m , and a 3 m cable with a $10^{10}\,\Omega$ sample will result in a 10 second RC time constant. This means that the electrometer reading will not stabilize within 0.25% of its final value in less than about one minute (about six time constants) when measuring such a SI sample. Let us consider what this means.

Usually, one minute is not too long to wait for a measurement. However, having to take 16 sets of data at one temperature for a sample which is temperature sensitive is a kind of challenge. As to temperature sensitivity, the resistivity and Hall coefficient of SI GaAs change by ~10% per Kelvin. Thus one would like to make 16 observations during a (fairly short) time with temperature stable to $\pm$ 0.05 K, or better. In order to solve these high resistance problems, a technique called static guard or guarding can be used[2,3]. Guarding is a technique using a conductor at essentially the same potential as the high impedance input, but supplied by a low impedance voltage source, to totally surround the sensitive input leads. As illustrated in Fig.2-1, we use triaxial cable and choose the inner shield as guard conductor, also maintaining it at the same potential as the high impedance center by connecting it to the output of a unity gain high impedance buffer amplifier. Since there is no potential difference between guard layer and center conductor, then there is no requirement to charge or discharge. The system time constant will therefore be reduced dramatically, by effectively eliminating system stray capacitance [4]. Another benefit from use of a guarding arrangement is that the leakage between the high

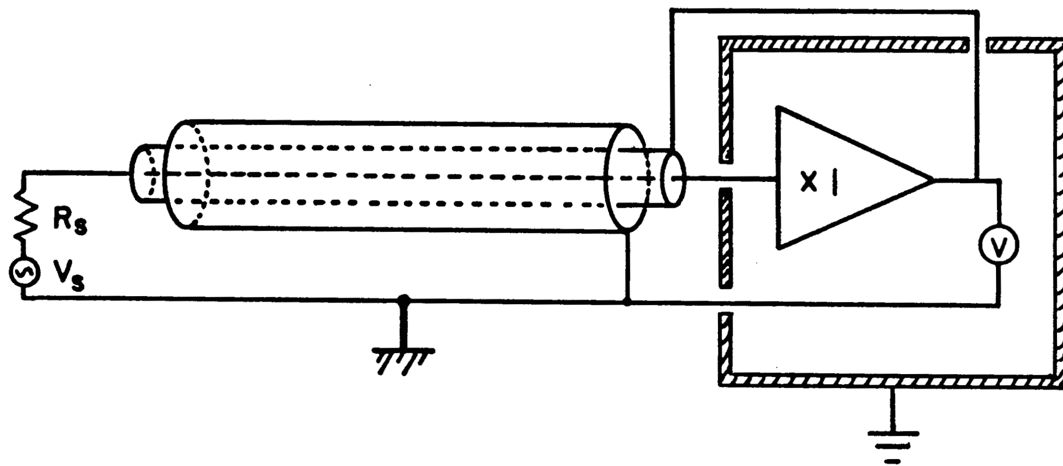


Figure 2-1 A triaxial guarding arrangement. The high impedance input is surrounded by a guard conductor which is connected to the unit gain electrometer buffer amplifier.

impedance center and the surrounding conductor can also be reduced to zero, since there is no potential difference between them.

It is well known that any two dissimilar metals joined together can generate a thermo-electric voltage from the junction. In general, the thermopower is a few tens of $\mu V/^{o}C$, the EMF being also proportional to the temperature differentials of junctions. In any Hall measurement system, from sample to measuring unit consists of soldering leads, connection cables, and amplifier input socket etc., involving various different metals. These metals can be at different temperatures, and the total thermal EMF will be the algebraic sum of the various contributions. Comparing the thermal EMF with a low level Hall voltage signal, one has a non-negligible error source in the Hall measurement. In order to reduce this error, it can of course be done by reducing the temperature gradient, but generally the sample has to measured with temperature differentials present. It is not feasible in a temperature-dependent measurement system for the sample and system to be always at the same temperature, but it is more practicable to keep both temperatures as constant as possible during a short period of time. When the sample and system are fixed at their respective temperatures, the corresponding EMF for the series of junctions is also fixed. And so one must take voltage readings by sending current in forward and reverse directions during that period of time. Since the junction thermal EMF is independent of the direction or magnitude of sample current, one can obtain a more correct signal by subtracting the reverse voltage reading from the forward voltage reading to cancel out the thermal EMF, and dividing the result by

two.

This cancellation of EMF error requires that temperature doesn't change during two voltage readings. From this one can expect that reductions of the system time constant will make any EMF error smaller. However, a rather long time constant is a natural behavior in high resistivity measurement. Thus the guarding technique is highly desired in building a high resistivity Hall effect measurement system, for reducing time constant and leakage error.

In the van der Pauw form of Hall measurement system, a multiplex switch or scanner is required for connecting the various pairs of contacts to voltage measuring and current supply units [5]. The ideal scanner or switch must provide high electrical isolation and low thermal EMF, as two conditions for building a high resistivity measurement system. The inside of a scanner consists of many pairs of metal junctions, which are normally separated by an insulator with good thermal conductivity: to reduce any temperature difference while maintaining electrical isolation. Unfortunately, most electrical insulators do not conduct heat well at room temperature. Therefore, a scanner which can meet low thermal EMF and good electrical insulation (two requirements at the same time) is almost impossible.

The best commercial available low voltage scanner is the Keithley 7059, which has less than $1\mu V$ contact potential but has only about $10^9\,\Omega$ input isolation resistance. Also, the best commercial low leakage scanner is the Keithley 7058, which has greater than $10^{15}\,\Omega$ channel isolation

resistance, but with a much larger contact potential of about 250 $\mu$V. In order to approach those two "ideal" requirements mentioned before, an arrangement of four electrometers with two scanners has been suggested [6]. In this arrangement, four electrometer buffer amplifiers transfer voltage signals from high impedance sample leads through a low voltage scanner to a voltmeter. Note that, so buffered, these voltage signals are of low impedance. Meanwhile, a current source supplies a constant current through a low leakage scanner to sample leads. Now high thermal EMF only exists in the current supply loop. This does not affect voltage measurement outside the loop, provided that the current can keep constant. Also the current leakage through the scanner and electrometer buffers themselves is negligible: compare their impedance ( $\sim 10^{14}\ \Omega$) with the sample resistance (no more than about $10^{10}\ \Omega$). A low leakage and low thermal EMF system can be achieved in this manner.

For a N-type conducting or failed semi-insulating sample, the Hall voltage is sometimes very small, and would be at the detection limit for a digital electrometer. Suppose, for instance, a highly conductive $10^{-4}\ \Omega$ cm sample. In order to avoid heating its contacts, the supply current must kept below 100 mA. This will generate a voltage drop about 100 $\mu$V for resistivity measurement. However, the Hall voltage will be only ~5 $\mu$V when $\mu_H = 1000$ cm$^2$/V-s and B = 5 KG. All electrometers or electrometer buffers have a natural limitation of voltage resolution of about 10 $\mu$V [7] due to thermal noise. Therefore, an electrometer is necessary for any semi-insulating sample, but may not be suitable for measuring a highly

conducting sample. If one's measurements have to encompass both highly conducting and highly semi-insulating samples, the high resistivity situation must use an electrometer, while the low resistivity situation must use a conventional DVM or even a nanovoltmeter.

## 2.2 System Developed for Such Measurements Versus Temperature

In our temperature dependent van der Pauw/Hall system, we use a modified Keithley low current scanner 7058 and a modified Keithley low voltage matrix scanner 7052 with the scanner mainframe 705 as a switching unit. The system also uses a Keithley 220 programmable constant current source, Keithley 196 programmable digital multimeter, and four home-made electrometer buffers. These high impedance buffers are made from electrometer-grade operational amplifiers, such as Analog Devices AD515 or Burr-Brown OPA128, which have less than 0.1pA bias current.

For different resistivity samples and different operating temperature ranges, we separate the system input by using two different sample holders. One for high resistivity samples using a fully guarded shielding arrangement can run from room-temperature up to 425 K (limited by melting of the In contacts we ordinarily employ). The other holder for low resistivity samples can operate from about 373 K down to 77 K by using a MMR [8] cooling stage and temperature controller. In both cases, current supply and voltage measurements are through the same scanner mainframe to the same

supply or measuring unit, and are controlled by an Apple-IIe computer (Fig.2-2).

As already noted, the resistivity of SI GaAs is very sensitive to temperature change, and 1° C will make a 10% difference [9]. Because of this, temperature control and measurement are very important in our system. We adjust the optimum PID setting [10] of an Oxford 3120 temperature controller, and place the platinum resistance sensor close to the heater to have the most responsive control. For accurate sample temperature measurement, we use a thermocouple as a second sensor. This is soldered to a small piece of copper sheet, mounted side by side with the sample on an alumina ceramic substrate (to provide the same thermal environment as the sample). The temperature is then read with an Omega model 670 thermometer. We also apply a layer of high electrical resistivity grease [11] between the sample and its ceramic substrate, as well as between ceramic substrate and aluminium heating block, to improve thermal conduction.

Several software routines were designed and added to our Hall measurement program. One is an ohmic test program, from which we can check on the I-V relation of contact pairs before or even during measurement. It is important to guarantee that there is no extra current injection from contacts in the chosen operational region. Usually the resistance of a SI GaAs sample is very high and can not be checked with a conventional curve tracer, so the electrometer and other high impedance units provide the ideal combination.

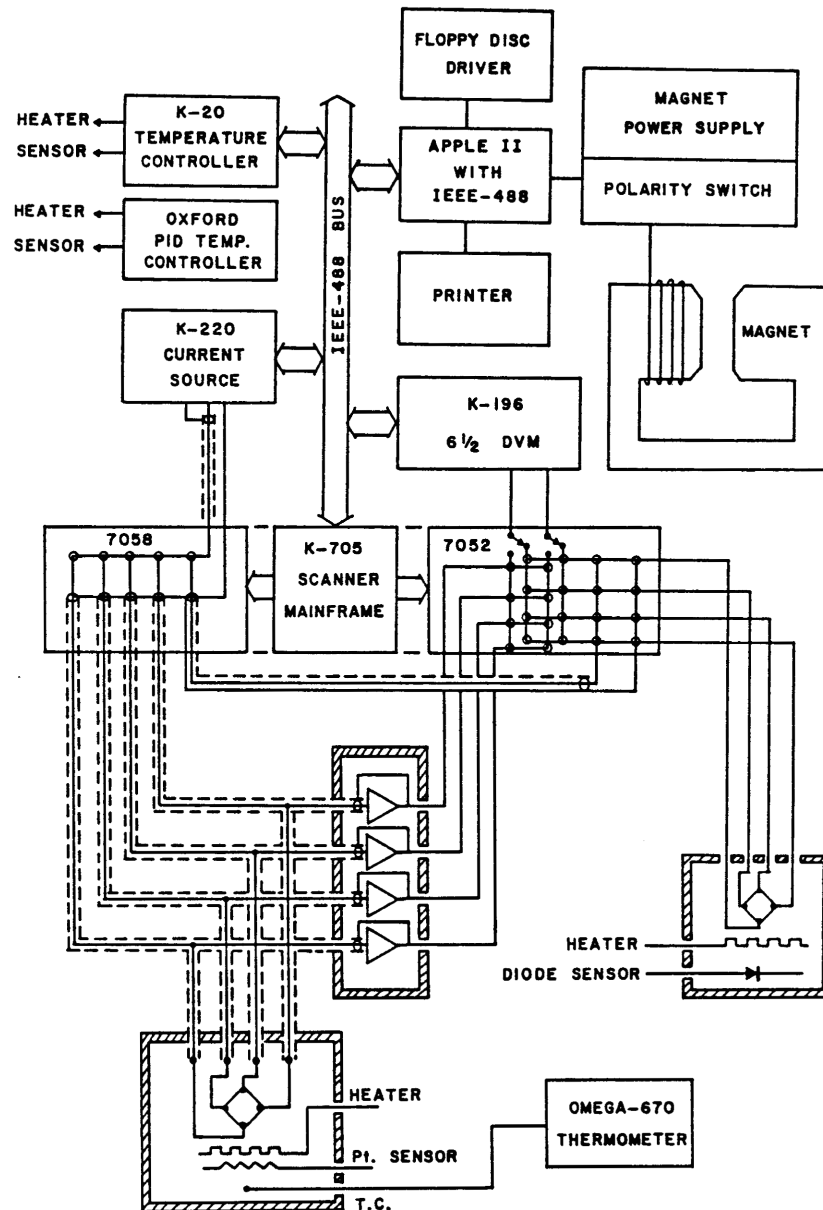


Figure 2-2 Schematic of the computer controlled Hall measurement system. Two separate ports are designed for high resistivity and low resistivity samples. Four electrometer buffers and triaxial cables are arranged for the high-impedance port. Also a low voltage switch and shielded coxial cables are arranged for the low-impedance port.

A second software routine developed for this work is a self adjusted current and holding time subprogram for temperature dependent Hall measurement. It is convenient to select and when necessary change to a suitable current as well as delay time by program commands during measurement, because the resistivity of SI GaAs will change five orders of magnitude from 290 K to 450 K during a typical measurement cycle.

Besides the instrumentation itself, sample preparation also plays an important role in getting correct data. Any leakage on the surface due to contamination can make a significant measurement error for a high resistivity sample. The detailed process for preparing the sample and applying ohmic contacts is described in appendix A.

## 2.3 Local Vibrational Mode (LVM) Absorption for Impurity Detection

If a Ga or As atom in a GaAs crystal has been replaced by a foreign atom, a different lattice vibration frequency will be created, because of the modified mass or bond condition. This vibration is localized in space and results in a band of optical absorption called "Local Vibration Mode (LVM)" absorption. This LVM absorption is phonon-creating not electronic, and can be detected in the mid to far-IR range. From the spectrum of the optical absorption coefficient $\alpha$, and a knowledge of the impurity LVM calibration factor f, one can calculate the impurity concentration N by using the equation

$$N = \int \alpha f \, d\bar{\upsilon}. \qquad (2\text{-}1)$$

This integration covers the narrow spectral range (usually less than 5 $cm^{-1}$) in which a specific impurity is LVM-active.

Unlike Si and Ge, GaAs is a partially ionic crystal which thus exhibits a very strong dispersion/absorption/reflection due to lattice vibration (called the Reststrahlen region) at around $h\nu \approx 35$ meV. This involves a transverse optical (TO) phonon with energy 33.25 meV and a longitudinal optical (LO) phonon with energy 36.13 meV, at room temperature. Figure 2-3 shows the optical absorption coefficient $\alpha$ through the Reststrahlen absorption region, and a few multiphonon lattice absorption peaks. The dashed curve and some data points show experiment values, while the solid curve is a theoretical model [12]. In addition to the strong single phonon absorption, there are some weaker overtone and combination multiphonon lattice absorption in the range 45-105 meV (Fig. 2-4) [12]. A possible assignment for the two-phonon absorption bands in conformity with selection rules of Birman [13] is listed in Table 2-1. The multiphonon lattice absorption spectrum is important to us in that any LVM absorption must be detected superimposed on this continuum.

LVM absorption locations and calibration factors f published by various workers are surveyed and listed in Table 2-2, for a number of substitutional impurities in GaAs. Since impurity associated LVM is a weak signal, sometime it is located near or overlapping the spectral location of those strong multiphonon lattice vibrations. It then becomes very hard to distinguish from the absorption background. The present study has

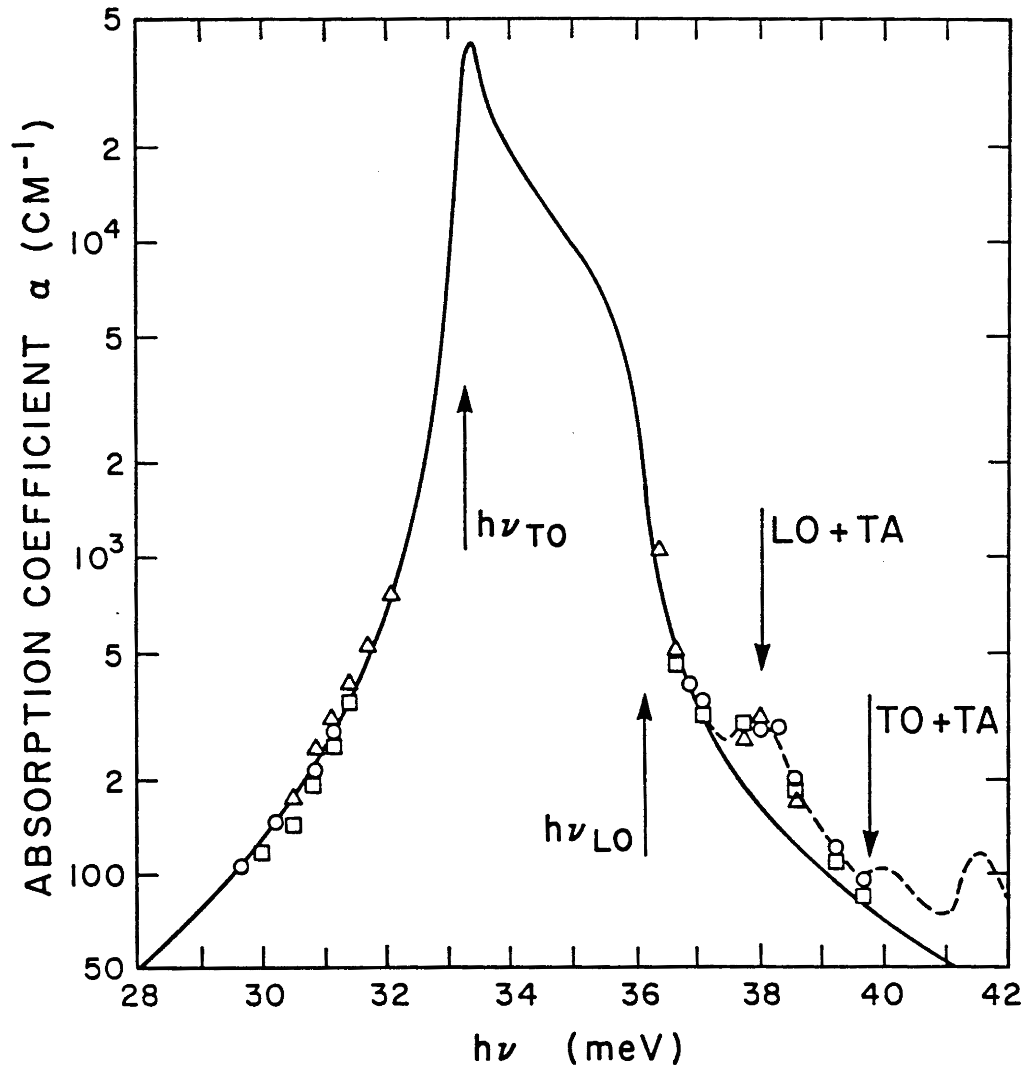


Figure 2-3 Optical absorption coefficient $\alpha$ through the Reststrahlen absorption region with a few multiphonon lattice absorption peaks indicated by arrows, after Blakemore [12].

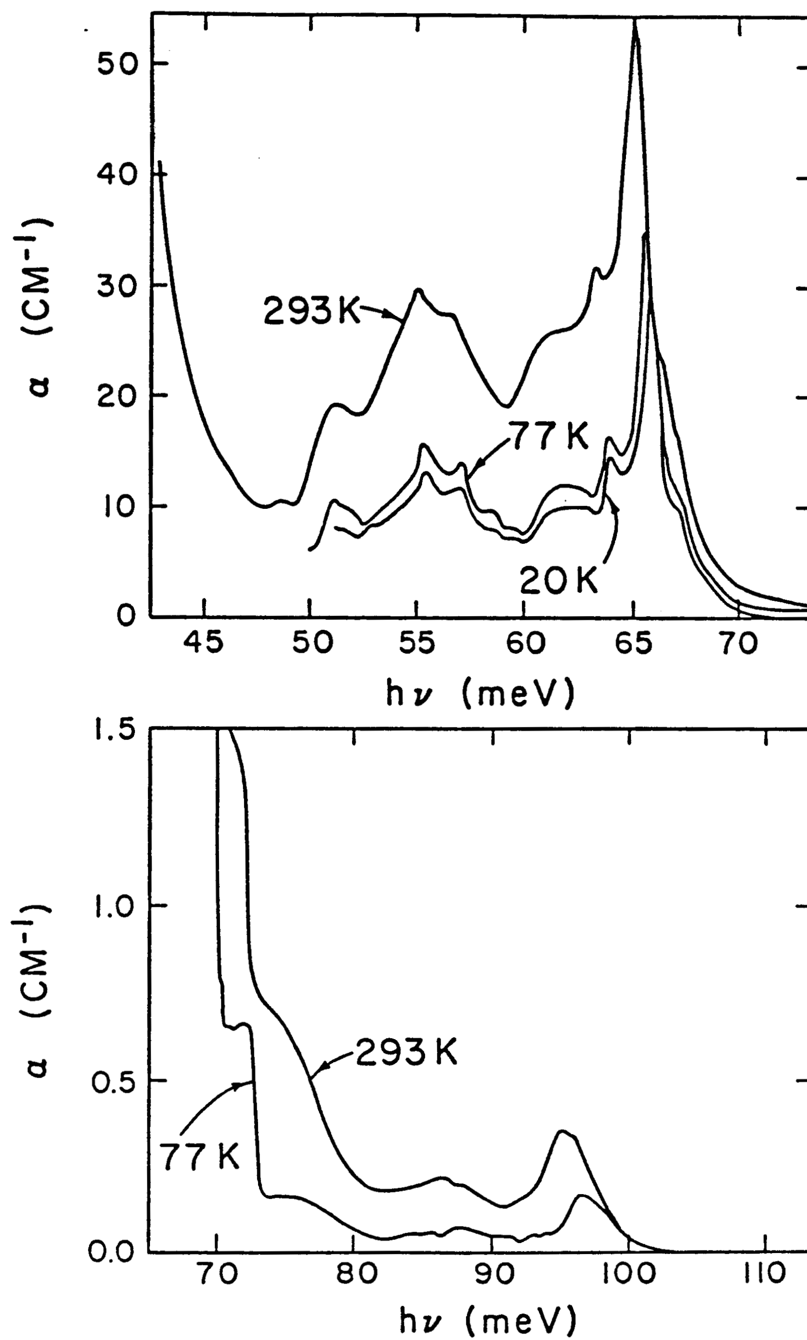


**Figure 2-4** GaAs optical absorption in the mid-IR, just above the Reststrahlen region of Fig. 2-3, after Blakemore [12].

Table 2-1 Prominent two-phonon absorption peaks in GaAs, and a set of possible assignments.

| $h\nu$ (meV) | Assignment | Brillouin zone location(s) |
|---|---|---|
| 38 | LO + TA | X, W |
| 40 | TO + TA | X |
| 41 | TO + TA | K |
| 44 | TO + TA | W |
| 49 | LO + LA | K |
| 51 | LO + LA | W |
| 55 | TO + LA | K |
| 57 | TO + LA | W |
| 62 | TO + LO | L, X |
| 64 | 2 TO | X |
| 66 | 2 TO | Γ, L |
| 71 | 2 LO | Γ |

Table 2-2 Spectral Locations of LVM Absorption Bands

| Impurity | LVM Band Location $\bar{\upsilon}$ ($cm^{-1}$) | $\varepsilon$ (meV) | Calibration Factor f ($cm^{-1}$) = $N/(\alpha \Delta\bar{\upsilon})$ | | Reference(s) |
|---|---|---|---|---|---|
| $Al_{Ga}$ | 362 | 44.9 | $3 \times 10^{16}$ | @ 77 K (?) | [17] |
| $^{28}Si_{Ga}$ | 384 | 47.6 | $6 \times 10^{16}$ | @ 77 K | [14] |
| $^{28}Si_{As}$ | 399 | 49.5 | $9 \times 10^{16}$ | @ 77 K | [14] |
| $^{11}B_{Ga}$ | 517 | 64.1 | $6 \times 10^{16}$ | @ 77 K (?) | [17] |
| $^{10}B_{Ga}$ | 540 | 66.9 | ------- | | [17] |
| $^{12}C_{As}$ | 580 | 71.9 | $1.3 \times 10^{16}$ | @ 300 K | [16] |
| | 582 | 72.1 | $8 \times 10^{15}$ | @ 77 K | [16] |
| $^{11}B_{As}$ | 601 | 74.5 | ------- | | [18] |
| $^{10}B_{As}$ | 628 | 77.9 | ------- | | [18] |

concentrated on the shallow donor $Si_{Ga}$ with LVM located at $\bar{\upsilon}$ = 384 $cm^{-1}$ and of FWHM bandwidth $(\Delta\bar{\upsilon}) \approx 0.4$ $cm^{-1}$[14,15], and the shallow acceptor $C_{As}$ with LVM located at $\bar{\upsilon}$ = 580 $cm^{-1}$ and of FWHM bandwidth $(\Delta\bar{\upsilon}) \approx 1.2$ $cm^{-1}$ [16]. The former (hν = 47.6 meV) is located between single-phonon and two-phonon strongly absorbing regions (background $\alpha \approx 10$ $cm^{-1}$). As a result, only a rather large $Si_{Ga}$ concentration can be detected. Things are rather more promising for $C_{As}$ acceptor detection, since this has its LVM band at hν = 72 meV, which sits on the decaying shoulder of two-phonon absorption toward weaker three-phonon absorption. The background $\alpha \approx 0.5$ $cm^{-1}$ is thus much weaker, and if sample and system are in good condition one can detect $\Delta\alpha_{min} \approx 10^{-2}$ $cm^{-1}$, corresponding to $C_{As}$ concentration as low as $10^{14}$ $cm^{-3}$. This detection limit is with f = 8 x $10^{15}$ $cm^{-1}$, and for measurement at T ≤ 77 K. Figure 2-5 shows carbon optical absorption spectra for a 4.25 mm thick slab of an "undoped" zone-melt grown SI GaAs crystal (VZM6) at 298 K and 66 K. These data were taken by 256 scan averaging with 0.5 $cm^{-1}$ resolution in a FTIR spectrometer.

The carbon data of Fig.2-5 were obtained in our laboratory using a Bio-Rad FTIR single beam spectrometer with maximum resolution $\delta\bar{\upsilon}$ = 0.1 $cm^{-1}$. This instrument can run over the range 450 - 4,000 $cm^{-1}$ using a MCT detector, and down to a lower wave number range by using a DTGS detector which was mandated for $Si_{Ga}$ or $Si_{As}$ detection. For reducing multiphonon lattice absorption, the FTIR was equipped with a CTI closed-cycle cooler, which has KBr windows transparent in the range from the visible to 250 $cm^{-1}$.

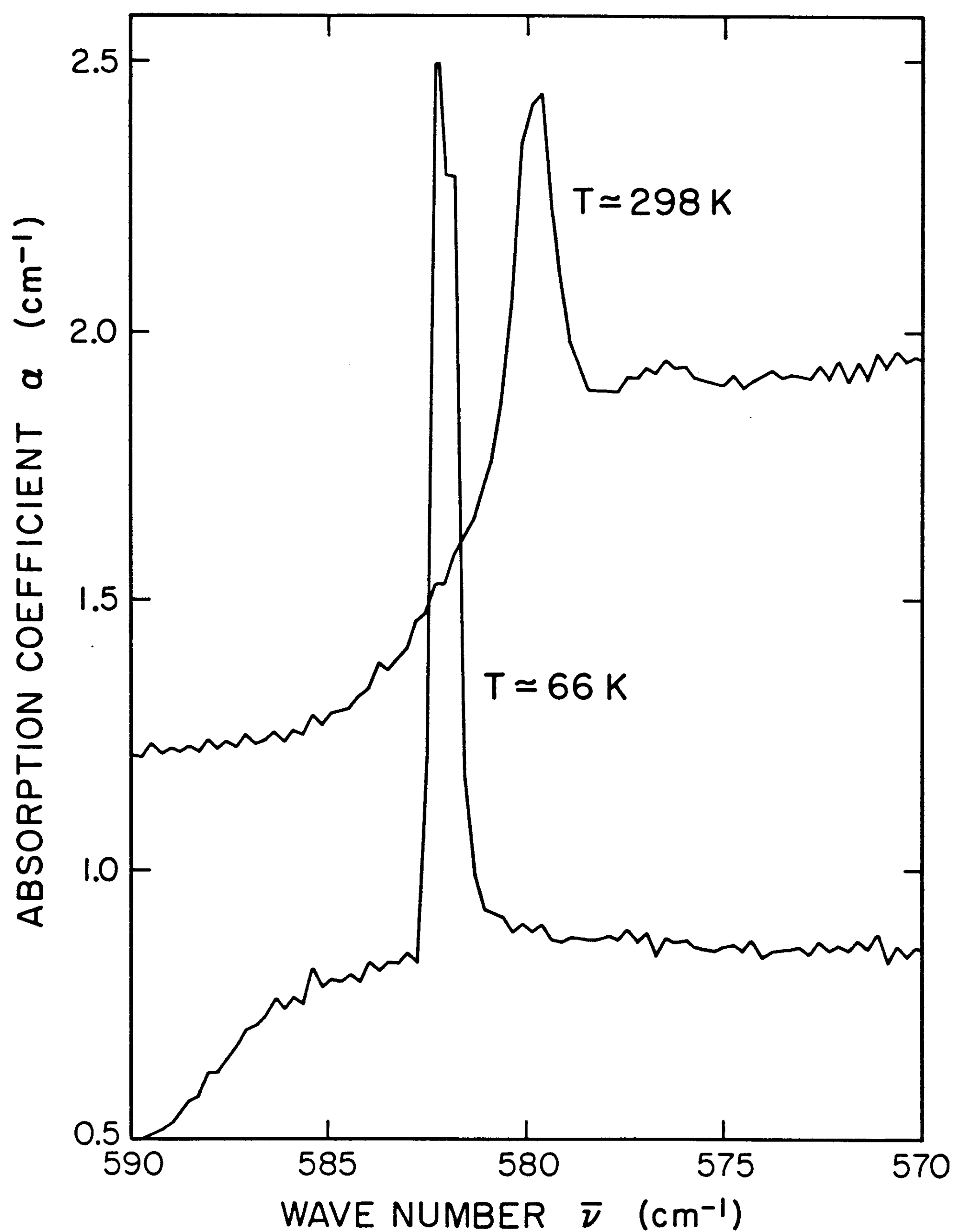


**Figure 2-5 FTIR $C_{As}$ optical absorption spectra for a 4.25 mm thick slab of crystal VZM6 at 298 K and 66 K.**

The sample for a LVM absorption measurement should be a double sided polished parallel slab. The absorption is weak, and one must use a slab several mm thick rather than a conventional (0.6 mm) wafer to get enough absorption. The first step in this measurement is to take the fraction of transmittance,

$$T = (I_t/I_0) = [1 - (I_r/I_0) - (I_a/I_0)] \qquad (2\text{-}2)$$

where $I_0$ is input energy, $I_r$ is the energy reflected, $I_a$ is the energy absorbed, and $I_t$ is the energy transmitted. Since the coherence length of non-laser light is much smaller than the sample thickness t, at least in this case it is not necessary to worry about multiple interference.

However, one will have multiple reflections due to the front and back polished surfaces. The fractional transmittance after addition of multiply reflected intensity components can be expressed as

$$T = (1 - R)^2 \exp(-\alpha t) [ 1 - R^2 \exp(-2\alpha t)]^{-1}$$
$$= (1 - R)^2 \exp(\alpha t) [ \exp(2\alpha t) - R^2]^{-1} \qquad (2\text{-}3)$$

This is is a quadratic equation for $\exp(\alpha t)$ of which the positive real root is

$$\exp(\alpha t) = [(1-R)^2/2T](1 + [1 + 4R^2T^2/(1 - R)^4]^{1/2}) \qquad (2\text{-}4)$$

and the absorption coefficient is

$$\alpha = (1/t) \ln([(1 - R)^2/2T] (1 + [1 + 4R^2T^2(1 - R)^{-4}]^{1/2})) \qquad (2\text{-}5)$$

For normal incidence, the reflectivity R can be expressed in terms of the real refractive index n and extinction coefficient k by

$$R = [(n - 1)^2 + k^2]/[(n + 1)^2 + k^2] \qquad (2\text{-}6)$$

Unless the absorption is very strong, the extinction coefficient $k \ll 1$. One can then omit the $k^2$ term in equation (2-6), which thus becomes

$$R = (n - 1)^2/(n + 1)^2. \quad (2\text{-}7)$$

At room temperature, and at low temperature ($T < 30K$), the refractive index n for GaAs [19] can be approximated in term of photon energy (in eV) by

$$n_{RT} = \{ 7.10 + 3.78[1 - 0.18(h\nu)^2]^{-1} - 1.97[(30.08h\nu)^2 - 1]^{-1}\}^{1/2} \quad (2\text{-}8)$$

and

$$n_{LT} = \{ 7.13 + 3.45[1 - 0.175(h\nu)^2]^{-1} - 1.88[(29.6h\nu)^2 - 1]^{-1}\}^{1/2}. \quad (2\text{-}9)$$

These can alternatively be expressed in terms of wave number ($\bar{\upsilon}$, in $cm^{-1}$) by

$$n_{RT} = \{ 7.10 + 3.78[1 - (\bar{\upsilon}/19000)^2]^{-1} - 1.97[(\bar{\upsilon}/268)^2 - 1]^{-1}\}^{1/2} \quad (2\text{-}10)$$

and

$$n_{LT} = \{ 7.13 + 3.45[1 - (\bar{\upsilon}/19280)^2]^{-1} - 1.88[(\bar{\upsilon}/272)^2 - 1]^{-1}\}^{1/2}. \quad (2\text{-}11)$$

In the transmittance experiments to be described, a computer program included these equations. It was thereby possible to convert a transmission spectrum to an absorption spectrum. By integration of the area of a LVM absorption band, we could obtain an impurity concentration from Equation (2-1), using a suitable calibration factor f.

## 2.4 Near and Mid-Infrared Measurements for EL2 Absorption, Impurity Photoionization, and Free Carrier Absorption

In addition to LVM absorption, the spectrum in the near and mid-IR ranges still has several interesting properties connected with SI GaAs

characterization. An important one is EL2 absorption in "undoped" GaAs. This has both photo-ionization and photo-neutralization aspects, ie., two processes. We can express the photo-ionization process as

$$EL2^{0} + h\nu \rightarrow EL2^{+} + e^{-} \qquad (2\text{-}12)$$

with a cross-section $\sigma^{o}_{n}(h\nu)$ of which the strength and spectral form was studied by Martin [20]. Also, we can express the photo-neutralization process as

$$EL2^{+} + h\nu \rightarrow EL2^{0} + h^{+} \qquad (2\text{-}13)$$

This has a cross-section $\sigma^{o}_{p}(h\nu)$ of which the strength and spectral form has been studied by Silverberg *et al*[21].

One can express the absorption due to all the EL2 present as

$$\alpha(h\nu) = N_{EL2^{0}}\sigma^{o}_{n}(h\nu) + N_{EL2^{+}}\sigma^{o}_{p}(h\nu). \qquad (2\text{-}14)$$

Here $N_{EL2^{0}}$ (or $N^{0}$ used in Fig.2-6) is the concentration of neutral EL2, and $N_{EL2^{+}}$ (or $N^{+}$ used in Fig.2-6) is the concentration of ionized EL2. Figure 2-6 is a room temperature EL2 absorption spectrum from sample III of a vertical zone melt crystal VZM6. The total EL2 absorption can be decomposed into the sum of two dashed curves in accordance with Equation (2-14). With the scalings of $\sigma^{o}_{n}(h\nu)$ and $\sigma^{o}_{p}(h\nu)$ published in references [20] and [21], one can fit the two dashed curves by $N_{EL2^{0}} \approx 6.4 \times 10^{15}$ cm$^{-3}$ and $N_{EL2^{+}} \approx 3.5 \times 10^{15}$ cm$^{-3}$. This means that the EL2 ionized fraction $P_i = N_{EL2^{+}} / (N_{EL2^{0}} + N_{EL2^{+}}) \approx 0.35$. That is consistent with an ionized fraction $P_i = (1 + n_0/n_D)^{-1} \approx 0.34$ for an adjacent sample, as deduced from electrical data reported in a subsequent chapter.

Depending on the energy level of an impurity or defect in the

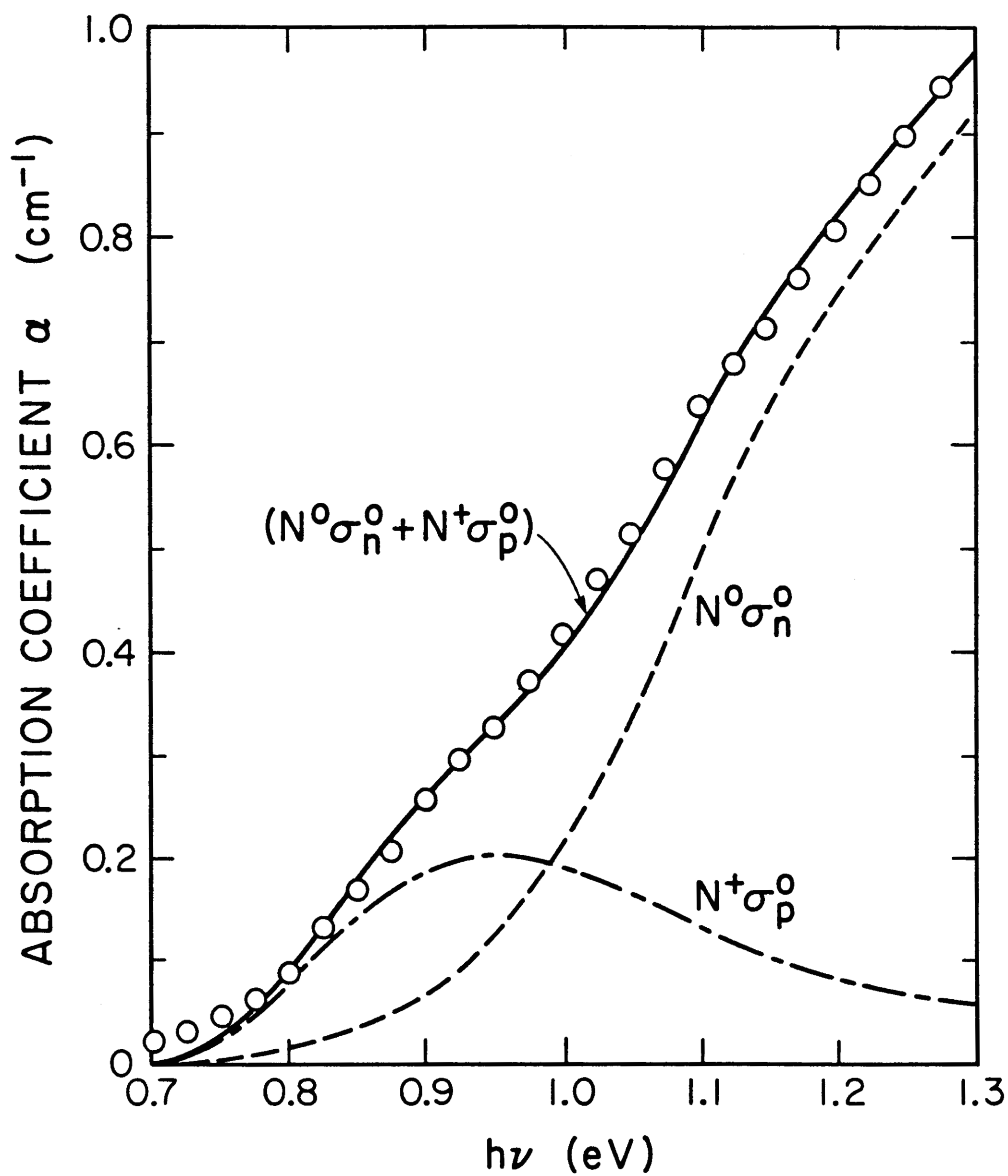


Figure 2-6 Optical absorption data of VZM6-III shown at 25 meV intervals, compared with the solid curve which is the sum of the two dashed curves ($N^o \sigma^o_n$) and ($N^+ \sigma^o_p$).

forbidden gap, the electronic transitions of impurities can create optical absorption in various infrared spectral ranges. For a shallow impurity, the ionization energy is only a few meV. One must detect such absorption in the far-IR range, and the sample must be cooled to liquid helium temperatures. But for an impurity whose energy is deep enough to hold a carrier at room temperature, photoionization will result in absorption in the near or mid-IR range.

Our study has concentrated on two deep acceptor impurities, Cr and Fe. Due to multi-valent and amphoteric properties of these impurities, the absorption process is more complicated than with EL2. The electronic configurations of $Cr_{Ga}$ in GaAs can be classified as $Cr^{1+}$ ($3d^5$, double acceptor), $Cr^{2+}$ ($3d^4$, one electron trapped or ionized acceptor), $Cr^{3+}$ ($3d^3$, lattice neutral), and $Cr^{4+}$ ($3d^2$, hole trap or ionized donor). In short, no less than four different charge states [22]. Since the ground state of $Cr^{1+}$ lies above the conduction band edge [23], $Cr^{3+} \Leftrightarrow Cr^{2+}$ transitions actually dominate the absorption in the range from 0.7 eV to intrinsic band gap.

Similar to Cr the configurations for iron as $Fe_{Ga}$, have charge states, $Fe^{1+}$ ($3d^7$, double acceptor), $Fe^{2+}$ ($3d^6$, one electron trapped or ionized acceptor), and $Fe^{3+}$ ($3d^5$, lattice neutral) [24]. In this case, $Fe^{1+} \Leftrightarrow Fe^{2+}$ and $Fe^{2+} \Leftrightarrow Fe^{3+}$ are the major transitions.

Free carrier absorption is very weak for SI GaAs, because the electron or hole densities are both less than $10^8$ $cm^{-3}$ for a sample with room temperature resistivity higher than $10^7$ $\Omega$-cm. This is especially so in the near-IR range, because free carrier absorption is proportional to $\lambda^3$ for GaAs

[25]. For a sample which fails to be semi-insulating, one can expect some absorption in the mid-IR, but still negligible in the near-IR region. We have measured near-IR free carrier absorption only for GaAs samples strongly doped with shallow donors or acceptors.

Some of our near to mid-IR data (2.5 - 25 μm) were obtained using a commercial Fourier transform infrared (FTIR) instrument. Actually, two such instruments were used; initially a Perkin-Elmer system, subsequently a Bio-Rad FTIR. A Perkin-Elmer grating spectrophotometer (Lambda-9) was also used for data from GaAs bandgap out to 2.5 μm. Two other near-IR grating spectrophotometers were assembled from components in our laboratory; these having the advantage - which the Lambda-9 does not provide - that the sample can be placed after the monochromator, just before the detector. Use of Ge and PbS detectors allowed us to cover the range 0.8 - 3.5 μm, with our own instruments.

A sample for such measurements should also be a parallel-faced slab, polished on both faces. Unless the absorption is very small, one can expect to measure absorption from the transmittance of a conventional thickness double side polished wafer. The equations used for the transmittance and absorption calculations are the same as those described in Section 2.3.

## REFERENCES: CH.2

1. D. C. Look, *Electrical Characterization of GaAs Materials and Devices* (John Wiley & Sons, New York 1989) p.38
2. Keithley Application Note #.100 , "Low Current Measurements"
3. Keithley Application Note #.710, "Guarding vs. Isolation in DMMs"
4. P. M. Hemenger, Rev. Sci. Instrum., **44**, 698, (1973)
5. ASTM, F76, Standard Method for Measuring Hall Mobility and Coefficient in Extrinsic Semiconductor single crystals.
6. Keithley Application Note #.510, "Hall and van der Pauw measurements of Semiconductors"
7. *Low Level Measurements for Effective Low Current, Low Voltage, and High Impedance Measurements* published by Keithley Instruments, Inc. revised third edition, June 1984, Cleveland, Ohio, U.S.A.
8. MMR, Microminiature Refrigerators, is a brand name of MMR Technologies, Inc.
9. L. Sargent, R-S. Tang, and J. S. Blakemore, in *Semi-Insulating III-V Materials: Malmo 1988*, edited by G. Grossmann and L. Ledebo, (Adam Hilger, Bristol, 1988), p. 183
10. PID represents Proportional, Integral, and Derivative.
11. Thermal joint compound, brand name Thermalcote™. This has a thermal conductivity = 0.43 (Btu- Ft)/(hr-$Ft^2$-$^oF$), combined with an electrical resistivity = $4 \times 10^{14}$ Ω-cm, and dielectric strength = 300 V/mil. An appropriate solvent is trichloroethane.

12. J. S. Blakemore, J. Appl. Phys. **53**, R124 (1982)

13. J. L. Birman, Phys. Rev. **127**, 1093 (1962); **131**, 1489 (1963)

14. J. Woodhead, R. C. Newman, A. K. Tipping, J. B. Clegg, J. A. Roberts, and I. Gale, J. Phys. D: Appl. Phys. **18**, 1575 (1985)

15. W. M. Theis and W. G. Spitzer, J. Appl. Phys. **56**, 890 (1984)

16. L. Sargent and J. S. Blakemore, Appl. Phys. Lett. **54**, 1013 (1989)

17. M. R. Brozel, J. B. Clegg, and R. C. Newman, J. Phys. D**11**, 1331 (1978)

18. G. A. Gledhill, R. C. Newman, and J. Woodhead, J. Phys. C**17**, L301 (1984)

19. J. S. Blakemore, J. Appl. Phys. **62**, 4528 (1987)

20. G. M. Martin, Appl. Phys. Lett. **39**, 747 (1981)

21. P. Silverberg, P. Omling, and L. Samuelson, Appl. Phys. Lett. **52**, 1689 (1988)

22. J. S. Blakemore, S. G. Johnson and S. Rahimi, in *Semi-Insulating III-V Materials: Evian1982*, edited by S. Makram-Ebeid and B. Tuck, (Shiva, Nantwich, UK, 1982), p. 172

23. A. M. Hennel, W. Szuskiewicz, M. Balkanski, G. Martinez, and B. Clerjaud, Phys. Rev. B **23**, 3933 (1981)

24. U. Kaufmann and J. Schneider, Festkorperprobleme xx (1980) pp. 87-113

25. W. G. Spitzer and J. M. Whelan, Phys. Rev. **114**, 59 (1959)

# CHAPTER 3

# COMPENSATION AND AMBIPOLAR CONDUCTION IN SI GaAs

## 3.1 The "Three-Level" Model for Undoped SI GaAs

Since the word "semi-insulator" or "semi-insulating GaAs" was introduced by Allen [1] in 1960, different models of compensation have been studied to understand the mechanism of the high-resistivity property of SI GaAs. He initially proposed a model with only two levels (a shallow donor-level and a deep acceptor-level lying below the intrinsic Fermi-level) to explain the variance from N-type to high-resistivity to P-type for his experimental data. However, this "two-level" model had difficulties in explaining the existence of high-resistivity N-type GaAs samples. Therefore, an electrically inactive "reservoir" level [1] was added by Allen to generalize his model, which one might call an early stage of the "three-level" model.

The first true "three-level" model for high-resistivity GaAs was probably the one proposed by Blanc and Weisberg [2], and successfully used by Woods and Ainslie [3] to explain so-called "oxygen doped" SI GaAs. This "three-level" model described GaAs containing shallow donors with density

$N_d$, deep donors with density $N_{DD}$, and acceptors with density of $N_a$. When the conditions $N_a > N_d$ and $N_{DD} > (N_a - N_d)$ are satisfied, the sample is of high resistivity.

For "undoped" SI GaAs, a "three-level" model is the most common and acceptable model to explain the compensation and the behavior of resistivity fluctuation during crystal growth. Kirkpatrick *et al.* [4] evaluated chemical impurities in various LEC grown GaAs crystals, and found out that carbon, silicon, and boron were principal impurities in "undoped" crystals. They also evaluated the electrical and optical properties of SI crystals and concluded that EL2 was the predominant deep level. Remember that boron as $B_{Ga}$ is electrically inactive in GaAs, and that EL2 is a deep donor defect. Remember also that carbon occurs predominantly as the acceptor $C_{As}$, whereas silicon in melt-grown GaAs favors the gallium site, for the $Si_{Ga}$ shallow donor. When $N_a > N_d$ and $N_{EL2} > (N_a - N_d)$ a sample is thus semi-insulating. In this model, the charge balance equation allows us to express

$$N_{EL2^+} = N_{EL2} - N_{EL2^0} = (N_a - N_d) + (n_o - p_o). \qquad (3\text{-}1)$$

The concentration of ionized EL2 is almost equal to the net shallow acceptor concentration when the free carrier densities are negligible small. In general, $N_d$ represents the sum of $Si_{Ga}$ and of all other shallow donors, and $N_a$ is the sum of $C_{As}$ and of other residual acceptors. Only when EL2 is partly ionized, will the Fermi level lock near the EL2 level. Because EL2 is close to midgap of GaAs, SI behavior looks near-intrinsic.

Beside the "three-level" model, a "four-level" model has been proposed by Lindquist [5] and by Martin *et al.* [6]. This model, adapted to

describe Cr doped SI GaAs, consists of four localized levels: a shallow and deep donor, and a shallow and deep acceptor. When a sample is semi-insulating, the Fermi level lies between these two deep levels.

Since there is no way to get 100% pure raw material, any undoped or unintentionally doped GaAs still contains certain amounts of residual impurities, in addition to native defects. The thermodynamics of crystal growth tell us that various defects will be created during a high temperature growing process. It is possible that more than three energy levels can be found in a real crystal. One should not surprised that a "five-level" or even more fancy models have been contemplated. However, the EL2 concentration is always in the order of $10^{16}$ $cm^{-3}$, which is higher by a factor of 10 or more than any other defects in "undoped" SI GaAs. Thus a "three-level" model can describe an "undoped" or "unintentionally doped" SI GaAs crystal very well.. Only samples which fail to be semi-insulating, in which the Fermi level is controlled by other levels which are shallow than EL2, need a complex compensation model.

## 3.2 Ambipolar Conduction Complications for Near-Intrinsic GaAs

There are two testing methods which are commonly used to determine the conduction type of semiconductors. One is Hall effect measurement, and the other is hot probe thermopower measurement. From a Hall effect measurement, one infers that the sample is P-type or N-type depending on

whether the Hall coefficient $R_H$ is positive or negative. Similarly for a thermo-electric power measurement, one also infers the conduction type from the sign of the Seebeck coefficient $\Theta$. The results of these two methods are not always consistent, especially in the case of Cr doped high-resistivity GaAs [7,8]. They might show N-type in a Hall measurement, but show P-type in a thermo-electric power measurement. This contradiction caused some initial interest in mixed conduction research [8,9]. Generally, the numbers of electrons and holes are quite different in an N-type or P-type semiconducting sample, and only one type of carrier dominates the conduction. The magnitude of the Seebeck or Hall coefficient can then be approximated well by using only one type of carrier. However, SI GaAs or any other near intrinsic semiconductor has numbers of electrons and holes close enough so that conduction is contributed by both types of carrier. In this situation, electrons and holes compete to determine the magnitude and even the sign of Hall or Seebeck coefficient. We can express the total conductivity as

$$\sigma = \sigma_p + \sigma_n = e(p_o \mu_p + n_o \mu_n). \qquad (3\text{-}2)$$

The ambipolar Hall coefficient [10] can then be written as

$$R_H = e\,(r_p\, p_o\, \mu_p^2 - r_n\, n_o\, \mu_n^2)/\sigma^2, \qquad (3\text{-}3)$$

where $r_p$ and $r_n$ are Hall correction factors for holes and electrons. The ambipolar Seeback coefficient [11] can be written as

$$\Theta = k\,\{p_o\, \mu_p[(5/2 - s') + \ln(N_V/p_o)] - n_o\, \mu_n[(5/2 - s) + \ln(N_c/n_o)]\}/\sigma, \quad (3\text{-}4)$$

where $s$ and $s'$ are the energy relaxation parameters for electrons and holes, numbers which depend on the combination of lattice and "impurity"

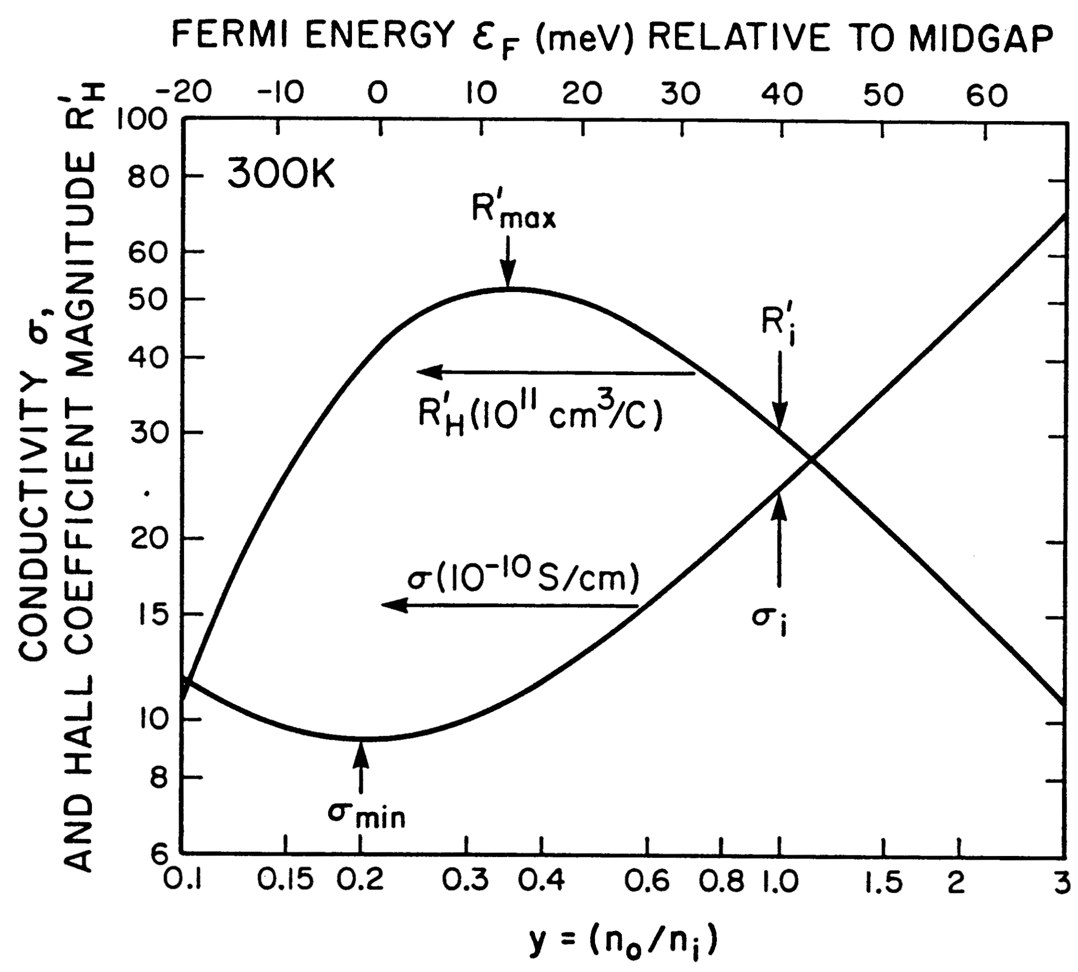


**Figure 3-1** Curves based on Eqs. (3-2) and (3-3) for the 300 K ambipolar conductivity $\sigma$ and the Hall coefficient magnitude $R'_H = -R_H$, vs the dimensionless $y = (n_o/n_i)$. Assumed values are $n_i = 2.25 \times 10^6$ $cm^{-3}$, $\mu_n = 25\,\mu_p = 6500\ cm^2/V\text{-}s$, and $r_n = 0.8\,r_p = 1.18$.

scattering.

If one is only concerned with the major terms which cause a sign change of $R_H$ and $\Theta$, one can reasonably neglect $r_p$ and $r_n$ in Eq.(3-3), since they both are not far from unity [12]. One also can pull out two block parenthesis terms in Eq.(3-4), since $s \approx s' \approx 1/2$ [13] and $\ln(N_V/p_o) \approx \ln(N_C/n_o) \approx \varepsilon_G/(2kT)$ for SI GaAs. In this like to mak treatment, Eqs. (3-3) and (3-4) will look like

$$R_H = e\,(p_o\,\mu_p^2 - n_o\,\mu_n^2)/\sigma^2 \qquad (3\text{-}5)$$

and

$$\Theta = k\,[2 + \varepsilon_G/(2kT)](p_o\,\mu_p - n_o\,\mu_n)/\sigma. \qquad (3\text{-}6)$$

We can see more clearly now that the terms which control sign changes are $(p_o\,\mu_p^2 - n_o\,\mu_n^2)$ in $R_H$ and $(p_o\,\mu_p - n_o\,\mu_n)$ in $\Theta$. Since $\mu_n$ is always higher than $\mu_p$ in GaAs, both $R_H$ and $\Theta$ are negative at the truly intrinsic condition: $p_o = n_o$. If we define $(\mu_n/\mu_p) \equiv b$, then $\Theta$ changes sign when $(p_o/n_o) = b$, and $R_H$ changes sign when $(p_o/n_o) = b^2$. Because $b > 1$, $\Theta$ will change sign sooner than $R_H$, as the $(p_o/n_o)$ ratio is increased from N-type towards P-type. Therefore, $R_H$ and $\Theta$ can be of different sign in the mixed conduction region, where $b < (p_o/n_o) < b^2$.

Resistivity $\rho$ (or conductivity $\sigma$ ) and Hall coefficient $R_H$ are the "raw" quantities in transport data. In a van der Pauw [14] type of Hall effect measurement, they can be directly expressed with measured resistance and Hall voltage by

$$\rho = \pi\, d\, f_{ab}\,(\ln 2)^{-1}\,(R_a + R_b)/2 \qquad (3\text{-}7)$$

and

$$R_H = 10^8 (d\, V_H)/(B\, I) \quad cm^3/C, \tag{3-8}$$

where d is the sample thickness (in cm), $f_{ab}$ is a geometric factor obtained from the two resistance ratio $R_a/R_b$, B is the magnetic field strength (in Gauss), and I is the current ( in Amperes) through the sample.

With a unipolar assumption, for example an N-type case, one can deduce the electron mobility from

$$\mu_n = \mu_{Hn}/r_n = |\sigma R_H/r_n| = |R_H/(\rho\, r_n)|, \tag{3-9}$$

and the electron concentration from

$$n_0 = r_n (e\, |R_H|)^{-1}. \tag{3-10}$$

This is a good approximation for any weakly N-type ("failed SI") GaAs, since the minority carrier density (hole density in this case) is negligibly small. However, when a sample is close to intrinsic or mixed conduction Eqs. (3-9) and (3-10) will no longer be suitable, as discussed above.

In order to simulate the ambipolar correction, we introduce two dimensionless quantities $\beta = (r_p/r_n)$ and $y = (n_0/n_i)$. For our convenience, we define the ambipolar Hall coefficient $R'_H = -R_H$, $R'_H$ being a positive quantity. Eq.(3-3) can thereby be expressed as

$$R'_H = r_n(e\, n_0)^{-1} [\, y^2 (b^2y^2 - \beta)/(1 + by^2)^2]. \tag{3-11}$$

If we define the square bracket term as

$$F(y) = [\, y^2 (b^2y^2 - \beta)/(1 + by^2)^2], \tag{3-12}$$

then Eq.(3-11) becomes

$$R'_H = r_n(e\, n_0)^{-1} F(y). \tag{3-13}$$

Therefore, the electron concentration can be described as

$$n_0 = r_n(e\, R'_H)^{-1} F(y). \tag{3-14}$$

Comparing Eq.(3-14) with Eq.(3-10), we can call F(y) an ambipolar correction multiplier, since it directly modifies the "raw quantity" $r_n(e\,R'_H)^{-1}$ into a "true" concentration $n_0$.

By the same token, we can treat the "raw" Hall mobility as

$$\mu_{Hn} = \sigma R'_H = r_n \mu_n[(b^2y^2 - \beta)\, b^{-1}\, (1 + by^2)^{-1}]. \qquad (3\text{-}15)$$

Again, we define the square bracket term in Eq.(3-15) as

$$G(y) = [(b^2y^2 - \beta)\, b^{-1}\, (1 + by^2)^{-1}]. \qquad (3\text{-}16)$$

Then Eq.(3-15) can be described as

$$\mu_{Hn} = \sigma R'_H = r_n \mu_n G(y). \qquad (3\text{-}17)$$

The true electron mobility can therefore be expressed by

$$\mu_n = \mu_{Hn}[r_n G(y)]^{-1} = \sigma R'_H (r_n)^{-1} [G(y)]^{-1}. \qquad (3\text{-}18)$$

The factor $[G(y)]^{-1}$ in Eq.(3-18) is an ambipolar multiplier for mobility correction, fulfilling a function analogous to F(y) in Eq.(3-14).

The equation F(y) is not only for calculation, but also provides a useful arbiter as to whether or not an ambipolar correction is necessary. Because of the mobility ratio in GaAs, F(y) is only 1% off from unity when $y \geq 3$, and asymptotically approaches unity when y is large enough. And so in what follows, execution of an ambipolar correction will be considered to be significant (to the 1% level) when $y \leq 3$. That turns out to be more or less equivalent to $z \leq 3$, where z is another dimensionless variable introduced shortly.

Figure 3-2 shows three curves, for variation of F(y) over the abscissa range $0.6 \leq y \leq 3$, with mobility ratio choices of $b = 15, 20,$ or $25$ and an assumed $\beta = (r_p/r_n) \approx 1.25$. Because values of b from 15 to 25 cover the

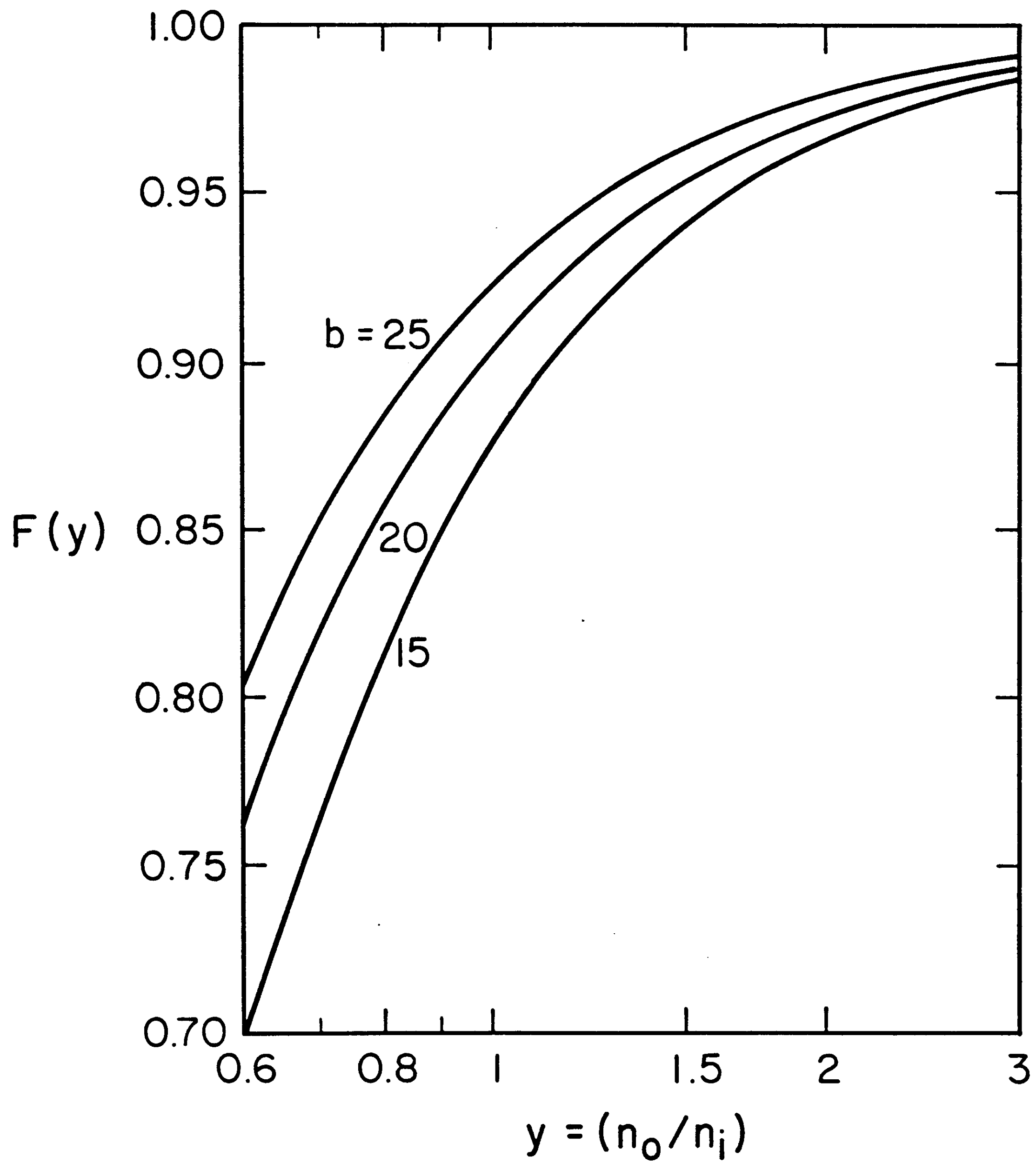


**Figure 3-2** Curves modeled on Eq.(3-12) for the factor F(y), showing the effect of near-intrinsic conditions on $R'_H$. For each curve it is assumed that $\beta = (r_p / r_n) \approx 1.25$, while the three curves are distinguished by $b = (\mu_n / \mu_p) = 15, 20$, or 25.

typical range of mobility ratio for SI GaAs, we know that $F(y)$ is not very sensitive to the value of b one chooses to use. $F(y)$ is also very insensitive to the number used for $\beta$.

We have the corrections Eqs.(3-14) and (3-18) if $y$ is known. Then we can get the ambipolar corrected electron concentration and mobility from raw Hall data. Now the question is: how to get $y(T)$ from the raw quantity $R'_H(T)$ or $\sigma(T)$. Since $\varepsilon_i(T)$ and $n_i(T)$ are both reasonably well quantified for GaAs (this will be shown in the next section), a knowledge of the intrinsic Hall coefficient $R'_i$ at any temperature is possible, and

$$R'_i = R'_H(n_0 = n_i) = r_n (e\, n_i)^{-1} [(b^2 - \beta)/(1 + b)^2]. \qquad (3\text{-}19)$$

If one compares the measured Hall coefficient $R'_H$ with the calculated intrinsic Hall coefficient $R'_i$ for that same temperature, one may obtain some information about y from it. Again, let us define a dimensionless quantity $z$ as

$$z = R'_i/R'_H = [y\, F(1)/F(y)] \qquad (3\text{-}20)$$

or

$$z(y) = [(b^2 - \beta)/(1 + b)^2]\, [\, y\, (b^2 y^2 - \beta)/(1 + b y^2)^2]^{-1}. \quad (3\text{-}21)$$

In Eq. (3-20), $z$ is calculated from measured Hall coefficient. And so if we insert reasonable numbers for $\beta$ and b, then Eq.(3-21) can be solved for y. Let us manipulate Eq.(3-21) into a polynomial equation in orders of $y$ as

$$y^4 b^2 + y^3 b^2 z(1+b)^2/(\beta - b^2) + y^2\, 2b + y z \beta (1+b)^2/(b^2 - \beta) + 1 = 0 \qquad (3\text{-}22)$$

or

$$y^4 + [z b^2 (1+b)^2/(\beta - b^2)] y^3 + [2/b] y^2 + [z b^{-2} \beta (1+b)^2/(b^2 - \beta)] y + b^{-2} = 0. \quad (3\text{-}23)$$

This is a real coefficient polynomial because $z$, b and $\beta$ are real numbers.

Since we know that the solution y should be a real root, we can solve it with computer by Newton's method, or any other available numerical method. Once y has been solved, it can be inserted into Eq.(3-12) and Eq.(3-16) to calculate F(y) and G(y). One can thereby obtain the corrected electron concentration and electron mobility from Eqs.(3-14) and (3-18).

However, b and $\beta$ are still unknown quantities. It is not possible to extract these numbers based on Hall data alone. It is thus necessary to solve this puzzle by some empirical approach.

To begin with, we should discuss $\beta = (r_p/r_n)$. The Hall factors $r_n$ and $r_p$ cover up a lot of complexity [15], in terms of scattering integrals. They are also functions of temperature, magnetic field, and doping density. However, the values of $r_n$ and $r_p$ do not depart *far* from unity. According to a result of Rode [16] reproduced in Fig.3-3, we should like to assume $r_n \approx$ 1.18 at 300 K and $r_n \approx 1.10$ at 400 K for a "weak-field and weak-doping" conditions. For calculation purpose, we linearize the curve as

$$r_n \approx 1.18 - 0.0008(T - 300), \qquad (3\text{-}24)$$

in the temperature range 250 to 450 K. Similarly, we wish to follow curve "r" of Lee and Look [17] as in Fig.3-4, and linearize the curve of $r_p$ as

$$r_p \approx 1.45 + 0.0015(T - 300), \qquad (3\text{-}25)$$

for the same temperature range as Eq.(3-24). Using the numbers from Eqs (3-24) and (3-25), $\beta$ can be evaluated as a function of temperature. It must be re-emphasized that the ambipolar correction analysis is *not* at all sensitive to the accuracy of one's choice for $\beta = (r_p/r_n)$. However, any error in one's simulation of $r_n$ itself is passed on directly as an error in the

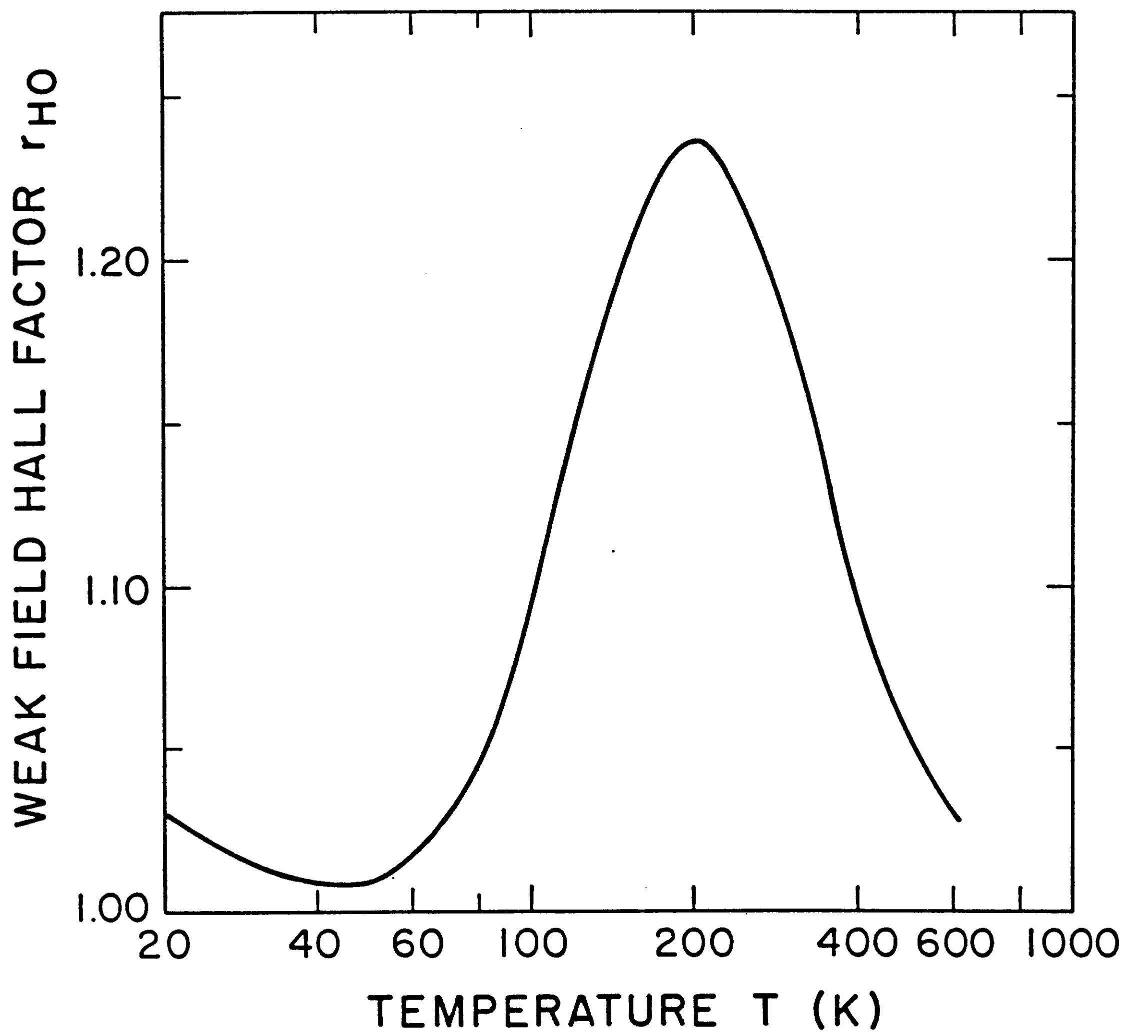


Figure 3-3 Theoretical weak-field Hall factor $r_H$ as a function of temperature, as calculated by Rode [16] for modestly doped N-type GaAs.

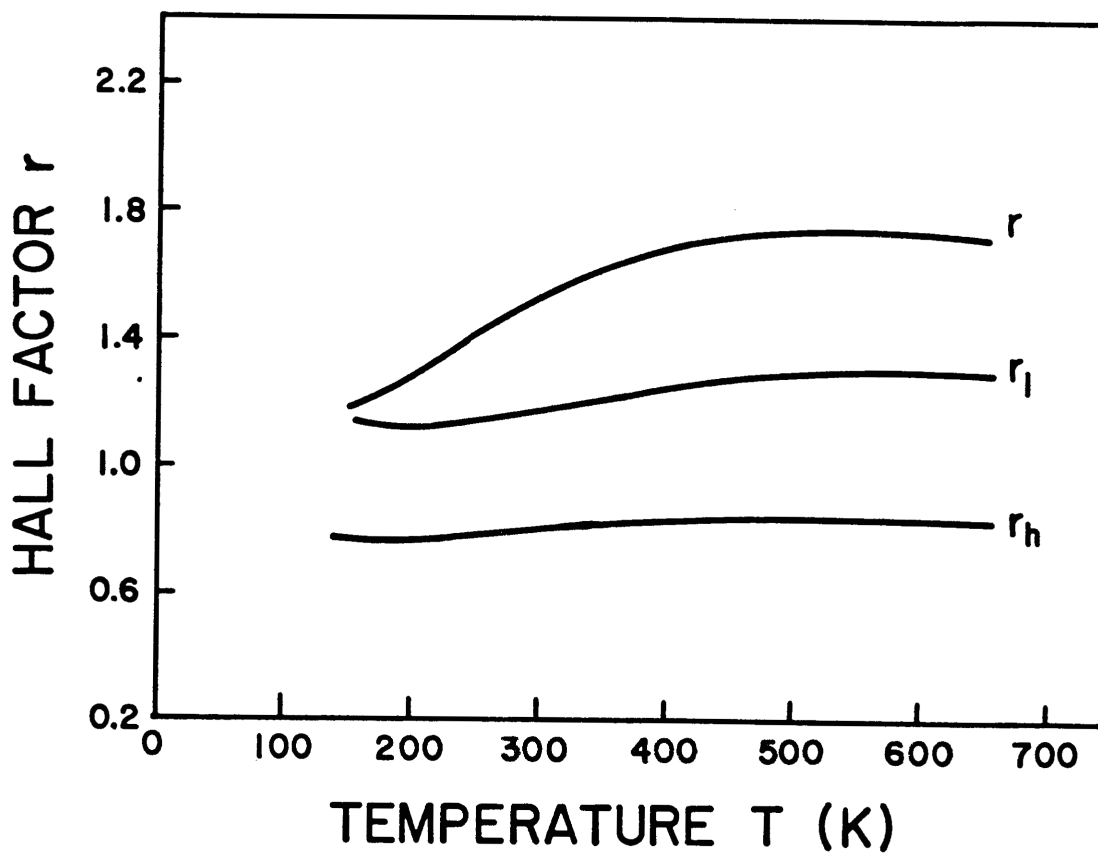


Figure 3-4 An experimental Hall factor r variation with temperature, and the effective factors $r_l$ for light holes and $r_h$ for heavy holes, after Lee and Look [17].

deduced $n_0$.

Secondly, we want to deal with the mobility ratio b. Since the scattering mechanisms are similar for electrons and holes in a given sample, it should possible to find a simple relation between $\mu_n$ and $\mu_p$. According to this assumption, Look [18] proposed an empirical form

$$b = (\mu_n/\mu_p) \approx 13 + 0.0009\mu_n \qquad (3\text{-}26)$$

for $\mu_n$ and $\mu_p$ at room temperature from published data. For temperature dependences of the lattice Hall mobilities, Blakemore [19] suggested that

$$\mu_{Hn} = (r_n\, \mu_n) \approx 9400\ (300/T)^{2.3} \quad cm^2\, v^{-1}\, s^{-1} \qquad (3\text{-}27)$$

and

$$\mu_{Hp} = (r_p\, \mu_p) \approx 400\ (300/T)^{2.3} \quad cm^2\, v^{-1}\, s^{-1}. \qquad (3\text{-}28)$$

around room temperature for "weak field" and "pure" GaAs. From these equations, we have a maximum Hall mobility ratio

$$(\mu_{Hn}/\mu_{Hp}) = (b/\beta) \approx 23.5 \qquad (3\text{-}29)$$

which is temperature independent. Although this is only postulated as true for very "pure" GaAs, we think that $(b/\beta)$ should not be markedly temperature sensitive for "weakly doped" (including SI) GaAs.

Equation (3-26) is a meritorious approach, which has been used by other authors [20]. However, when we have checked it with the mobility ratio for stronger doping, it appears possible that Eq.(3-26) might over-estimate the value of b in low mobility cases. For low effective mass conduction band electrons should start to have their mobility impaired by impurity scattering or by microscopic inhomogeneity more easily than the light-heavy combination valence band holes. Some of our work accordingly

used a slightly modified version of Eq.(26), via:

$$b(T) = (\mu_n/\mu_p) \approx 8 + 0.002\mu_n(T) \qquad (3\text{-}30)$$

for the temperature range around 290-425K. This did not give us the final solution since $\mu_n$ still is a unknown factor, but it provided us with a crude guide for approaching the values of z, y, and F(y). Fortunately, F(y) is not very sensitive to the value chosen for b in Fig.3-2. Therefore, one can make a reasonably intelligent guess as to an initial value for b, and make a correction later. Based on the quotation by Martin *et al.* [6] that $b(400) \approx 15$ at 400 K, and the 300 K value estimated by us $b(300) \approx 20$, our analyses have often employed

$$b(T) = 20 - 0.05(T - 300) \qquad (3\text{-}31)$$

as the initial guess. Once the estimated and corrected $\mu_n$ is obtained, one can plug that value into Eq.(3-30) to get a modified b for further iterations of the calculation.

Since the values of $\beta$ and b are determined by empirical formulae, it is pointless to express the value of y to more than three digits of accuracy, even though one can do that by computer without any problem. With this in mind, it motivated us to create a simple function which could numerically approximate F(y) for correction. However, y is a function of z. It is convenient for us to express Eq.(3-14) directly in term of z

$$n_0 = r_n(e\,R'_H)^{-1}\,F(y(z)) = r_n(e\,R'_H)^{-1}\,f'(z), \qquad (3\text{-}32)$$

where $f'(z)$ is a function we wish to know, or to simulate effectively. For dealing with near-intrinsic SI GaAs, the simple form $f(z)$ is very effective, where

$$f(z) = [1 - 1/(bz^2)]^2 \approx f'(z) \qquad (3\text{-}33)$$

in this work. The differences of f(z) and F(y) are compared and plotted in Fig. 3-5 for the specific numerical choice b = 20. They are fairly close on the n side of intrinsic, and still close until one reaches y or z less than ~ 0.8. In practice, $n_0 > 0.8\ p_0$ is the case for most "undoped" SI GaAs. Using f(z), the estimated (corrected) electron concentration is given by

$$n_0(\text{est}) = r_n(e\ R'_H)^{-1}\ f(z). \qquad (3\text{-}34)$$

Once $n_0$(est) is obtained, it can then be used to give a reasonable estimate for y. From here, one can go back to calculate F(y) and G(y) of Eqs.(3-12) and (3-16). A refined $n_0$ and $\mu_n$ can then be obtained, with an accuracy for $n_0$ limited by the reliability of the raw Hall data, and by the fidelity of the simulation used for $r_n(T)$.

## 3.3 Usefulness of Temperature-Dependent Electrical Transport Data

Bulk resistivity, and carrier concentrations, are the most important and directly measurable quantities for any semiconducting sample. A lot of useful information such as compensation and scattering mechanisms, can be deduced using these transport data. Especially, the temperature-dependent carrier concentration $n_0(T)$ for SI GaAs allows us to monitor whether or not the Fermi level is controlled by a deep level and to check the ionization fraction or occupancy factor of any specific level within the band gap.

The intrinsic band gap of GaAs is well-known and modeled by

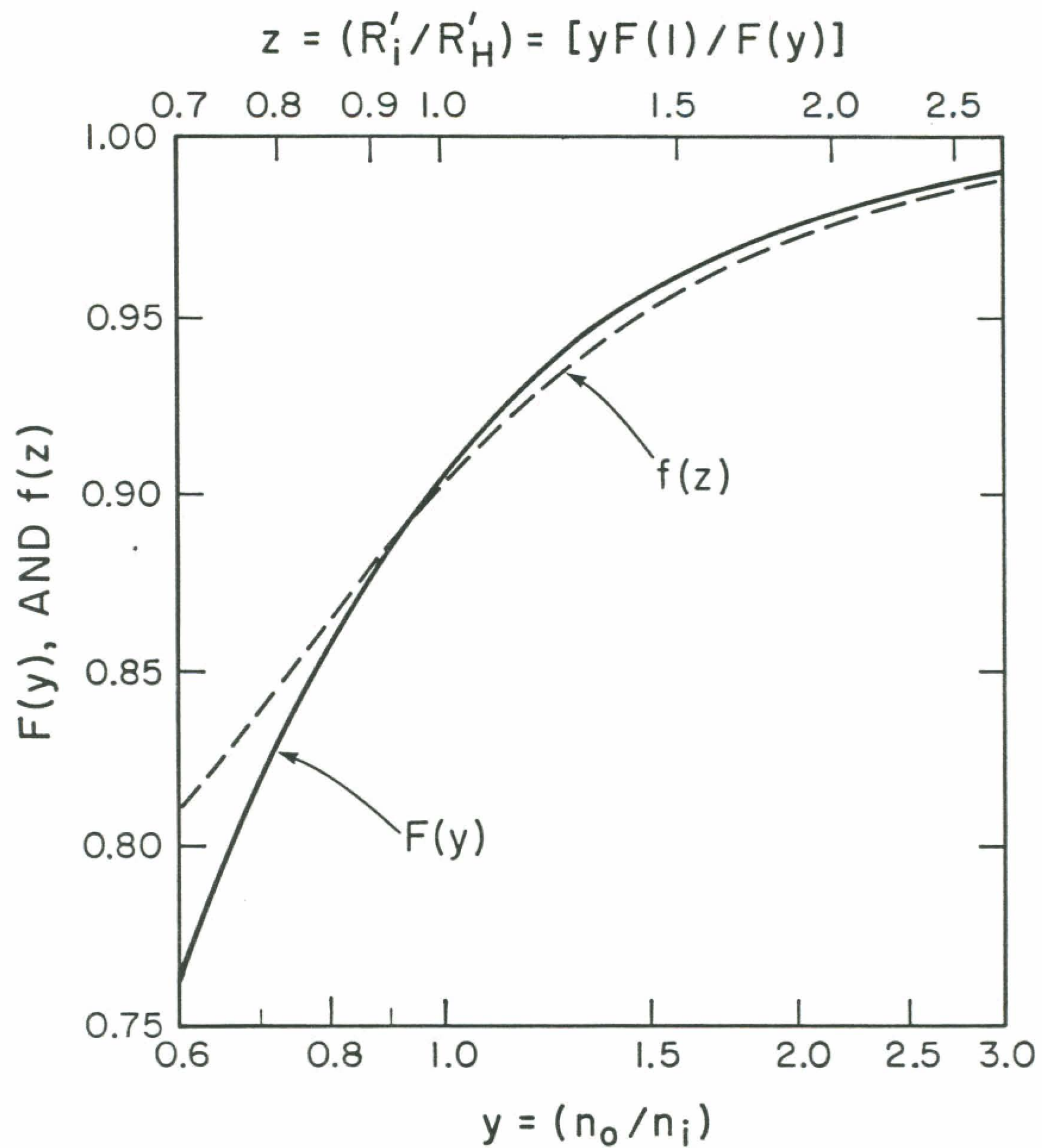


Figure 3-5 Graphical comparison of correction factors F(y) (solid curve) and f(z) (dashed curve) from Eqs.(3-12) and (3-33). In both cases, it is assumed that $b = 20$ and $\beta \approx 1.25$.

Thurmond [21] in the form

$$\varepsilon_i(T) = 1519 - 0.5405\, T^2 / (T + 204) \quad \text{meV}. \qquad (3\text{-}35)$$

For non-degenerated GaAs, the intrinsic carrier density can be expressed as

$$n_i(T) = (N_c\, N_v)^{1/2} \exp(-\varepsilon_i / 2kT). \qquad (3\text{-}36)$$

The effective densities of states in the conduction and valence bands can be represented by [22]:

$$N_c(T) \approx 8.1 \times 10^{13}\, T^{3/2} \quad \text{cm}^{-3} \qquad (3\text{-}37)$$

and

$$N_v(T) \approx 1.9 \times 10^{15}\, T^{3/2} \quad \text{cm}^{-3} \qquad (3\text{-}38)$$

in the temperature range (290 ~ 450K) we are interested in. With the quantities above , we are able to model Eq.(3-36) in the form

$$n_i(T) = 3.9 \times 10^{14}\, T^{3/2} \exp(-\varepsilon_i / 2kT). \qquad (3\text{-}39)$$

The Fermi energy can usually be expressed as

$$\varepsilon_F(T) = \varepsilon_c - kT \ln(N_c/n_0) \qquad (3\text{-}40)$$

or

$$\varepsilon_F(T) = \psi + kT \ln(n_0/n_i), \qquad (3\text{-}41)$$

where

$$\psi(T) = (\varepsilon_c + \varepsilon_v)/2 + (kT/2) \ln(N_v/N_c) \qquad (3\text{-}42)$$

is the intrinsic Fermi level. It is convenient to define zero energy at band gap center $(\varepsilon_c + \varepsilon_v)/2$ in this case. According to the values for $N_c$ and $N_v$ above, Eq.(3-42) reduces to

$$\psi(T) \approx (T/7.32) \quad \text{meV} \qquad (3\text{-}43)$$

After these processes, the Fermi level can be evaluated from the value of $n_0(T)$ through the numerical equation

$$\varepsilon_F(T) = (T/7.32) + 0.086169T \ln(n_0/n_i) \quad \text{meV.} \qquad (3\text{-}44)$$

In semi-insulating or high-resistivity GaAs, all shallow levels should be totally ionized by compensation, but a deep level with energy not far from the Fermi level may have non-negligible numbers of both "filled" and "empty" states. Assume a deep donor level located at energy $\varepsilon_D = (\varepsilon_c - \varepsilon_d)$, with $N_{di}$ states ionized and $N_{dn}$ states neutral. One can express the occupancy probability $P_e$ as [23]

$$N_{dn}/(N_{dn} + N_{di}) = P_e(\varepsilon_D) = \{1 + \beta' \exp[(\varepsilon_c - \varepsilon_d - \varepsilon_F)/kT]\}^{-1}, \qquad (3\text{-}45)$$

where $\beta' = (g_i/g_n)$ is the spin degeneracy weighting factor of that level. If we know the free energy $\varepsilon_d$ and spin degeneracy factor $\beta'$ of that donor level then the ionized fraction can be obtained from

$$N_{di}/(N_{dn} + N_{di}) = P_i(\varepsilon_D) = 1 - P_e(\varepsilon_D) \qquad (3\text{-}46)$$

A similar approach can be used for an acceptor level with energy $\varepsilon_A = (\varepsilon_v + \varepsilon_a)$. The occupancy probability (filled with an electron) or ionized fraction is then

$$N_{ai}/(N_{an} + N_{ai}) = P_i(\varepsilon_A) = [1 + \beta' \exp(\varepsilon_v + \varepsilon_a - \varepsilon_F)/kT]^{-1}. \qquad (3\text{-}47)$$

For Cr-doped SI GaAs, since the absolute free energy [24] of the $Cr^{2+}/Cr^{3+}$ acceptor level, and the spin degeneracy factor ($\beta' = 5/4$) [25] are both known factors, one can insert these into Eq.(3-47) to get the ionization factor $P_i(\varepsilon_A)$. In not intentionally doped SI GaAs, the level we are concerned with is EL2, but the spin degeneracy factor for EL2 is still not clear in the GaAs community because of the ambiguity of this defect's microscopic nature. We have to solve this problem by avoiding use of the spin degeneracy factor.

Based on published data for the electron capture and emission

coefficients of EL2, Blakemore [24] deduced the "mass action density" $n_D^*$ of EL2 from detailed balance reasoning, the result expressed as

$$n_D^* = (e_n/c_n) = 1.85 \times 10^{15}\, T^{3/2} \exp(-0.748/kT)\ \text{cm}^{-3}. \qquad (3\text{-}48)$$

Also the "mass action density" can be expressed as

$$n_D^* = \beta' . N_c \exp[-\varepsilon_t / kT]. \qquad (3\text{-}49)$$

If one quotes the equilibrium electron concentration as

$$n_0 = N_c \exp[-(\varepsilon_c - \varepsilon_F)/ kT]. \qquad (3\text{-}50)$$

then Eq.(3-45) can be expressed in term of $n_D^*$ and $n_o$ as

$$P_e(\varepsilon_D) = (1 + \beta' \exp(-\varepsilon_t/kT) \exp[(\varepsilon_c - \varepsilon_F)/kT])^{-1} = (1 + n_D^*/n_0)^{-1}. \qquad (3\text{-}51)$$

Now, the ionization factor of EL2 becomes

$$P_i(EL2) = 1 - (1 + n_D^*/n_0)^{-1} = (1 + n_0/n_D^*)^{-1}. \qquad (3\text{-}52)$$

It is thereby possible to derive $P_i(EL2)$ without knowing the spin degeneracy factor $\beta'$.

The Fermi level and ionization factor obtained in the above equations are temperature dependent. From their behavior, we can acquire a clearer picture in assessing the properties of SI GaAs under various conditions.

## REFERENCES: CH.3


1. J. W. Allen, Nature, **187**, 403 (1960)
2. J. Blanc and L. R. Weisberg, Nature, **192**, 155 (1961)
3. J. F. Woods and N. G. Ainslie, J. Appl. Phys. **34**, 1469 (1963)
4. C. G. Kirkpatrick, R. T. Chen, D. E. Holmes, P. M. Asbeck, K. R. Elliott, R. D. Fairman, and J. R. Oliver, in *Semiconductors and Semimetals Vol. 20*, 192, 206 (1984)
5. P. F. Lindquist, J. Appl. Phys. **48**, 1262 (1977)
6. G. M. Martin, J. P. Farges, G. Jacob, J. P. Hallais, and G. Poiblaud, J. Appl. Phys. **51**, 2840 (1980)
7. G. R. Cronin and R. W. Haisty, J. Electrochem. Soc., **111**, 874 (1964)
8. T. Inoue and M. Ohyama, Solid State Commun. **8**, 1309 (1970)
9. L. A. Balagurov, E. M. Omel'yanovskii, and L. Ya. Pervova, Sov. Phys. Semicond. **8**, 1051 (1975)
10. D. C. Look, *Electrical Characterization of GaAs Materials and Devices*, (John Wiley & Sons, New York 1989).
11. R. A. Smith, *Semiconductors*, (Cambridge Univ. Press 1978) p.155
12. K. Seeger, *Semiconductor Physics An Introduction*, Springer Series in Solid-State Sciences 40, (Springer-Verlag, 3rd edition, 1985) p. 58
13. $s \approx s' \approx 1/2$ for mostly lattice scattering which can be seen in Chapter 6 of Ref.11.
14. L. J. van der Pauw, Philips Res. Rep. **13**, 1 (1958)

15. B. K. Ridley, *Quantum Processes in Semiconductors*, Ch.3, Ch.4 (Oxford Univ. Press, 2nd edition, 1988)

16. D. L. Rode, in *Semiconductors and Semimetals Vol. 10*, 1 (1975)

17. H. J. Lee and D. C. Look, J. Appl. Phys. **54**, 4446 (1983)

18 D. C. Look, in *Semi-Insulating III-V Materials: Nottingham 1980*, edited by G. J. Rees, (Shiva, Orpington, UK, 1980), p. 183

19. J. S. Blakemore, J. Appl. Phys. **53**, R123 (1982)

20. J. J. Winter, H. A. Leupold, R. L. Ross and A. Ballato, in *Semi-Insulating III-V Materials: Evian 1982*, edited by S. Makram-Ebeid and B. Tuck, (Shiva, Nantwich, UK, 1982), p. 134

21. C. D. Thurmond, J. Electrochem. Soc. **122**, 1133 (1975)

22. J. S. Blakemore, J. Phys. Chem. Solids 49, 627 (1988)

23. J. S. Blakemore, *Semiconductor Statistics*. Ch.3, (Dover, New York, 1987)

24. J. S. Blakemore, in *Semi-Insulating III-V Materials: Hakone 1986*, edited by H. Kukimoto and S. Miyazawa, (Ohmasa,Toyko, 1986), p. 389

25. U. Kaufmann and J. Schneider, Festkorperprobleme **20**, 87 (1980)

# CHAPTER 4

# RESULTS FOR "UNDOPED" GaAs CRYSTALS GROWN BY VARIOUS METHODS

## 4.1 Rationale for the Results Described Here

As a Preliminary for this chapter, it is useful for the reader to appreciate that the work reported on in this dissertation has a thrust towards characterization of numerous GaAs crystals which had been melt-grown elsewhere - by various persons, and by a variety of growth techniques. For a reader whose own interests lie in the growth of epilayers, fabrication of device structures, etc., it may seem a handicap to the present work that our measurements were not made on bulk GaAs crystals grown by ourselves, but the choice to work with wafers and samples from large melt-grown crystals prepared elsewhere was a deliberate one.

GaAs crystals have been grown from the melt since the 1950s, as already noted in Chapter 1. However, melt-grown monocrystal GaAs of high quality has become available only in comparatively recent years (this being especially true for "undoped" or "not intentionally doped" SI GaAs), as growth systems of increased size and complexity have been developed. Material suitable in quality for device substrates of the 1990s does not come

from small, simple, growth chambers; but from large-scale growth systems which are very costly to operate. (Thus the "raw" 99.99999% In and As for one growth can cost up to $5,000, and there are other major costs per resulting crystal.)

The natural result has been that the best GaAs to study comes from a few commercial suppliers, both those who grow crystals only for in-house use (such as AT&T Bell Laboratories), and those who sell GaAs to the outside. The resources of the US Naval Research Laboratory have also been adequate for that laboratory to maintain a viable crystal growing effort, and results with some of this NRL-grown material are described later in this chapter. A modest bulk growth program also continues (as of 1990) at the Lawrence Berkeley DoE Laboratory.

The high cost of operating a state-of-the-art GaAs bulk growth facility has thus obliged academia to retire from this aspect of GaAs activity. The termination in 1988 of a DARPA-funded LEC GaAs growth activity at Arizona State University is one notable recent example. For a number of years, very small Horizontal Bridgman (HB) GaAs crystals were grown in the laboratory of H. C. Gatos at MIT, but the intent there was a study of GaAs defect chemistry, not the creation of "high quality" material.

If one grows very small crystals, at least there can be an opportunity in an academic setting for a reasonable fraction of the material to be used. When each crystal amounts to several kilograms, only a tiny fraction of each crystal is required for characterization: the remainder is usable in a commercial setting, but not in a university one. Probably more than 99% of

the GaAs grown in the above-noted ASU program was disposed of as gallium scrap.

Given the economics of GaAs bulk growth, the academic community can make a much more meaningful contribution by exerting a leadership role in characterization, with actual growth left to those organizations where it makes sense. Information derived from experiments such as those described in this thesis can be useful (a) to those who have been involved in the actual growth, and (b) for those who use GaAs wafers as substrates for device fabrication. We can also, via publication, show the commercial sector how they can improve their own characterization efforts.

If one is dependent on commercially-purchased wafers - as is the case for many university research programs - the work is subject to two limitations: (1) budget restrictions may limit a student to a very narrow variety of samples, and (2) just how the crystals yielding those samples were grown is apt to be shrouded in mystery.

The work to be described in this thesis was not limited in the above way, for we have been fortunate that those who grow GaAs crystals, and those who use them for device fabrication, have been eager to provide us with numerous and diverse wafers at no cost. Some of those wafers were "loaned" for nondestructive optical tests only before proceeding on a device fabrication path. Other wafers and thicker "slug" samples were outright donations, with the understanding that electrical and optical data derived by us would be shared with the donor party. Such collaboration has led to some joint publications.

Among those who have donated GaAs to us may be noted "undoped" Liquid Encapsulated Czochralski (LEC) material from Westinghouse Electric Co. (a "captive" grower, producing crystals only for in-house use), and the commercial vendors Johnson Matthey Electronics (formerly Cominco), Litton-Airtron, Spectrum Technology Inc., and Morgan Semiconductor Division of Ethyl Corp. (It may be somberly noted that Spectrum and Morgan both dropped out of the GaAs growth business during 1989.) We have also been able to work with LEC SI GaAs from various Japanese and European suppliers, and this has been most useful for us in assessing what *is* the state of the art, year by year. Most importantly, we have often been privy to specific information on the growth and thermal history of the GaAs provided us for study.

Valuable also has been an opportunity to compare LEC GaAs with that melt-grown by other methods. All of these other methods have some catching up to do compared with LEC so far as crystal *size* is concerned (100 mm diameter is as of 1990 readily available from numerous LEC suppliers, while other methods yield crystals of 3" diameter or smaller), yet several of these look promising for providing GaAs of low-to-vanishing dislocation density. Dislocations are not a problem for direct-implant MESFET devices, but are most undesirable for various optoelectronic applications. Thus in our work we have welcomed opportunities to characterize GaAs grown by both Horizontal Bridgman (HB) and Vertical Bridgman (VB) methods (courtesy of Crystal Specialties Int'l), by the Vertical Gradient Freeze (VGF) method (from AT&T Bell Laboratories, and from American Xtal Technology

Inc.), and by the Vertical Zone Melting (VZM) method (from Naval Research Laboratory).

From all of this material, amounting to hundreds of wafers and other samples, representative data have been selected to report in this thesis: measurements on "undoped" GaAs in this chapter, and for variously-doped GaAs in Chapter 5. GaAs grown without intentional doping (but with aims of compensation control) is intended to be SI, though some examples in this chapter will show that this objective is not always achieved. Doped GaAs can - using shallow donors or acceptors - be strongly N-type or P-type, though Chapter 5 will also report on SI Cr-doped GaAs, and on Fe-doped GaAs which can (depending on the amount of iron present) be either SI or fairly high resistivity P-type.

## 4.2 Electrical Data for a Range of Samples from Near-Intrinsic to "Failed SI"

The SI form of melt-grown GaAs is attractive as a substrate for device and integrated circuit (IC) purposes, since the high resistivity provides interdevice isolation. Throughout the 1980s, this property of SI GaAs has been a major driving force in the design of digital ICs, and of microwave analog ICs. In the coming decade, the properties of SI GaAs are expected to play an increasingly significant role for optoelectronics, as this moves from single devices towards integration, a path which has been pursued slowly and tortuously over the past 20 years.

From 1964 to about 1980, SI GaAs depended on chromium compensation, and it is true that some users still specify SI GaAs:Cr for their device substrates. However, an interest in "undoped" or "unintentionally-doped" SI GaAs has commanded much of the recent literature, and provides the subject matter of this chapter. For such a crystal, there is in practice a small shallow donor concentration of impurities such as $Si_{Ga}$ and $Se_{As}$ (the total $N_d$ being a few times $10^{15}$ $cm^{-3}$ at most), and a concentration $N_a$ of shallow acceptors such as $C_{As}$. The hope is that $N_a > N_d$, and such GaAs would be P-type except for the intervention of deep-level donor defects, most prominently EL2. When in fact $N_{EL2} > (N_a - N_d) > 0$, the Fermi energy $\varepsilon_F$ is controlled by partial EL2 occupancy, and semi-insulating (SI) behavior results.

The above set of inequalities requires that shallow acceptors such as carbon be present in a modest but adequate amount. Too much carbon, and the material is P-type. Too little carbon, and the EL2 levels are essentially 100% filled. This allows the Fermi energy to float higher in energy, becoming "pinned" by one of the less populous other defect species. The result is "Failed SI" material, with $n_0(300) > 10^8$ $cm^{-3}$ and $\rho_{300} < 10^7$ $\Omega$-cm, falling outside the usual specification range for SI GaAs.

Of the many SI and failed-SI "undoped" GaAs samples we have studied, this section of the chapter picks out six samples representative of the range of room temperature electron concentration from $8 \times 10^6 < n_0(300) < 2 \times 10^{11}$ $cm^{-3}$; that is, from near-intrinsic material to emphatically failed-SI GaAs. The sources of these samples are not reported here (to protect

those who kindly provided less-than-ideal material for our enjoyment), but it should be commented that these six samples represent both US and overseas suppliers, and more than one growth method. Later in this chapter, data are presented for material by three identified growth methods: VB in Section 4.3, VGF in Section 4.4, and VZM in Sections 4.5 and 4.6.

For the six samples discussed in the present section, 300 K electrical properties are listed in Table 4-1. Note that some of these samples are of very high-resistivity, but the Hall coefficient $R_H$ is still lower than one third of the intrinsic Hall coefficient $R_i$, so an ambipolar correction is not necessary in this analysis. Figure 4-1 shows a conventional semi-logarithmic plot of resistivity versus reciprocal temperature, which is useful since resistivity is such a familiar property. For the four samples 3 to 6 (all meeting the conventional SI criterion), this plot is quite close to linearity throughout; whereas the failed SI samples 1 and 2 show a departure from linearity at lower temperatures. If one describes a linear plot for resistivity in terms of

$$\rho = \rho_0 \exp(\Delta E / kT), \qquad (4\text{-}1)$$

then the appropriate parameters for these six samples are as listed in Tab.4-2. We can see from Fig.4-1 and/or Tab.4-2 that EL2 has control for samples 3 to 6, but not for samples 1 or 2.

Figure 4-2 shows the electron Hall mobility versus temperature. It is interesting that the mobility is markedly impaired for the two samples of *lower* resistivity, and we have observed the same phenomenon with

Table 4-1 300 K properties for the various samples

| Sample No. | $\rho$ ($\Omega$ cm) | $-R_H$ ($cm^3/C$) | $\mu_{Hn}$ ($cm^2/V s$) | $n_0$ ($cm^{-3}$) | $\varepsilon_F$ (meV) | $P_i$ | $N_{Carb}$ ($10^{14}$ $cm^{-3}$) |
|---|---|---|---|---|---|---|---|
| 1 | $2.1 \times 10^4$ | $3.7 \times 10^7$ | 1730 | $2.0 \times 10^{11}$ | 335 | $1.3 \times 10^{-5}$ | <2 |
| 2 | $1.3 \times 10^6$ | $3.1 \times 10^9$ | 2450 | $2.4 \times 10^9$ | 220 | $1.1 \times 10^{-3}$ | <2 |
| 3 | $1.4 \times 10^7$ | $8.3 \times 10^{10}$ | 6150 | $8.8 \times 10^7$ | 135 | 0.029 | ~4 |
| 4 | $5.5 \times 10^7$ | $3.0 \times 10^{11}$ | 5475 | $2.5 \times 10^7$ | 102 | 0.096 | 12 |
| 5 | $7.6 \times 10^7$ | $5.0 \times 10^{11}$ | 6550 | $1.5 \times 10^7$ | 89 | 0.151 | .... |
| 6 | $1.7 \times 10^8$ | $9.2 \times 10^{11}$ | 5430 | $8.0 \times 10^6$ | 73 | 0.246 | 28 |

Table 4-2 Parameters necessary for a fit of the resistivity and electron density data for samples 1-6 into the form of Eqs.(4-1) and (4-2).

| Sample No. | $\rho_0$ ($\Omega$-cm) | $\Delta E$ (eV) | A ($cm^{-3}$ $K^{-3/2}$) | $\Delta H$ (eV) |
|---|---|---|---|---|
| 1 | $1.1 \times 10^{-4}$ | 0.500(for T≥320K)* | $5.2 \times 10^{14}$ | 0.425 |
| 2 | $1.4 \times 10^{-6}$ | 0.724(for T≥340K)* | $1.8 \times 10^{16}$ | 0.640(for T≥330K)* |
| 3 | $8.8 \times 10^{-7}$ | 0.785 | $1.4 \times 10^{17}$ | 0.768 |
| 4 | $2.3 \times 10^{-6}$ | 0.795 | $5.9 \times 10^{16}$ | 0.779 |
| 5 | $5.8 \times 10^{-6}$ | 0.780 | $1.9 \times 10^{16}$ | 0.763 |
| 6 | $9.1 \times 10^{-6}$ | 0.789 | $7.0 \times 10^{15}$ | 0.751 |

*For these samples, the lines curve too much for this type of fit at lower temperature.

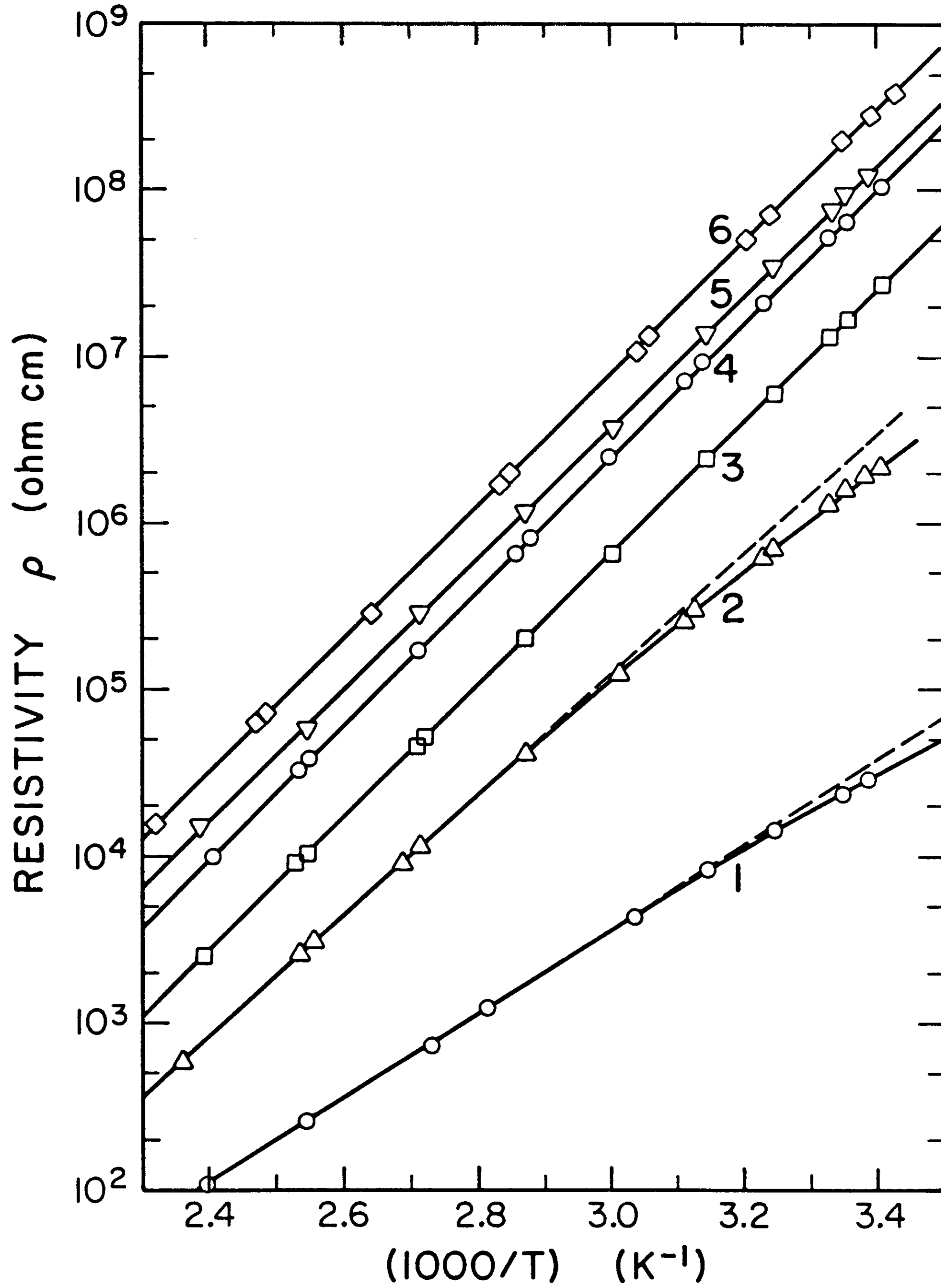


Figure 4-1 Resistivity vs reciprocal temperature for samples 1-6.

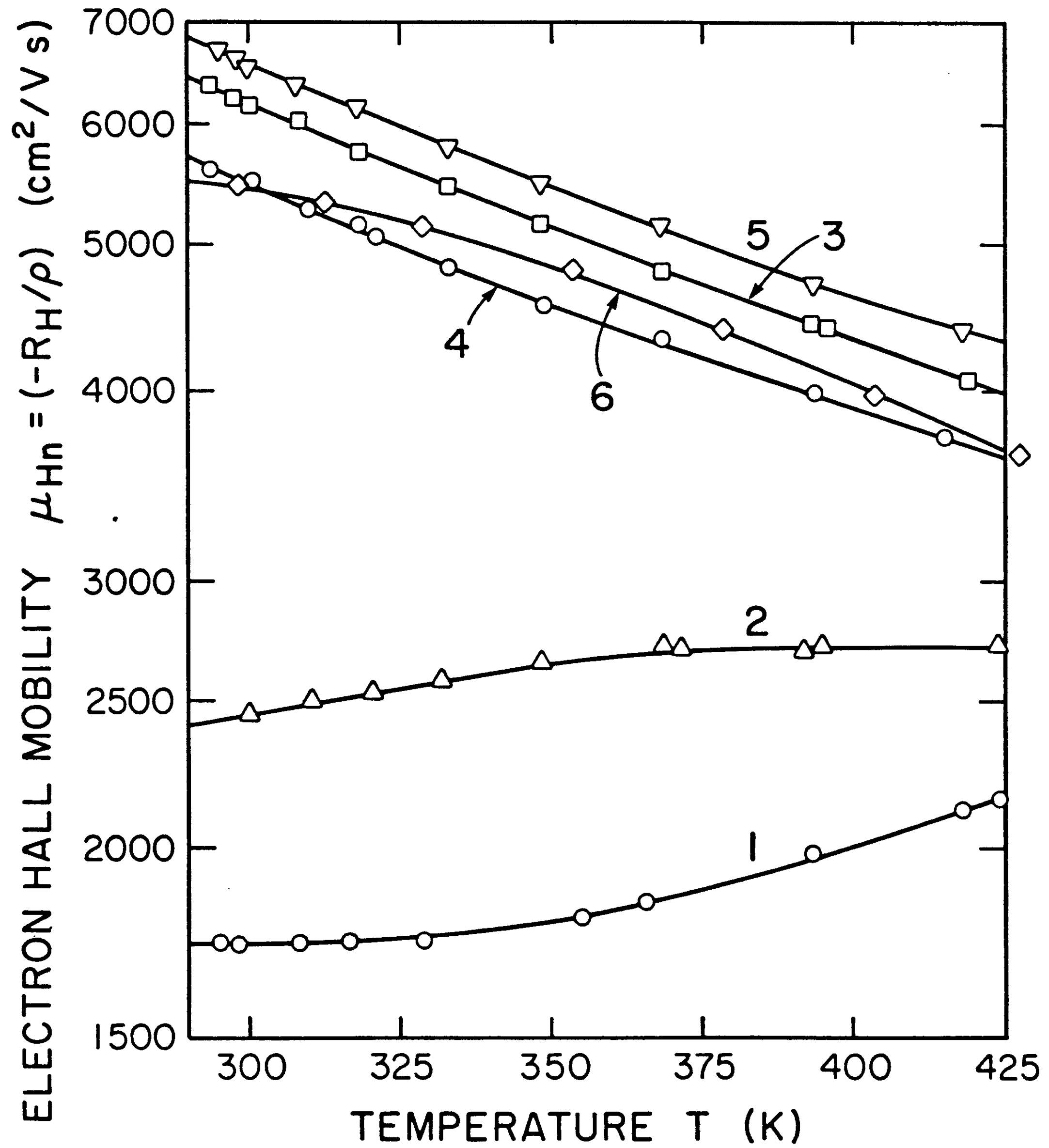


**Figure 4-2 Electron Hall mobility vs temperature for samples 1-6.**

numerous samples from other failed SI crystals. It is only reasonable to conjecture that the poor mobility in such a material is caused by local inhomogeneity of $(\varepsilon_s - \varepsilon_F)$. Such fluctuations have been proposed by Robert *et al.* [1] and Pistoulet *et al.* [2] for SI GaAs itself, although failed SI material should be even more susceptible since control of the Fermi level now rests upon other kinds of defects which are shallower in energy *and less numerous* than EL2.

Figure 4-3 shows a semi-logarithmic plot of electron density as inferred from the Hall coefficient ($n_0 = r_n / eR'_H$) versus reciprocal temperature. Such data are often simulated by

$$n_0 = A\, T^{3/2} \exp(-\Delta H / kT), \qquad (4\text{-}2)$$

where $\Delta H$ is the activation energy (or enthalpy). This could be done successfully over the entire temperature range for five of the six samples using the parameters listed in Tab.4-2. As noted in that table, there was more curvature than could be accounted for by a simple $T^{3/2}$ factor for the lower-temperature part of the data for sample 2. Even so, one can clearly see that the activation enthalpy $\Delta H$ for sample 1 and 2 does not "belong" to EL2. However, $\Delta H$ is a quite imperfect guide of the separation between $\varepsilon_s$ and the dominant electron trap (EL2 in this case), and great significance should not be read into the ~30 meV range of enthalpies among samples 3 to 6.

A valuable insight of the temperature dependent Fermi level $\varepsilon_F(T)$ is shown in Fig.4-4, derived from $n_0(T)$ of each sample. Since EL2 is the midgap defect level of most interest for SI GaAs, it is useful to examine

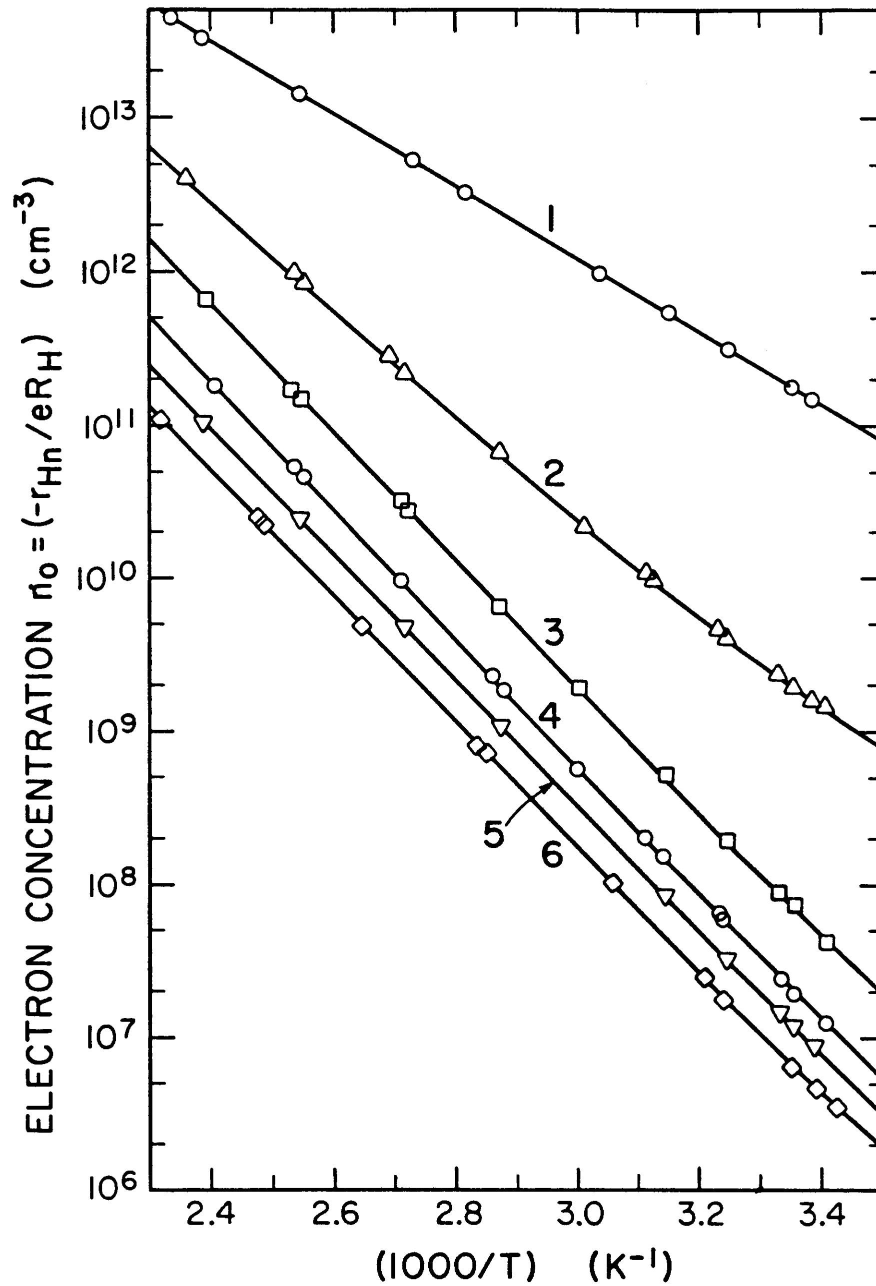


Figure 4-3 Electron concentration (derived from the Hall coefficient) vs reciprocal temperature for samples 1-6.

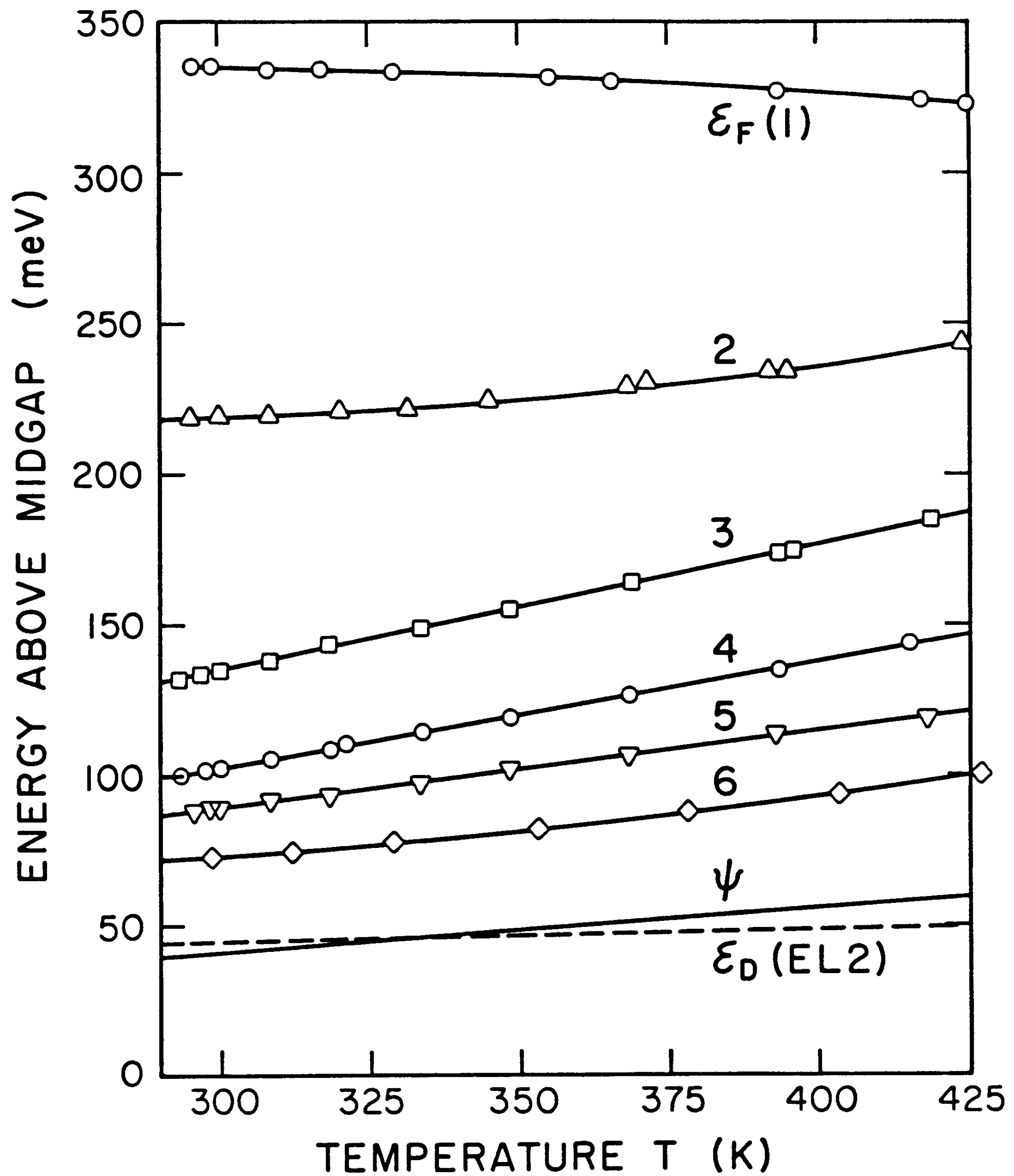


Figure 4-4 Fermi energy $\varepsilon_F$ for samples 1-6, the intrinsic Fermi level $\psi$, and the EL2 level $\varepsilon_D$, all plotted vs temperature, with midgap used as the zero for the ordinate scale.

Fig.4-4 together with Fig.4-5 which shows the EL2 ionized fraction $P_i(T)$. Because of the generality of Eq.(3-52), the values of $P_i(T)$ are still valid even when EL2 is not the level responsible for "locking" the Fermi level, which of course is the fate of samples 1 and 2. Since the total EL2 in each of samples 1-6, as measured by near-IR absorption, is in the order of $10^{16}$ cm$^{-3}$, to within ± 20% , an *approximate* ordinate scale for $N_{EL2^+}$ (the ionized EL2 center concentration) is shown on the right-hand edge of Fig.4-5. If SI GaAs was truly representable by a simple three-level model, then one would expect $P_i$ to be temperature invariant until T became large enough to make $(n_0 - p_0)$ a significant component of Eq.(4-1), which Fig.4-5 shows not to be quite true. Under this assumption, the ionized EL2 concentration $N^+$ is just simply equal to the difference of shallow acceptor and trace donor concentrations in the temperature range 290 to 425 K, and

$$N^+ = (N_{EL2} - N^o) = (N_a - N_d), \tag{4-3}$$

where $N^o$ denotes the neutral EL2 concentration. Meanwhile, from Eq.(3-45), one can also write

$$(N^o + N^+)/N^o = [1 + \beta' \exp(\varepsilon_D - \varepsilon_F)/kT] \tag{4-4}$$

and get

$$\varepsilon_F = \varepsilon_D + kT \ln[N^o/(\beta' N^+)]. \tag{4-5}$$

In such a case, $\varepsilon_F$ should rise (when $N^o > \beta' N^+$) with temperature to be a constant multiple of kT away from the absolute free energy $\varepsilon_D$. However, one can see that the above-noted expectations are only partly fulfilled for the SI samples 3 to 6, and are in total disagreement with what happens for the failed SI samples 1 and 2.

The carbon concentration was measured by mid-IR range local vibration mode (LVM) absorption for five of these six samples, and the results are listed in the final column of Tab.4-1. Except for samples 1 and 2, each has enough compensating acceptors to allow control of $\varepsilon_F$ by EL2. (This beneficial control was only barely achieved with sample 3, where $P_i \sim 0.03$.) Why does the calculated $P_i$ decline slightly with warming? Two possibilities can be mentioned. First, it will be recalled that calculating $P_i$ requires $n_D^*$ from Eq.(3-48); and in citing the numerical form of $n_D^*$ it was noted that this was based on wide-range $e_n$ data but more limited $c_n$ data [3], not extending far above room temperature. Thus, we can be rather confident about $P_i$ values calculated for 300 K, but less so about the extension to higher temperatures. The 300 K value $P_i \sim 0.25$ for sample 6, shown in Tab.4-1 and Fig.4-5, while derived from $R_H$ data, is also in accord with the $N^+/N^0$ ratio we deduce from near-IR absorption in this material.

The second possible reason why $P_i$ of samples 3 to 6 slopes gently down towards the right is the consequence of too simplistic a view of charge balance in SI GaAs. It seems likely that $\varepsilon_F(T)$ for each of these samples remains low enough not to produce any significant temperature dependence in the populations of electrons on the various shallower kinds of trap known to exist in the upper half of the intrinsic gap for melt-grown GaAs [4]. Thus, where could any extra electrons have come from to make $P_i$ creep towards a smaller value? The answer may lie in the assumption we, and many others who work with SI GaAs, make here that EL2 is *one* kind of defect with *one* ground-state energy $\varepsilon_D$. That fails to take into account the possible

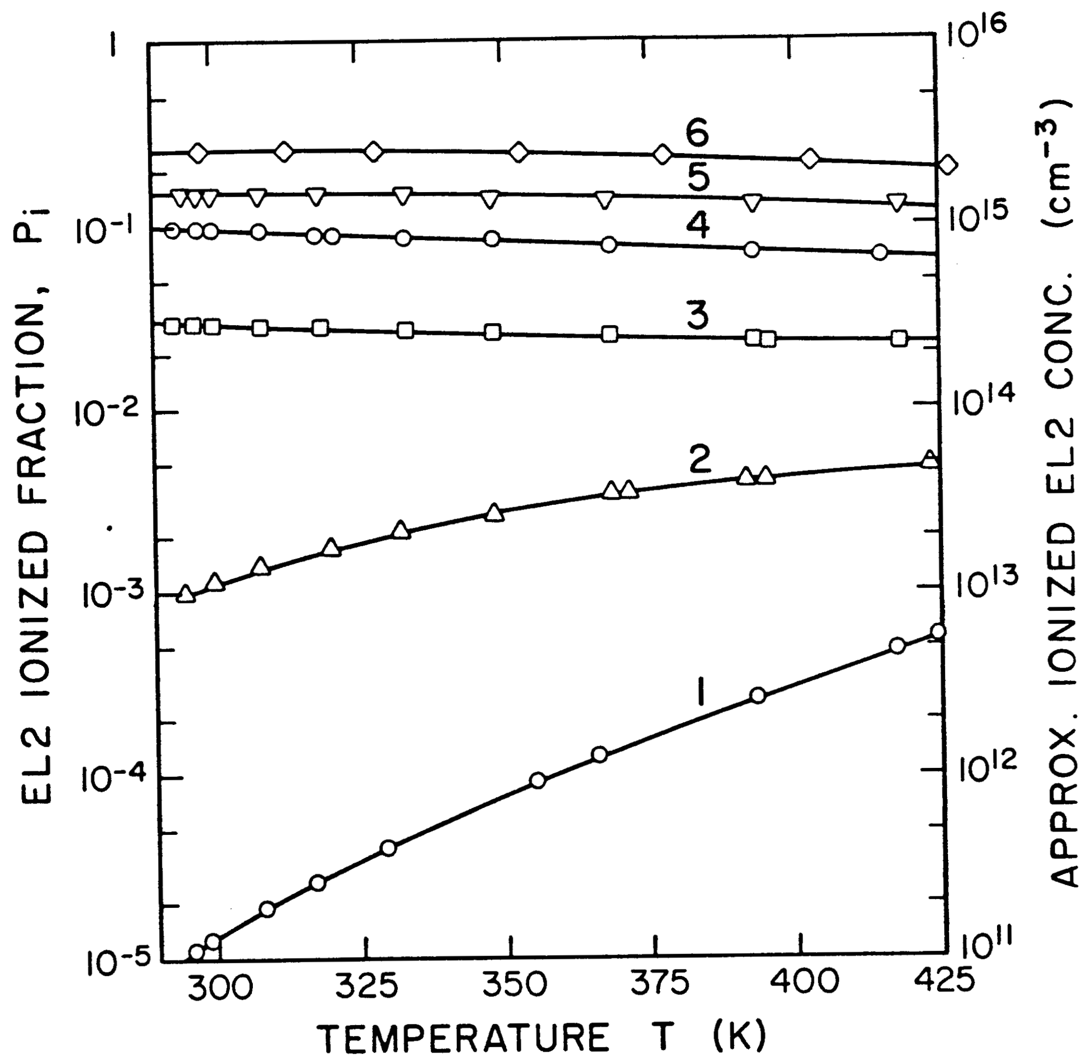


Figure 4-5 The EL2 ionization fraction $P_i$ vs temperature for the six samples. Since $N_{EL2} \sim 10^{16}$ $cm^{-3}$ for all samples, the ordinate scale at the right gives an *approximate* scaling for the ionized EL2 concentration.

complications of an EL2 family of defect complexes [5] with a finite range of ground-state energies. It was because of our awareness that the various SI GaAs crystals might have a different mix of EL2 family components that we commented in connection with Fig.4-3 and Tab.4-2 that great significance should not be attached to the slightly varying $\Delta H$ enthalpies among samples 3 to 6. In any event, the apparent negative slope of $P_i$ may be just that: appearance rather than reality.

In contrast, the increase of $P_i$ with temperature is clearly significant for samples 1 and 2. One can see most clearly for sample 1 in Fig.4-4 that $\varepsilon_F$ is pinned by a defect level some 0.3 eV below the conduction band, possibly the entity known as EL6 [4]. Note from the right-hand-side ordinate scale in Fig.4-5 that the numbers of electrons involved in being thermally transferred from EL2 into shallower traps are less than $10^{14}$ $cm^{-3}$. Thus, a relatively modest concentration of such a trap can have an opportunity to seize control when too few acceptors are present for EL2 to exercise its usual dominance.

## 4.3 Electrical Data for Undoped VB-Grown Crystals

When a pyrolytic boron nitride crucible is used, high-resistivity SI GaAs single crystals of circular (100) cross-section can be grown by the so-called vertical Bridgman (VB) method. Due to the low temperature gradient, these VB crystals have a lower dislocation density than LEC crystals which

are currently so widely used in the GaAs IC industry. Of typical samples from five such (100)-oriented and "undoped" SI crystals we report on here, conditions in three were close enough to intrinsic so that an ambipolar correction (for hole conduction) was necessary, especially in converting from Hall coefficient to electron concentration in our analysis.

The 300 K room temperature properties and some raw as-measured quantities of samples P through T are listed in Tab.4-3. In this table, we also list F(y), f(z), and other parameters used for ambipolar correction. The correction is trivially small for samples P and Q, mildly affects samples R and S (affecting the deduced electron concentration $n_0$ by ~ 2%), and has a larger effect for near-intrinsic sample T. Figure 4-6 shows a conventional Arrhenius semilogarithmic plot of corrected electron concentration versus reciprocal temperature for these samples. For comparison, a temperature dependent intrinsic carrier concentration $n_i(T)$ is plotted as a dashed line. One comment concerns specifically sample T, for which $n_0 \sim 1.5\, n_i$ at room temperature, but which has become essentially *intrinsic* by 400 K, because of the dominance of EL2 partial ionization on charge balance, Fermi energy, etc. The other comment divides the samples into two categories, with sample P, Q, and R all having a very slight *upwards* curvature in the plot of $\log(n_0)$ vs (1000/T), whereas samples S and T both have a slight *downwards* curvature in that plotting arrangement.

All of the above can be demonstrated more effectively by a plot of calculated Fermi energy versus temperature, as is done in Fig. 4-7. One can thereby see how $\varepsilon_F$ for sample T is forced steadily towards the intrinsic

Table 4-3 Properties of the five VB-grown SI samples at T = 300 K : raw as-measured values and quantities derived from these. Assumed that $n_i(300) = 2.25 \times 10^6$ cm$^{-3}$, and $r_n = 1.18$ ($= 0.8\ r_p$)

| Measured, assumed, or derived quantity | Sample | | | | |
|---|---|---|---|---|---|
| | P | Q | R | S | T |
| Measured Hall coefficient Magnitude, $R'_H$ (cm$^3$/c) | $2.045 \times 10^{11}$ | $4.605 \times 10^{11}$ | $1.095 \times 10^{12}$ | $1.345 \times 10^{12}$ | $2.068 \times 10^{12}$ |
| Resistivity, $\rho$ ($\Omega$ cm) | $3.25 \times 10^7$ | $7.28 \times 10^7$ | $2.53 \times 10^8$ | $2.43 \times 10^8$ | $4.57 \times 10^8$ |
| Ambipolar Hall mobility, $(\sigma R'_H) \equiv \mu_H$ (cm$^2$ / V s) | 6300 | 6325 | 4325 | 5530 | 4530 |
| Assumed ratio $(\mu_n/\mu_p) \equiv b$ | $\sim 22$ | $\sim 22$ | $\sim 17$ | $\sim 20$ | $\sim 18$ |
| Calculated, $R'_i$ (cm$^3$/c) | $2.99 \times 10^{12}$ | $2.99 \times 10^{12}$ | $2.91 \times 10^{12}$ | $2.96 \times 10^{12}$ | $2.93 \times 10^{12}$ |
| Ratio $(R'_i/R'_H) \equiv z$ | 14.6 | 6.5 | 2.65 | 2.20 | 1.41 |
| Function $f(z)$ | 0.9996 | 0.998 | 0.983 | 0.979 | 0.945 |
| $n_{est} = f(z)(r_n/eR'_H)$ (cm$^{-3}$) | $3.60 \times 10^7$ | $1.596 \times 10^7$ | $6.61 \times 10^6$ | $5.36 \times 10^6$ | $3.37 \times 10^6$ |
| $[n_{est}/n_i] \equiv y$ | 16.0 | 7.1 | 2.94 | 2.38 | 1.50 |
| Function $F(y)$ | 0.9996 | 0.998 | 0.986 | 0.982 | 0.951 |
| $n_0 = F(y)(r_n/eR'_H)$ (cm$^{-3}$) | $3.60 \times 10^7$ | $1.596 \times 10^7$ | $6.63 \times 10^6$ | $5.38 \times 10^6$ | $3.39 \times 10^6$ |
| $(\varepsilon_F - \text{midgap})$ (meV) | 112 | 91 | 69 | 63 | 51 |
| $(1 + n_0/n^*)^{-1} = P_i$ | 0.068 | 0.140 | 0.282 | 0.327 | 0.435 |

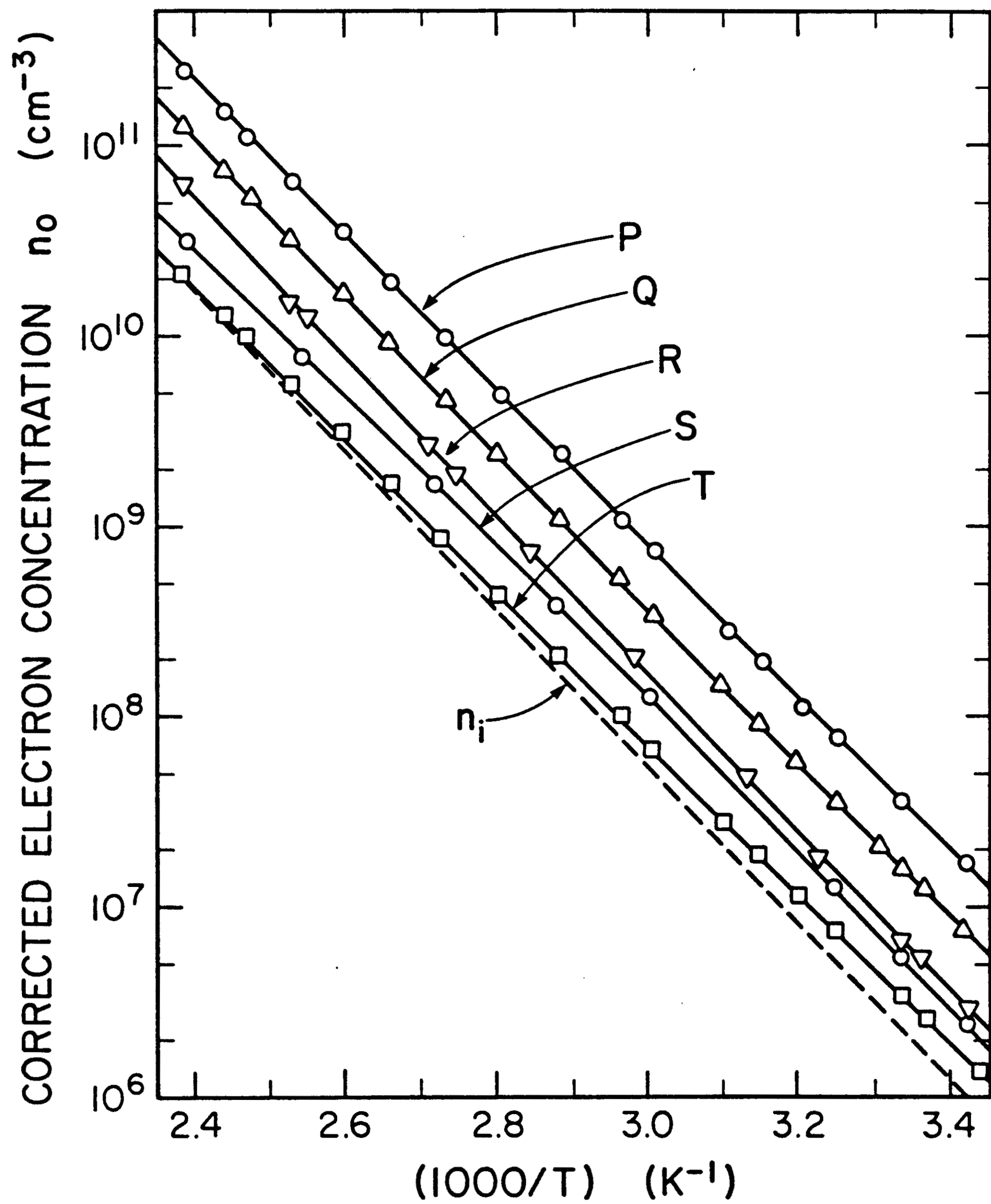


Figure 4-6 The ambipolar corrected carrier concentration $n_0$ vs reciprocal temperature for samples P through T. For comparison, a dashed line shows the course of the intrinsic concentration $n_i(T)$.

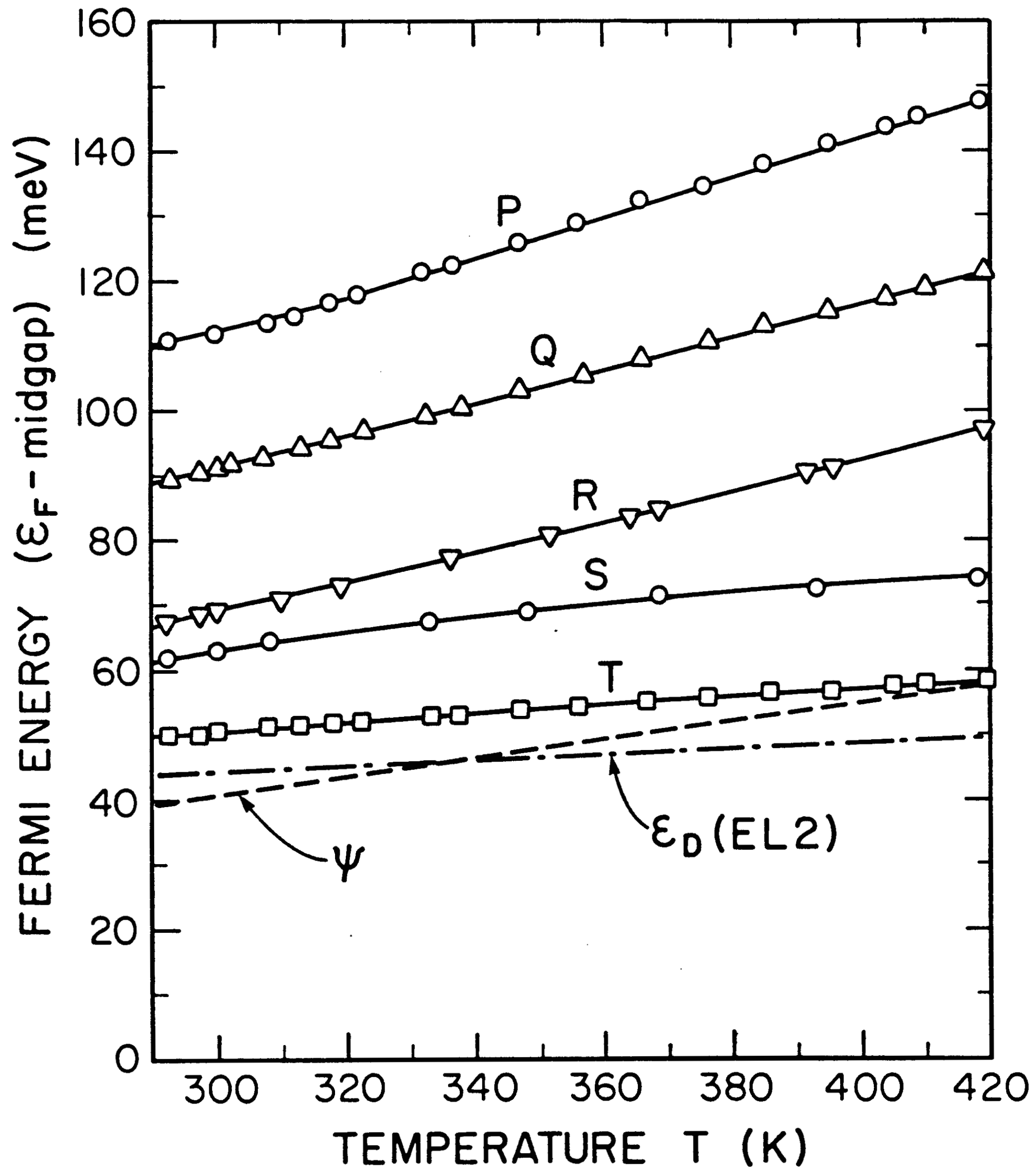


Figure 4-7 Fermi energy $\varepsilon_F$ for samples P through T, the intrinsic Fermi level $\psi$, and the EL2 level $\varepsilon_D$. All plotted versus temperature, with midgap $(\varepsilon_c + \varepsilon_v)/2$ used as the zero for the ordinate scale.

Fermi level $\Psi$ on warming, so that it can remain a constant (fractional) multiple of kT above $\varepsilon_D$, as is required for the ratio ($N^+/N^0$) of EL2 sites to be almost temperature invariant, as described by Eq.(4-5).

Fig.4-8 shows the ionized fraction of the EL2 level in these five crystals. For the weakly compensated samples P and Q, and even R, the calculated $P_i$ declines with temperature for the same reason as explained in Section 4.2. However, for the highly compensated samples S and T the situation is slightly different, with $P_i$ maintained fairly constant over the measuring temperature range. This also might be further evidence that EL2 has multiple ground-states.

## 4.4 Brief Comment on Undoped VGF Crystals

It was pointed out in Section 1.2 that the VB method (subject of data reported in Section 4.3) and the VGF method of GaAs crystal growth have much in common. For both, the melt is contained in a cylindrical crucible with a seed well at the base. In contrast to the VZM method (concerning which data are presented in Sections 4.5 and 4.6), the VB and VGF methods both start with the *entire* charge molten - except, of course, for the seed! The essential difference is that in VB growth, the capsule containing this crucible is lowered with respect to the hot zone of the surrounding furnace, whereas in VGF growth there is no physical motion. Instead, the location of the $T_m$ - 1513 K isotherm in the furnace is moved slowly upwards under

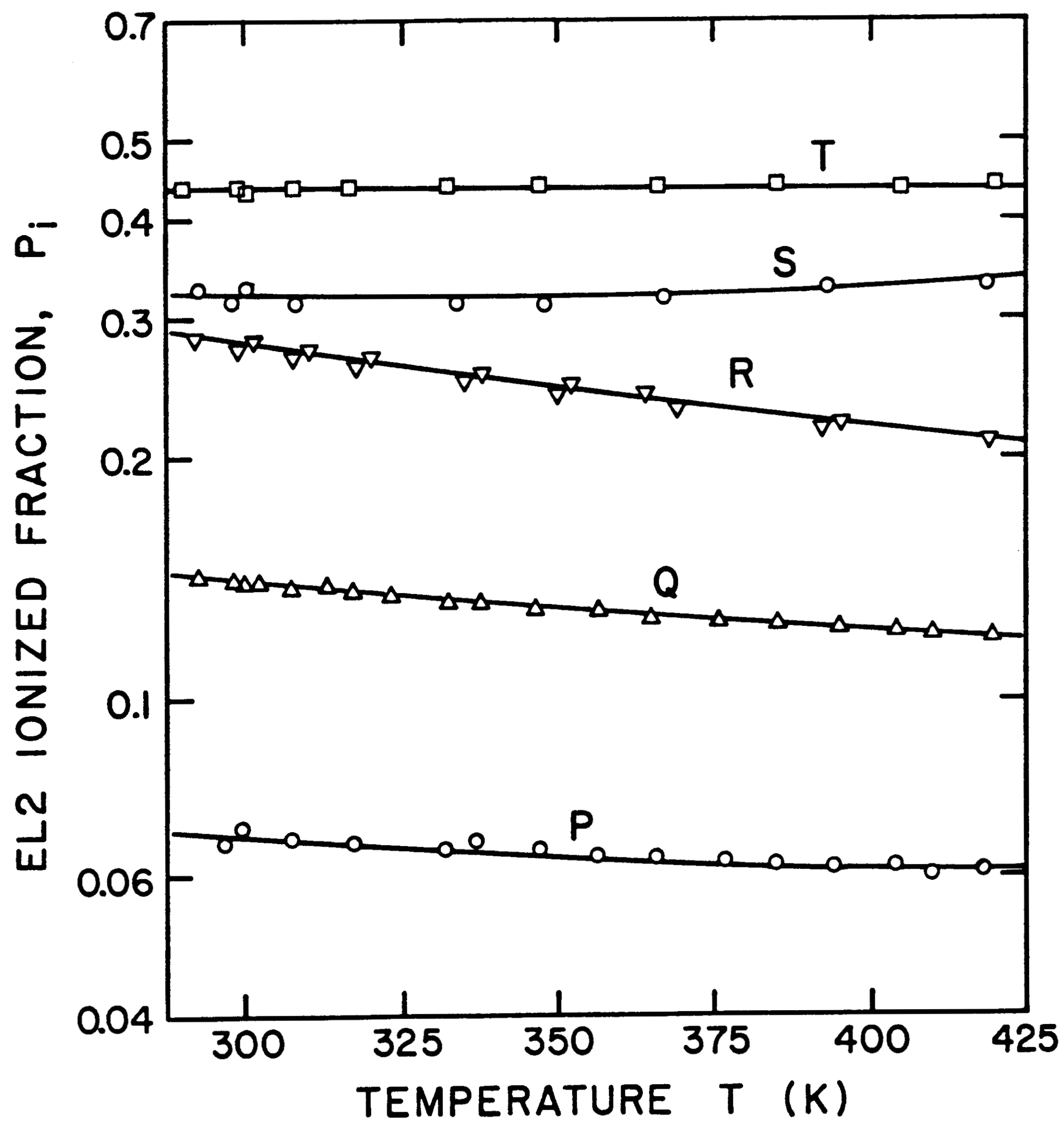


Figure 4-8 The EL2 ionization fraction $P_i$ vs temperature for VB samples P through T.

electronic control.

It has been possible for us to make observations with VGF-grown GaAs crystals from both AT&T Bell Laboratories, and American Xtal Technology (AXT). Some interesting data for doped VGF material will be reported in Chapter 5, notably for an iron-doped crystal grown at AT&T. In the present section, brief comments only are made concerning the undoped (that is, not intentionally doped) VGF GaAs we have studied from these two crystal growth facilities. The present writer was only peripherally involved in EL2 measurements and mapping for wafers from various undoped AT&T crystals, and those results [6] lie outside the scope of this thesis. It is, however, worth commenting that the concentration of $C_{As}$ acceptors we detected was quite small for both AT&T and AXT materials. This was of course measured by LVM absorption as discussed in Section 2.3, but the carbon LVM band (at 580 $cm^{-1}$ for room temperature, at 582 $cm^{-1}$ for low temperature, as illustrated in Fig.2-5) was very weak for the AT&T material, and indicative of $N_{Carb} \approx 1 \times 10^{15}$ $cm^{-3}$ for several samples of AXT GaAs.

Whereas the LEC method can yield $N_{EL2} \sim 1.3 \times 10^{16}$ $cm^{-3}$ for undoped GaAs grown from a slightly As-rich melt and given a suitable post-growth anneal [7] (such as 8 - 15 hours at 900° C), the EL2 concentration rarely exceeds $10^{16}$ $cm^{-3}$ for undoped SI GaAs grown by the various non-LEC methods. This was true for the VB material reported on in Section 4.3, for the VZM material to be described in Sections 4.5 and 4.6, and has also been the case for undoped VGF material examined by us. Figure 4-9 shows a

spectral trace of the near-IR absorption for a typical sample of undoped SI GaAs grown by AXT using the VGF method. The dashed line superimposed on the data corresponds to neutral EL2 photoionization (i. e., as with the $N^0 \sigma^0_n$ curve in Fig.2-6), with no need to add a $N^+ \sigma^0_p$ contribution. The latter was, of course, to be expected in view of the small concentration of carbon acceptors detectable in this material. The scaling of the dashed curve in Fig.4-9 corresponds, using the well-known calibration by Martin [8], to a total EL2 concentration $N_{EL2} = 6 \times 10^{15}$ cm$^{-3}$ for that sample. This is adequate to maintain a SI status, even though only 50% of that present in modern LEC material. From a device standpoint, it may be remarked that SI GaAs with a low EL2 concentration yields a lower activation efficiency for direct silicon implants [9,10]. That would not, however, be of any concern to a user who planned to employ VGF-growth SI GaAs as a substrate for epitaxy.

### 4.5 Data for VZM and Zone-Refined GaAs

Back in 1952, the technique of zone refining (ZR) was first described by Pfann [11] of Bell Labs as a means to manipulate impurity distributions in melt-growth of a semiconductor crystal. Adaptation of this to "floating-zone" vertical format was reported shortly thereafter by Keck and Golay [12], with silicon specifically in mind at that time. For GaAs, the volatility of arsenic during melt-growth presents problems which were not encountered

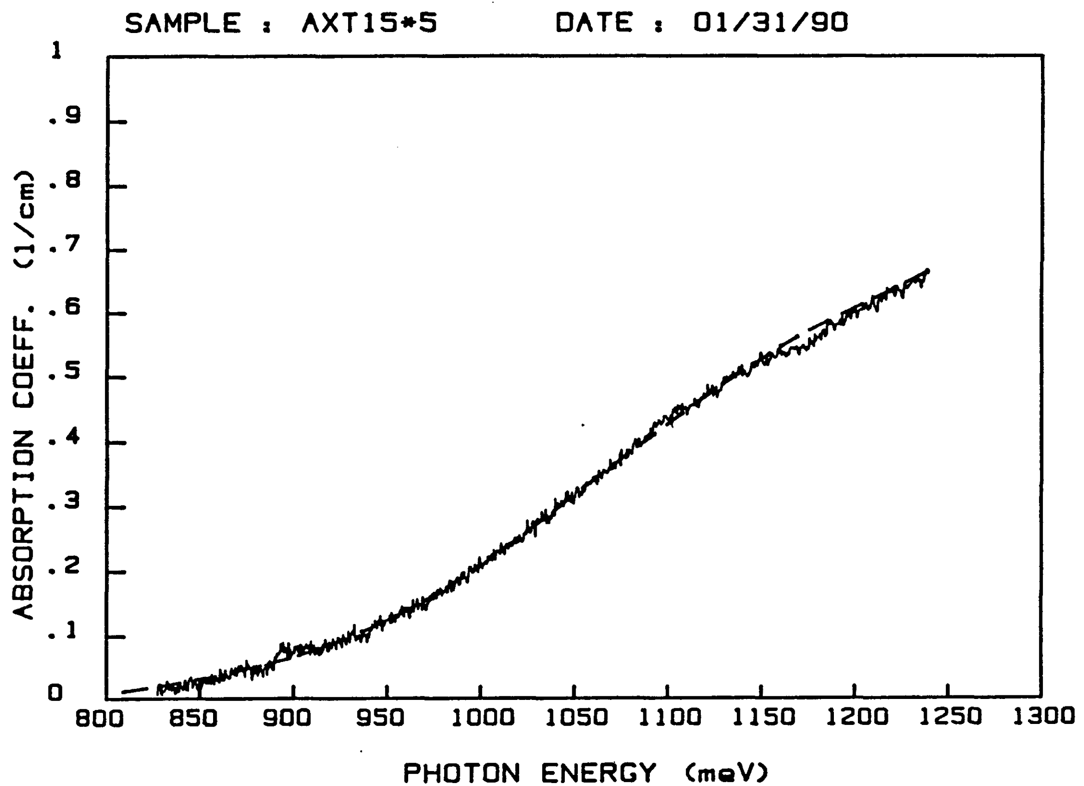


Figure 4-9 The room temperature absorption coefficient $\alpha$ vs photon energy (in meV) for VGF sample AXT15. The dashed curve is plotted with the pure neutral EL2 absorption spectrum which was reported by Martin [8]. This is scaled for $N_{EL2^o} = 6 \times 10^{15}$ $cm^{-3}$.

in Ge or Si growth. Several researchers overcame that problem, and have attempted to zone refine GaAs, but their efforts were frustrated by a lack of suitable high-purity non-reactive growth system components [13,14]. A successful new version of a furnace design and method for vertical zone melt (VZM) and zone refining growth of GaAs has recently been reported by Swiggard [15].

Two VZM grown crystals, and one zone refined crystal, were provided to us by Swiggard. We measured the EL2 and $C_{As}$ shallow acceptor concentrations, plus electrical parameters for these three "undoped" SI GaAs crystals. Two VZM grown crystals were named VZM6 and VZM8. For each of these there was a single passage of molten zone from a (100)-oriented seed towards the top, where crystallization was completed. One zone refined crystal, named ZR13, was grown and refined by a series of 14 zone passes. As illustrated in Fig.4-10, each crystal was cut into numbered sections, each about 25 mm high, which is approximately equal to the length of the molten zone. From each section of a crystal, three adjacent wafers were cut for various measurements. One of these was a 3 mm thick slab for FTIR carbon acceptor concentration measurement. Two thinner wafers (~ 0.6 mm) were cut adjacent to these thick slabs, of which one was used for electrical measurement, and the other for EL2 concentration measurement. For easy comparison, some 300 K electrical properties of the various samples are summarized in Tab. 4-4.

For section III of VZM6 and sections I to III of VZM8, ambipolar corrected electron concentrations $n_0(T)$ and as-measured resistivity $\rho(T)$ are

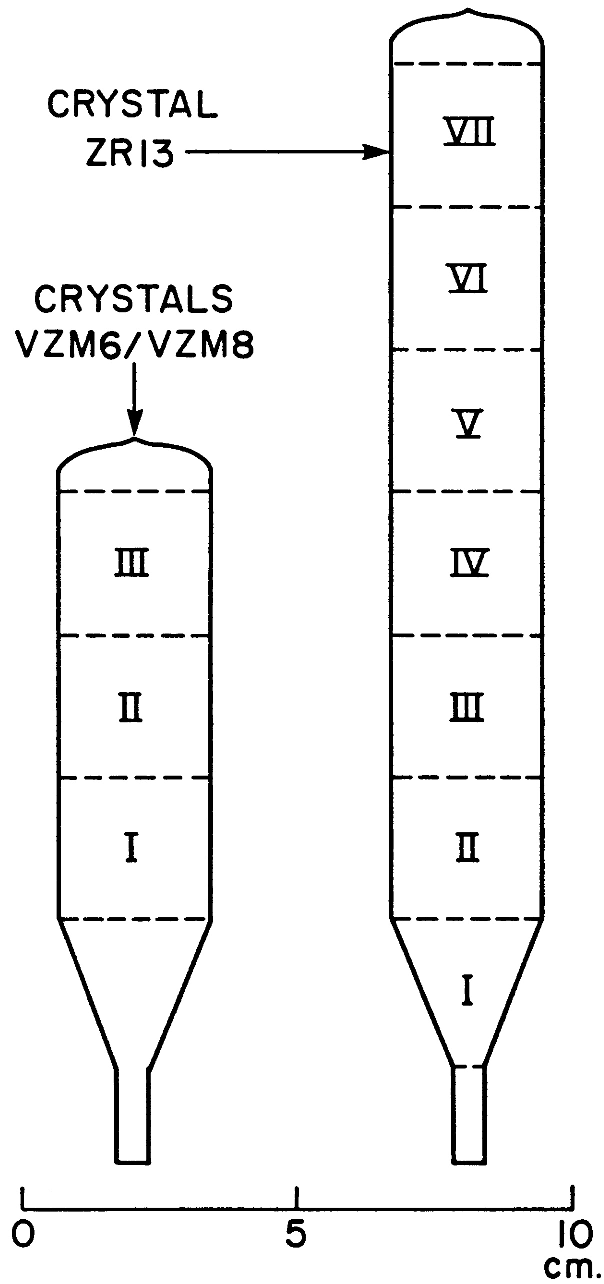


Figure 4-10 Cross-sectional views of the two VZM crystals and the zone-refined crystal. These indicate how a crystal was divided into numbered sections.

Table 4-4
300 K electrical properties for vertical zone melt and zone refined crystals.

| Crystal number and section | Resistivity $\rho_{300}$ ($\Omega$ cm) | Electron Hall mobility $\mu_{Hn}$ (cm$^2$/V s) | Electron concentration $n_0(300)$(cm$^{-3}$) | Deduced ionized EL2 fraction $P_i$ |
|---|---|---|---|---|
| VZM6-III | $5.75 \times 10^8$ | 2400 | $5.18 \times 10^6$ | 0.34 |
| VZM8-I | $2.09 \times 10^8$ | 5250 | $6.68 \times 10^6$ | 0.28 |
| VZM8-II | $1.08 \times 10^8$ | 5590 | $1.23 \times 10^7$ | 0.18 |
| VZM8-III | $1.40 \times 10^7$ | 3940 | $1.33 \times 10^8$ | 0.019 |
| ZR13-I | $5.78 \times 10^8$ | 1008 | $1.26 \times 10^7$ | 0.17 |
| ZR13-II | $5.59 \times 10^8$ | 3815 | $3.37 \times 10^6$ | 0.44 |
| ZR13-III | $4.15 \times 10^8$ | 4165 | $4.19 \times 10^6$ | 0.38 |
| ZR13-IV | $2.82 \times 10^8$ | 4425 | $5.85 \times 10^6$ | 0.31 |
| ZR13-V | $2.54 \times 10^6$ | 2585 | $1.12 \times 10^9$ | 0.002 |
| ZR13-VI | $4.61 \times 10^2$ | 3425 | $4.67 \times 10^{12}$ | 0.000 |
| ZR13-VII | 0.59 | 2700 | $4.63 \times 10^{15}$ | 0.000 |

shown in semi-logarithmic form versus a reciprocal temperature scale in Figs.4-11 and 4-12. From slopes of these two figures, we know that (apart from VZM8-III) the other three samples are controlled by the same kind of deep level, which we know is EL2. This will be seen more clearly from the deduced Fermi energy $\varepsilon_F(T)$ and calculated EL2 ionized fraction $P_i(T)$ for these samples, which are plotted in Figs.4-13 and 4-14. We can see that those three samples show the same tendency, with a slightly decreasing trend in Fig.4-14. This is of course the same as with some near-intrinsic samples described in sections 4.2 and 4.3 which were controlled by fractional EL2 compensation. From Fig.4-13, the Fermi levels of these three samples are inclined to the intrinsic Fermi level $\psi(T)$ staying a few kT away from the free energy $\varepsilon_D(T)$ of EL2. This behavior also confirms that VZM8-I, VZM8-II, and VZM6-III are controlled by EL2.

A temperature dependence of $\mu_{Hn}$ for these four samples is shown in Fig.4-15. Sample VZM6-III has poor mobility, which is not surprising because of the non-optimum nature of this first GaAs VZM growth.

Fig.4-16 shows the room temperature carbon acceptor LVM band for three samples of crystal VZM8. Each of these was measured with 0.5 $cm^{-1}$ resolution, and with an average over 256 scans. Using the calibration factor

$$f_{RT} = N_{Carb} /(\alpha\Delta) \approx (13 \pm 3) \times 10^{15}\ cm^{-1} \qquad (4\text{-}6)$$

recommended by Sargent and Blakemore [16], the LVM band areas correspond to carbon concentrations of $4.4 \times 10^{15}$, $3.1 \times 10^{15}$ and $2.6 \times 10^{15}$ $cm^{-3}$ for samples 8-I, 8-II and 8-III respectively. The variation of $N_{Carb}$, decreasing from section I to section III in crystal VZM8, happens because

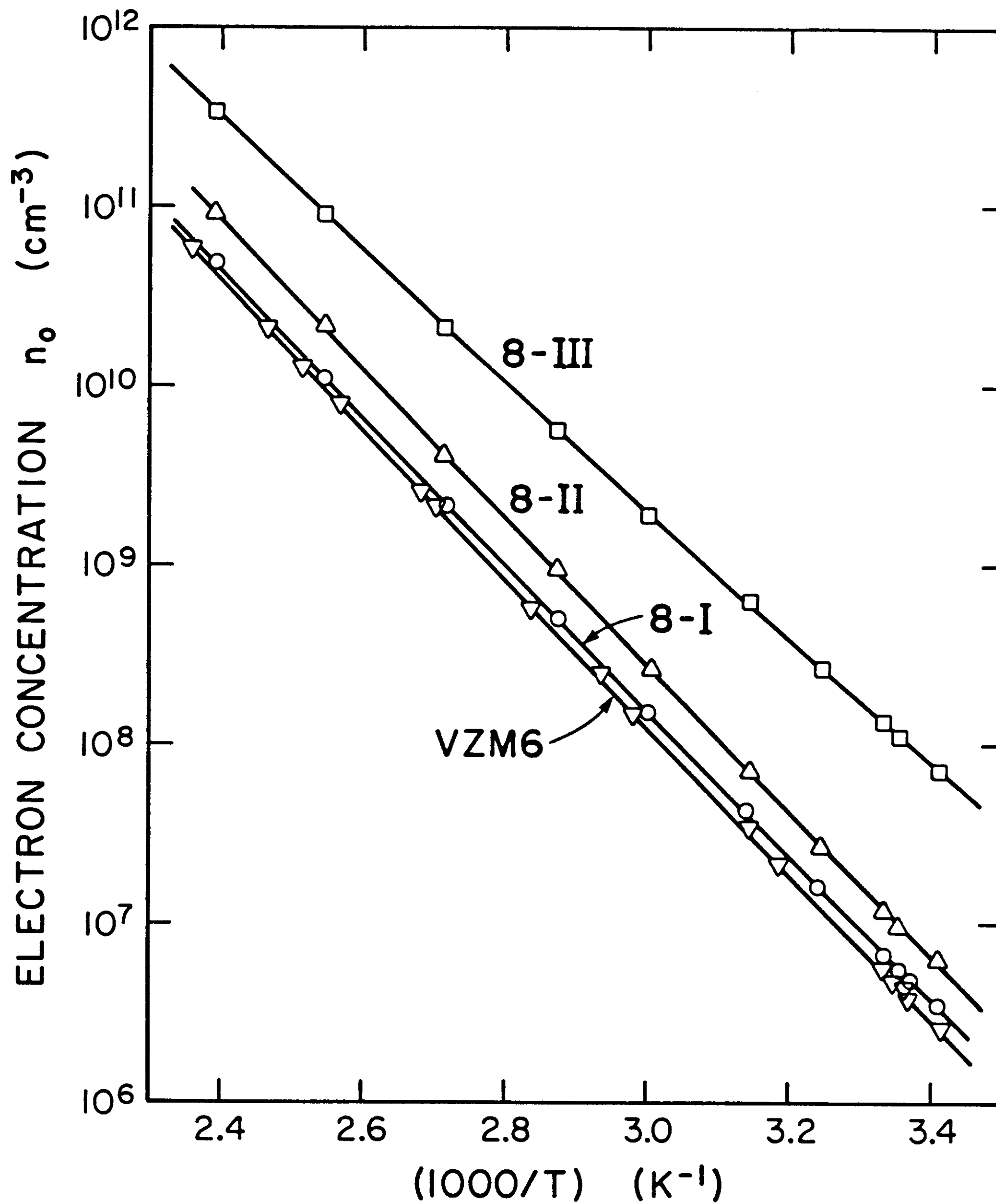


Figure 4-11 Electron concentration vs reciprocal temperature for four VZM samples. An ambipolar correction was required for the data of VZM6 and (VZM)8-I.

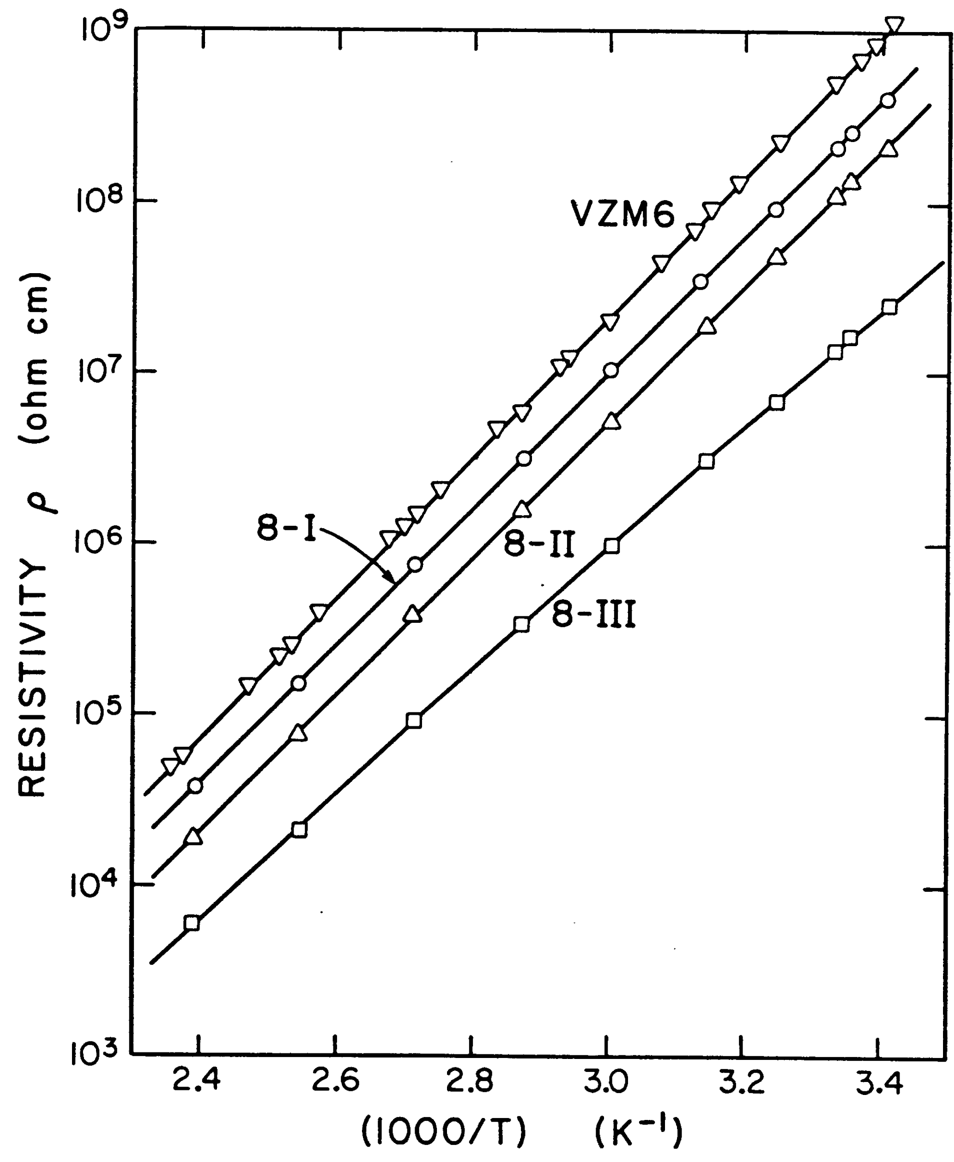


**Figure 4-12 Resistivity vs reciprocal temperature for four VZM samples.**

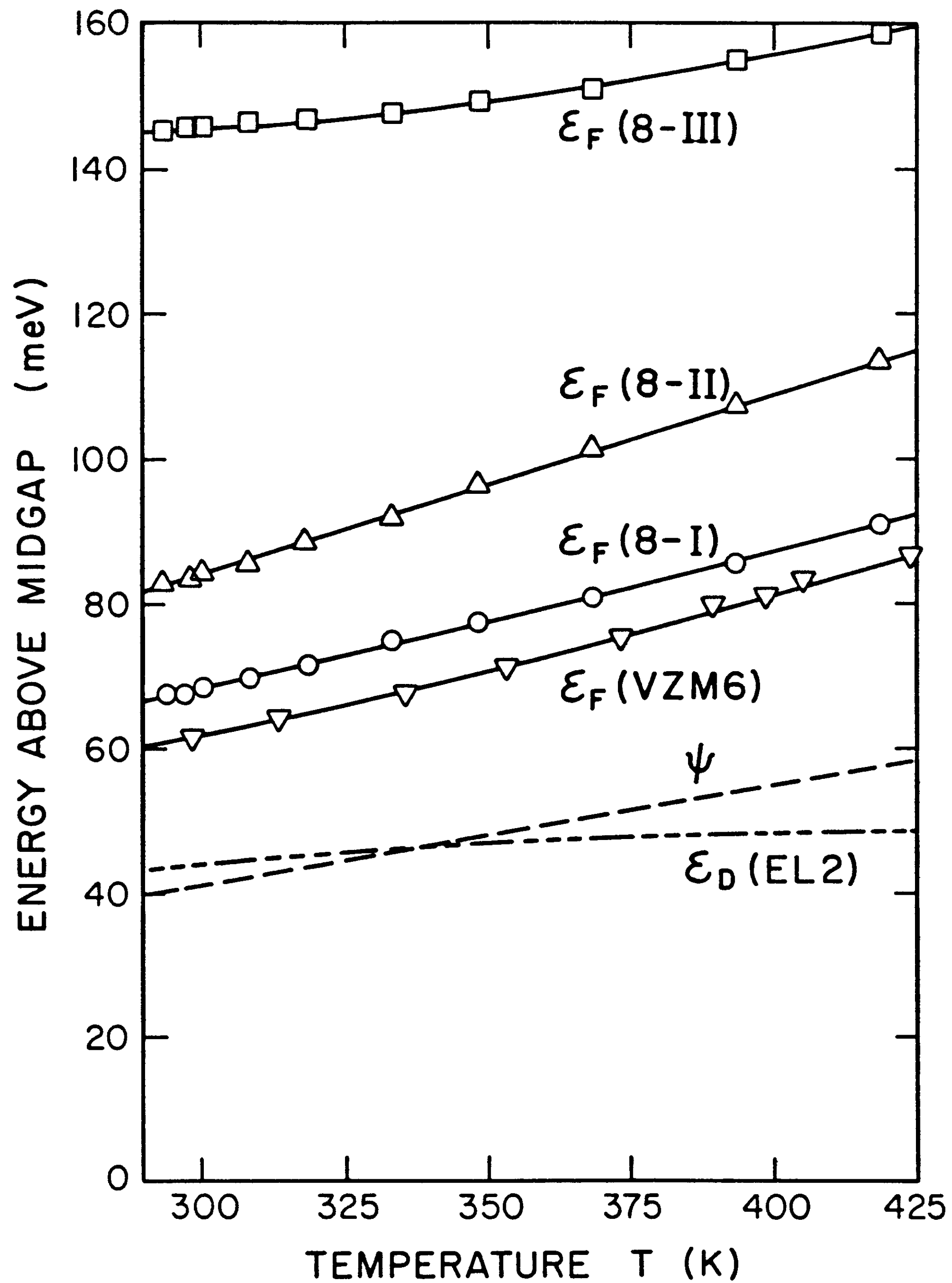


Figure 4-13 Fermi energy versus temperature for each of the four VZM samples, with midgap used as zero for the ordinate. Also, as before, showing the EL2 free energy $\varepsilon_D$ and the intrinsic Fermi energy $\psi$.

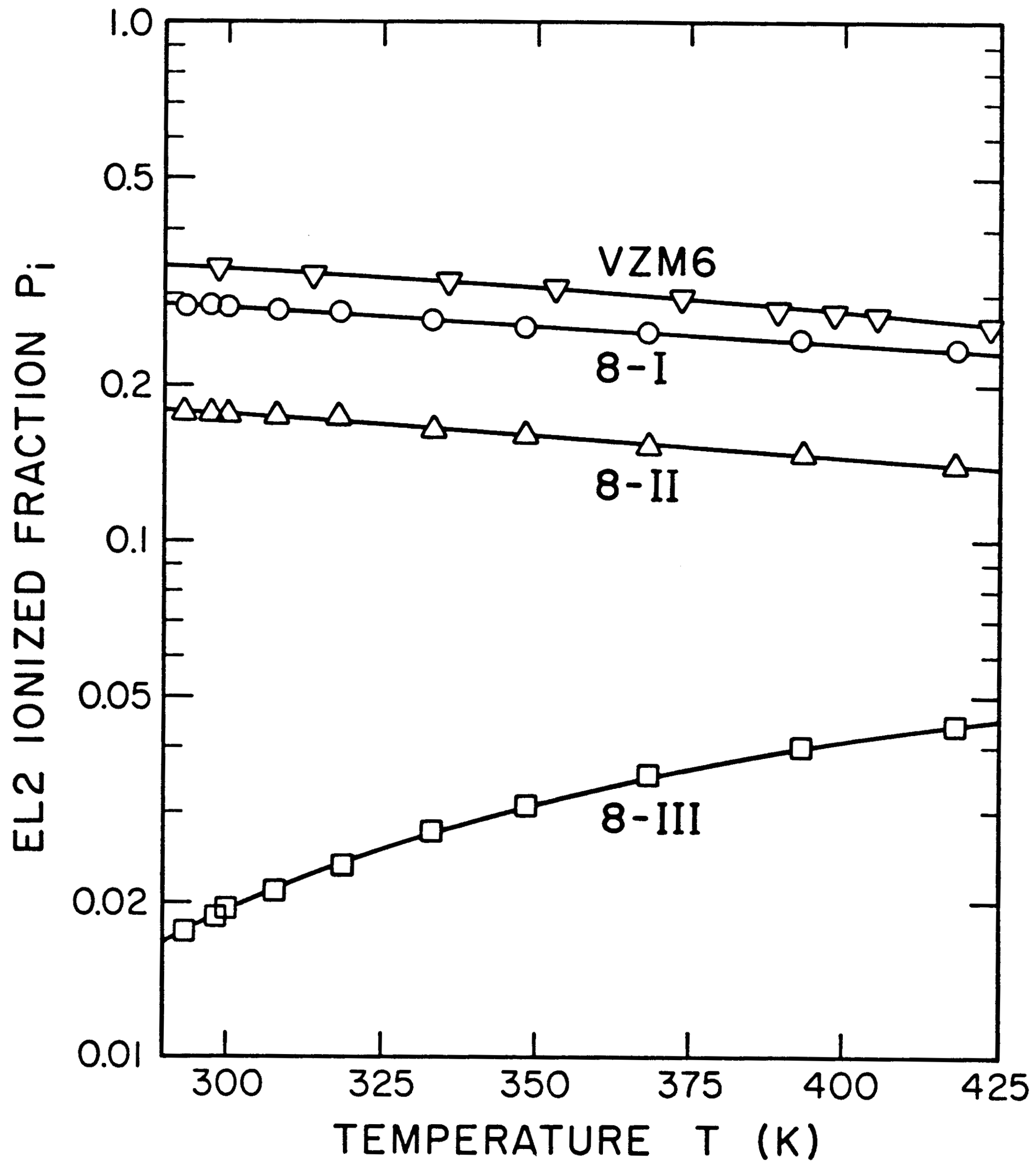


Figure 4-14 EL2 ionization fraction $P_i$ vs temperature for four VZM samples.

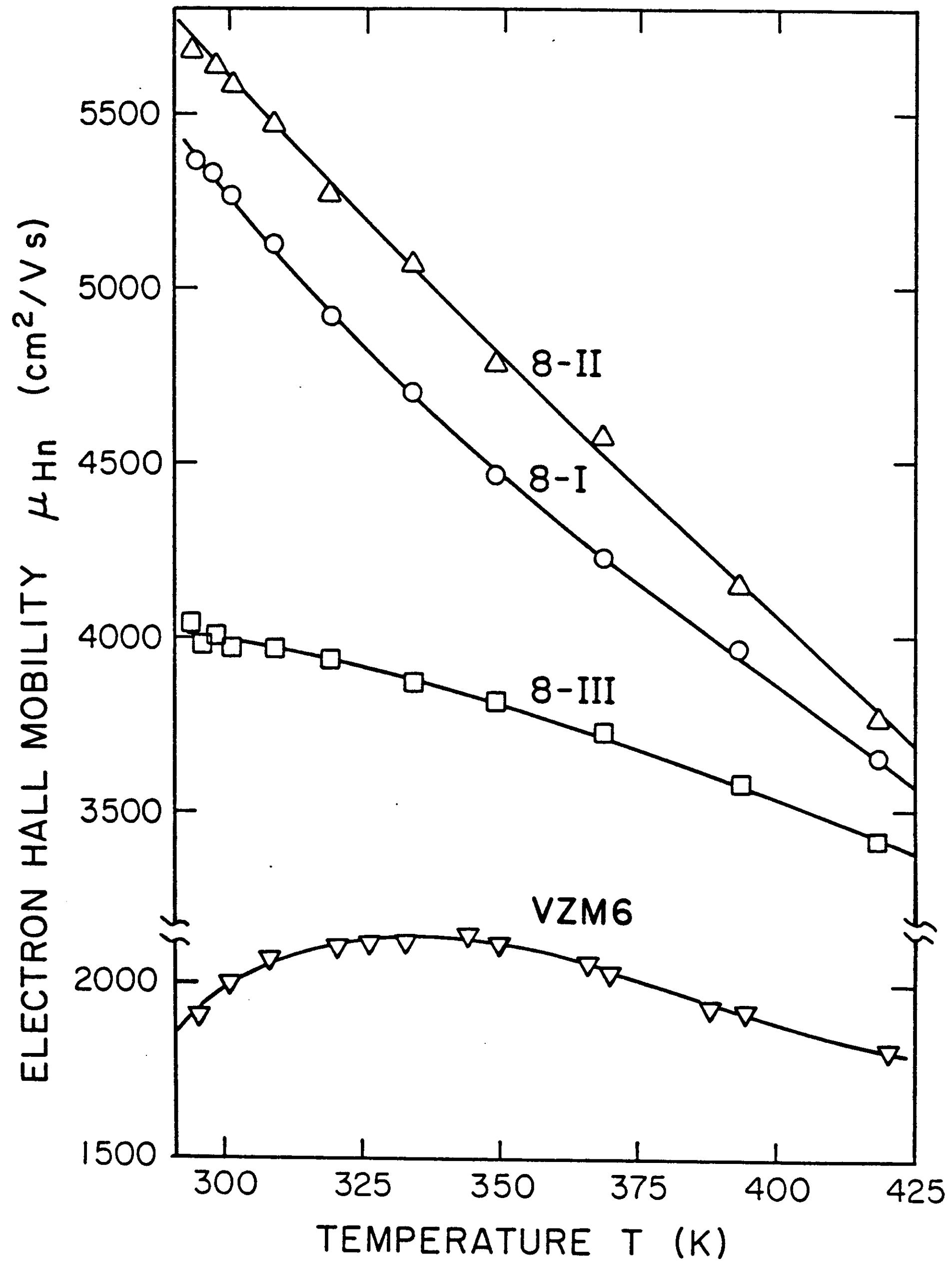


**Figure 4-15 Electron Hall mobility vs temperature for four VZM samples.**

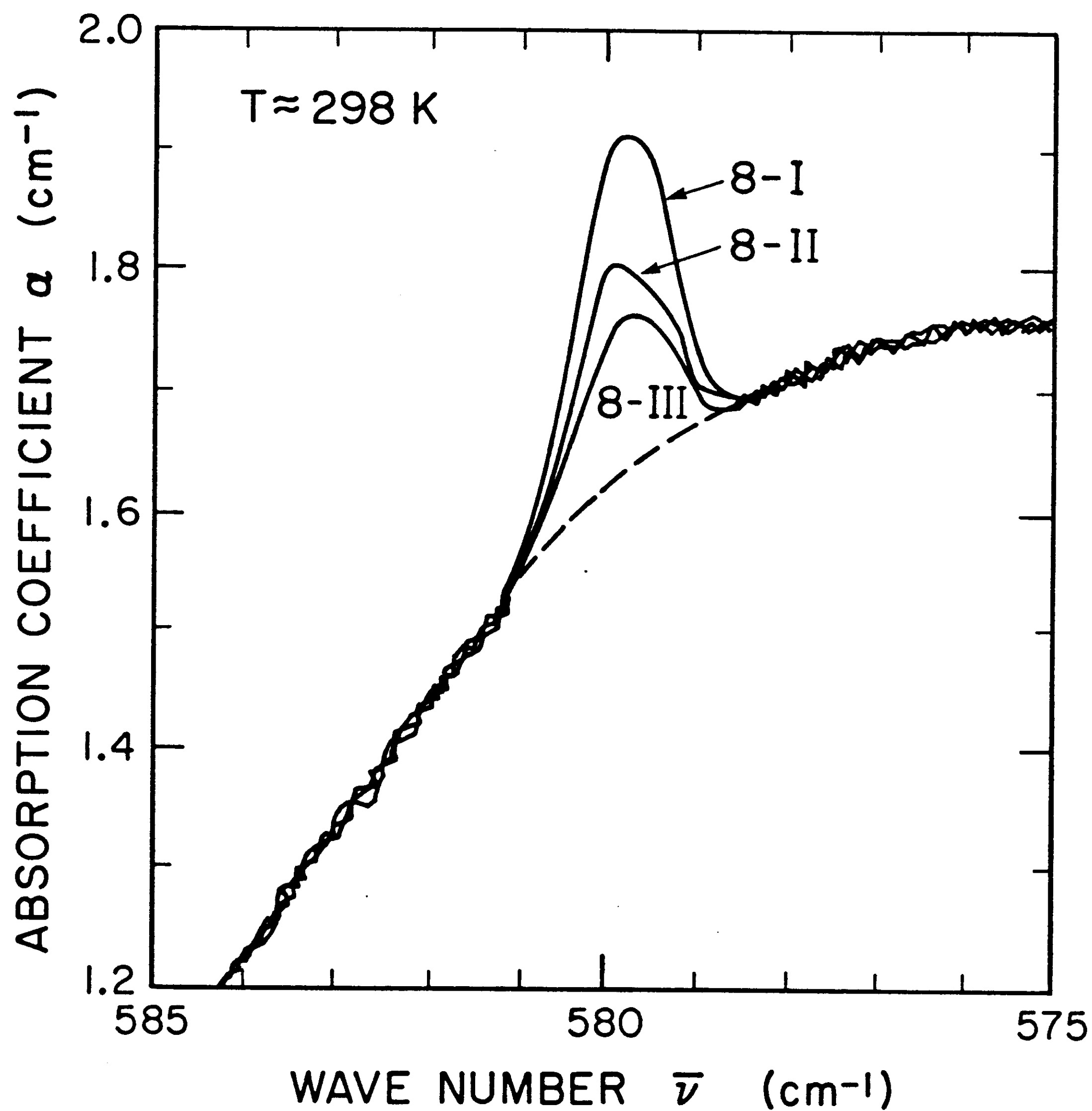


**Figure 4-16 Room temperature carbon LVM absorption band traces for samples (VZM) 8-I to 8-III.**

the segregation coefficient of carbon is larger than unity, and so this impurity is rejected from the melt during growing process. The accumulation of carbon is even more pronounced in a multiple pass zone refined crystal such as ZR13.

While commenting on carbon LVM measurements, it can further be noted at this juncture that the room temperature and low temperature $C_{As}$ LVM data of Fig. 2-5 were obtained for a thick sample of VZM6-III. This material came, of course, from an early trial of the VZM growth technique, without perhaps adequate care in contaminant avoidance, and the *strong* carbon LVM band demonstrable in Fig. 2-5 corresponds to $N_{Carb} \approx 1 \times 10^{16}$ $cm^{-3}$. That substantial carbon content would have made the material P-type had it not also been for the presence of an appreciable quantity of shallow donors (most likely dominated by $Si_{Ga}$). The mutual presence of these shallow acceptors and donors did lower the mobility, as can be seen by the lowest curve in Fig. 4-15.

Nevertheless, the material of VZM6-III *was* semi-insulating, with an ionized EL2 fraction $P_i \approx 0.34$ (see Table 4-4 and Fig.4-14) as inferred from electrical data. As will now be seen, that electrical value for $P_i$ was validated by near-infrared absorption data [17].

We evaluated the room temperature variation of optical absorption coefficient $\alpha$ for the thick sample of VZM6-III over the spectral range $0.7 \leq h\nu \leq 1.3$ eV, as shown earlier in this thesis as Fig.2-6 and repeated here as Fig.4-17. The spectral dependence could be expressed as a linear combination of absorption from photoionization of $EL2^o$ and

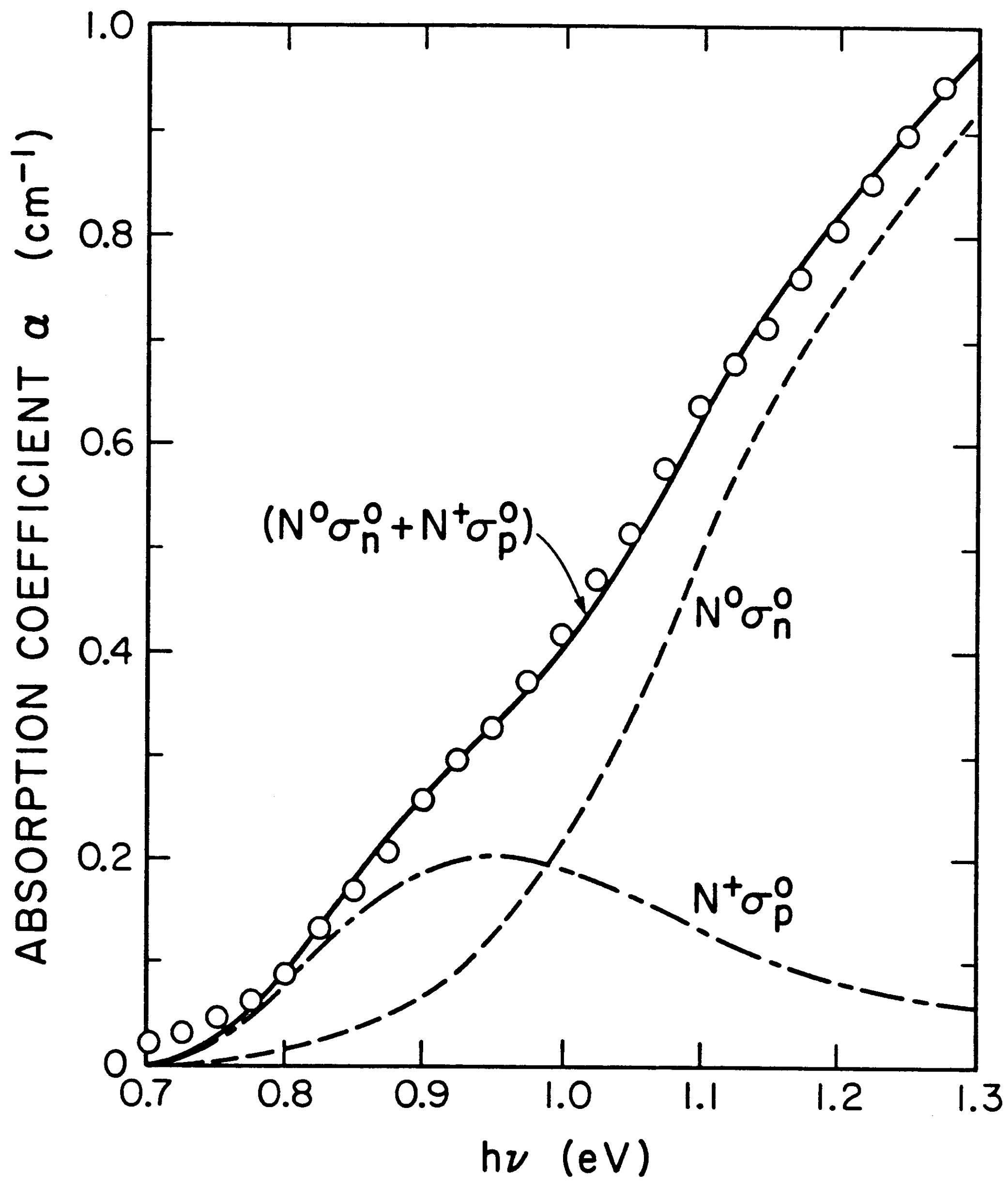


**Figure 4-17 Optical absorption data of VZM6-III shown as a linear combination of absorption from photoionization of $EL2^0$ and photoneutralization of $EL2^+$.**

photoneutralization of $EL2^+$, and gave a result that the total $N_{EL2}$ equals about $1.0 \times 10^{16}$ $cm^{-3}$ with 35% ionized. That is in good agreement with the electrically-derived value $P_i = 0.34$ listed in Tab.4-4.

Fig.4-18 shows a map of the absorption behavior for a polished wafer of VZM6, taken at 1.1 µm. The mean absorption coefficient is $\langle \alpha \rangle = 0.70$ $cm^{-1}$. Since $P_i$ is rather large in this wafer, the optical density is affected to a perceptible extent by $EL2^+$ sites, and this figure cannot be regarded as a true map of $EL2^o$. Indeed, as we know from the above spectral dependence, $N^o \approx 0.65\ N_{EL2} \approx 0.65 \times 10^{16}$ $cm^{-3}$. The map does show, however, that the variance of the (neutral) EL2 population is ~13%. Nevertheless, Fig.4-18 shows no four-fold symmetry (as is sometimes seen for GaAs grown under conditions that encourage dislocation climb) [18,19]. A comparable map made at a wavelength beyond the EL2 absorption range was featureless, showing no stress birefringence fringes [20,21]. This was, indeed, expected in view of the small dislocation density ($N_D \approx 2000$ to 5000 $cm^{-2}$) in the VZM grown GaAs.

Similar maps were made at wavelengths close to the 1.5 µm range for three thin polished wafers from crystal VZM8. Again, and as expected, no stress birefringence was detected. Maps made at a shorter infrared wavelength (1.0 µm) once again found EL2 to be distributed in a manner with no crystallographic significance. Fig.4-19 shows a map made at 1.0 µm for the wafer from crystal section VZM8-I. The mean absorption in this case is consistent with $N_{EL2} \approx 1.0 \times 10^{16}$ $cm^{-3}$, with $P_i \approx 0.28$. For the successive portions of crystal VZM8, the total amount of EL2 detected optically was

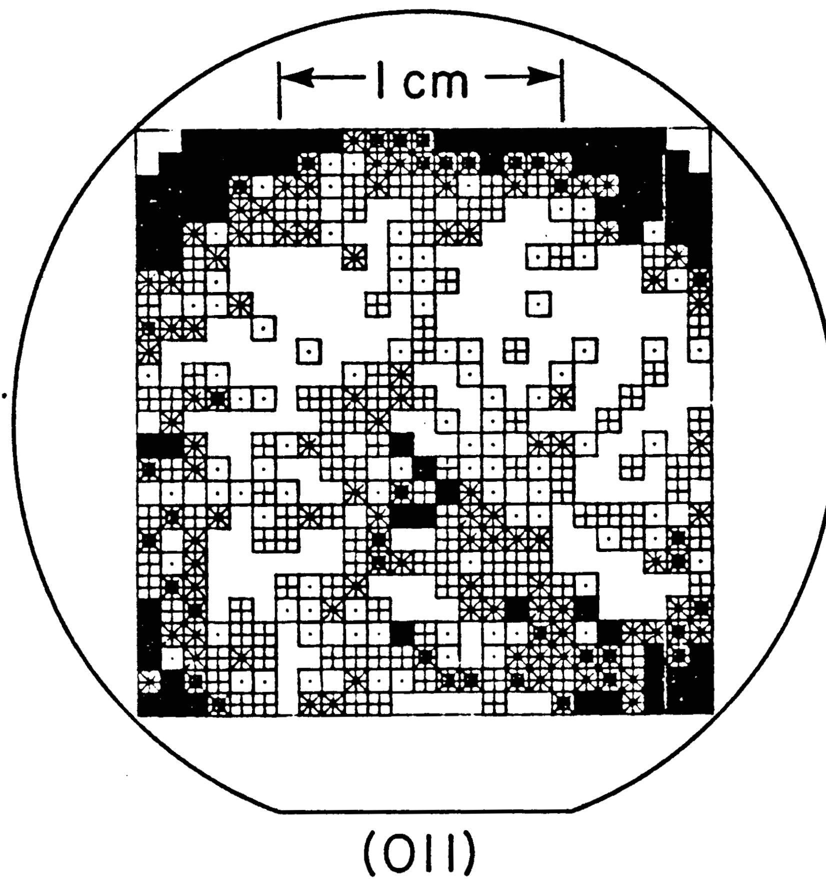


Figure 4-18 Near-IR absorption coefficient map (25 x 25 pixels, for a square 20 mm on a side), made at 1.1 μm for a polished thin wafer (t ≈ 0.6 mm) of crystal VZM6.

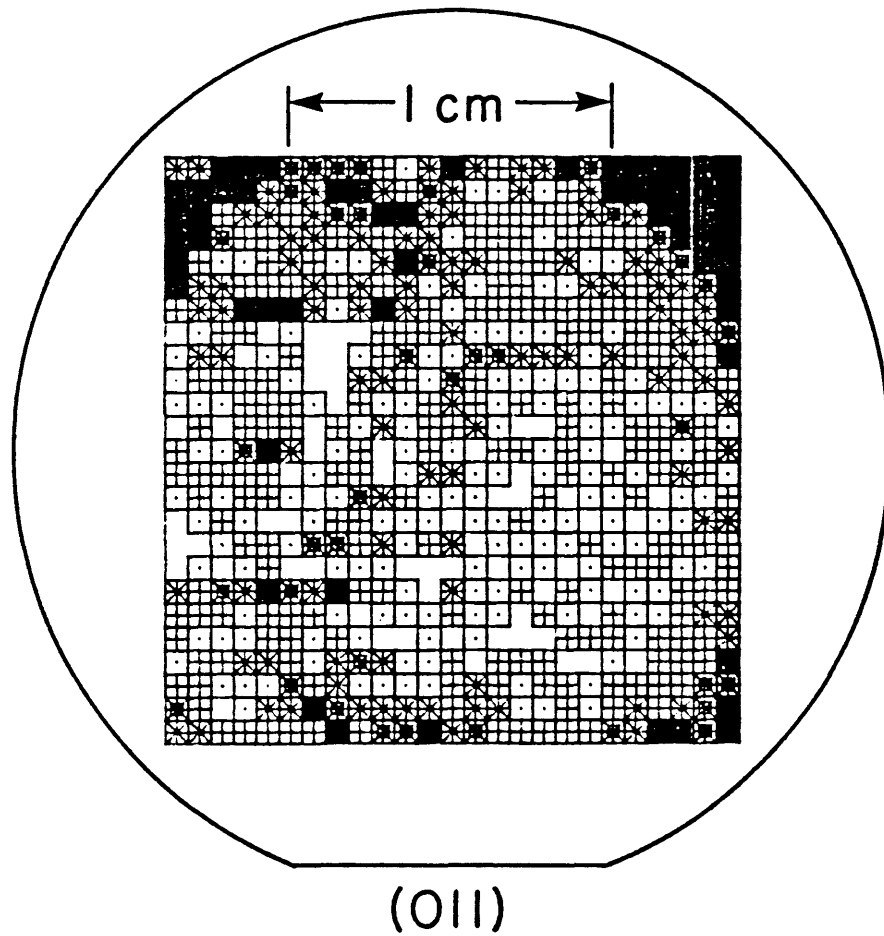


Figure 4-19 Absorption map (25 x 25 pixels, for a square 17.5 mm on a side) made at 1.0 μm for a-0.6 mm-thick wafer from crystal section VZM8-I.

approximately the same, with of course almost all EL2 in the neutral condition for wafer 8-III.

Let us now turn to the multiple pass zone refined crystal ZR13. As previously, we examined the electrical samples from each section of crystal ZR13 by resistivity and Hall coefficient measurement over a temperature range from ~290 K to ~420 K. The Hall coefficients $R_H$ of the first four sections of this crystal (lowest four, counting upwards from the seed) are more than about one-third of the intrinsic value $R_i$. Thus, an ambipolar correction is necessary in deducing the electron concentration $n_0(T)$ and electron Hall mobility $\mu_{Hn}(T)$ from raw as-measured data relating to sections 1 through 4. The electron concentrations and resistivities of for the first several sections of ZR13 are plotted in Figs.4-20 and 4-21. In Fig.4-20, a dashed line was plotted to show how the intrinsic concentration $n_i$ varies over that temperature range, and to demonstrate how close $n_0(T)$ is to intrinsic for the material of sections I to IV. Indeed, for section II, the material crosses over the intrinsic line ($p_0 > n_0$) when the temperature is higher than 385 K. From Fig.4-20 and Tab.4-4, we can see that samples spread from very high-resistivity through failed SI to n-type conducting in crystal ZR13. This is a good indication that some shallow donor impurities (such as silicon and selenium, both of which have less than unity segregation coefficient) were swept from the lowest section towards the top (section VII) by the zone refining process.

Figs.4-22 and 4-23 show, respectively, the Fermi energies and EL2 ionization fractions for the lowest four sections of crystal ZR13. Fig.4-22

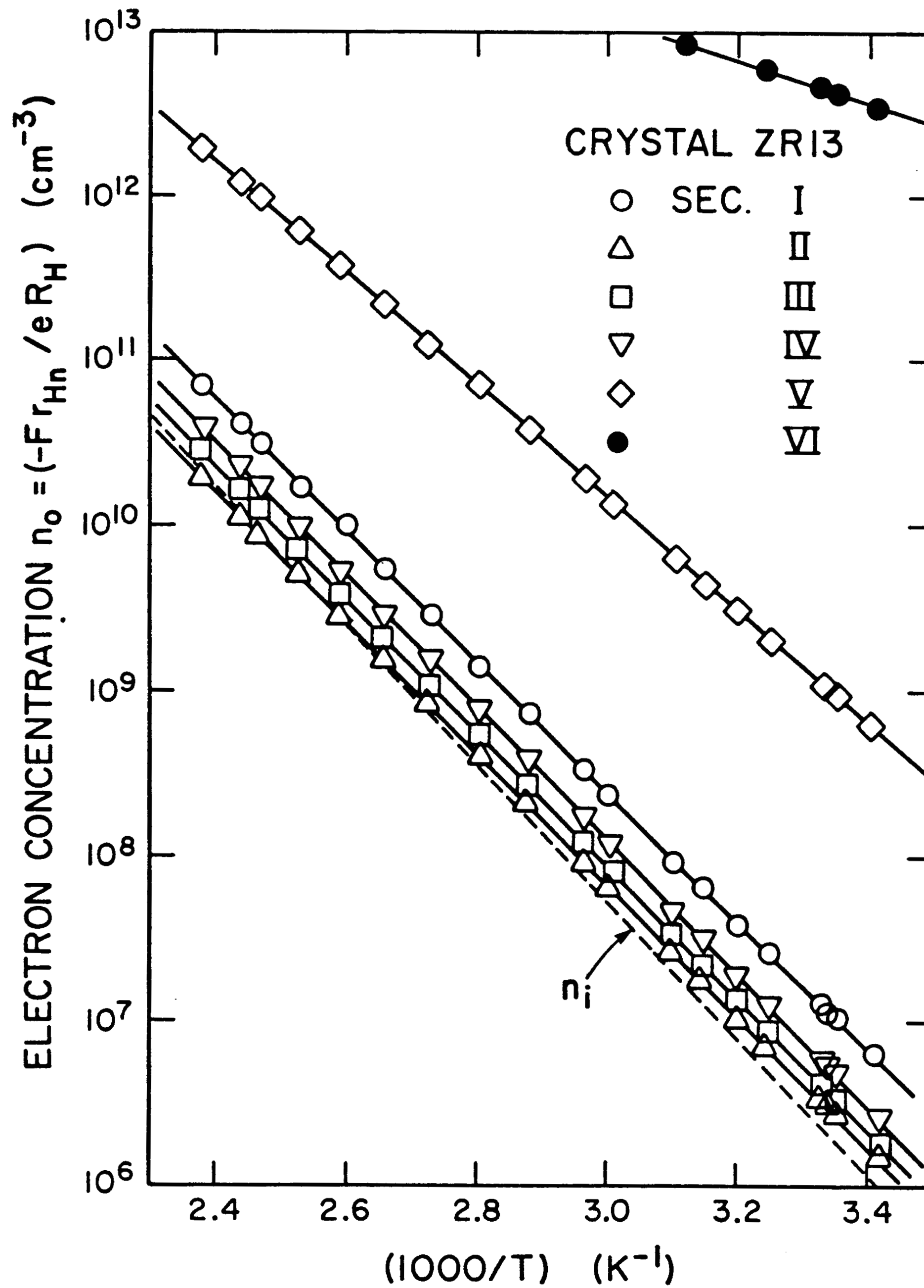


Figure 4-20 Electron concentration versus reciprocal temperature for samples from the first six sections of Crystal ZR13. The dashed line is the intrinsic concentration $n_i(T)$.

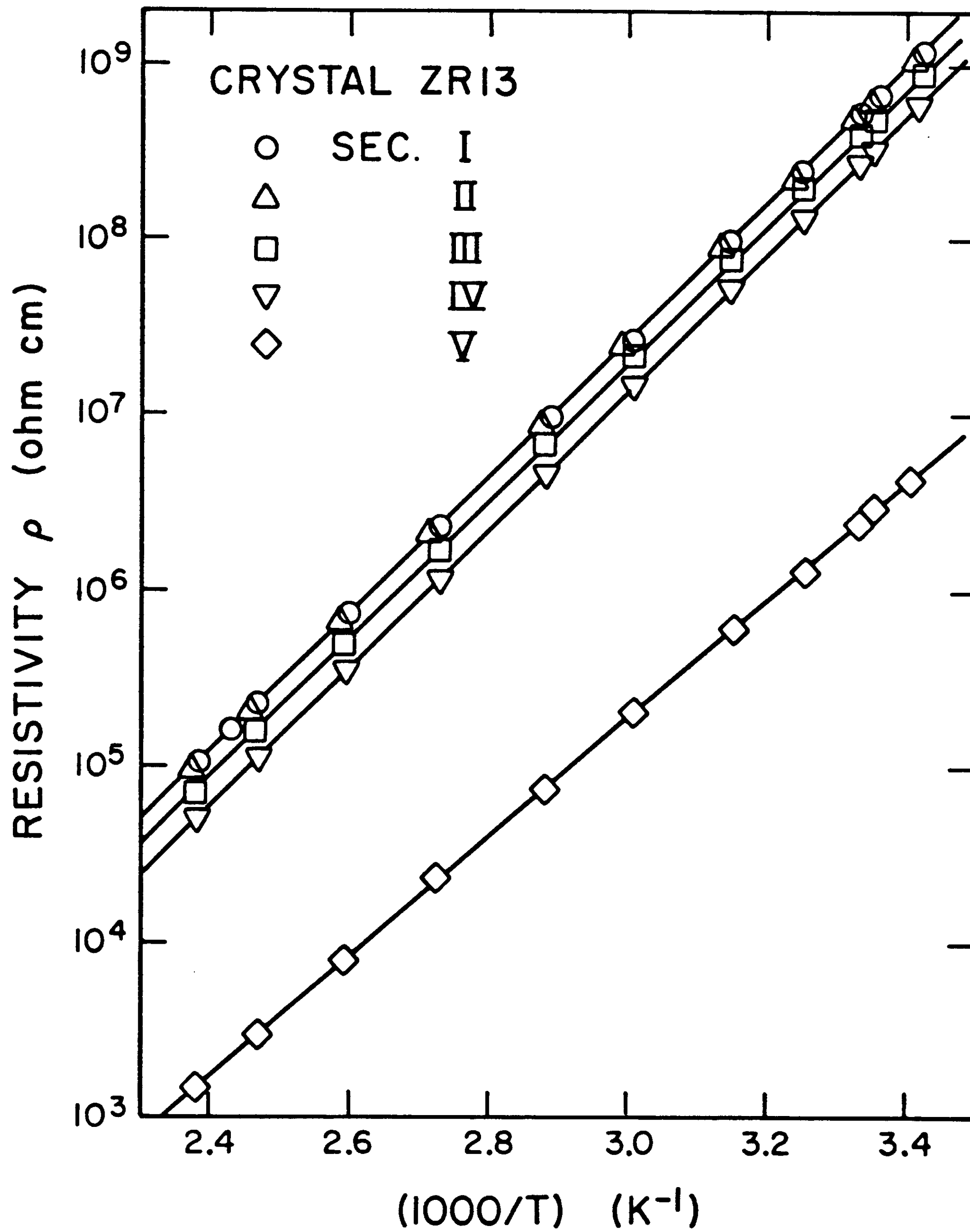


Figure 4-21 Resistivity versus reciprocal temperature for samples from the first four sections of Crystal ZR13.

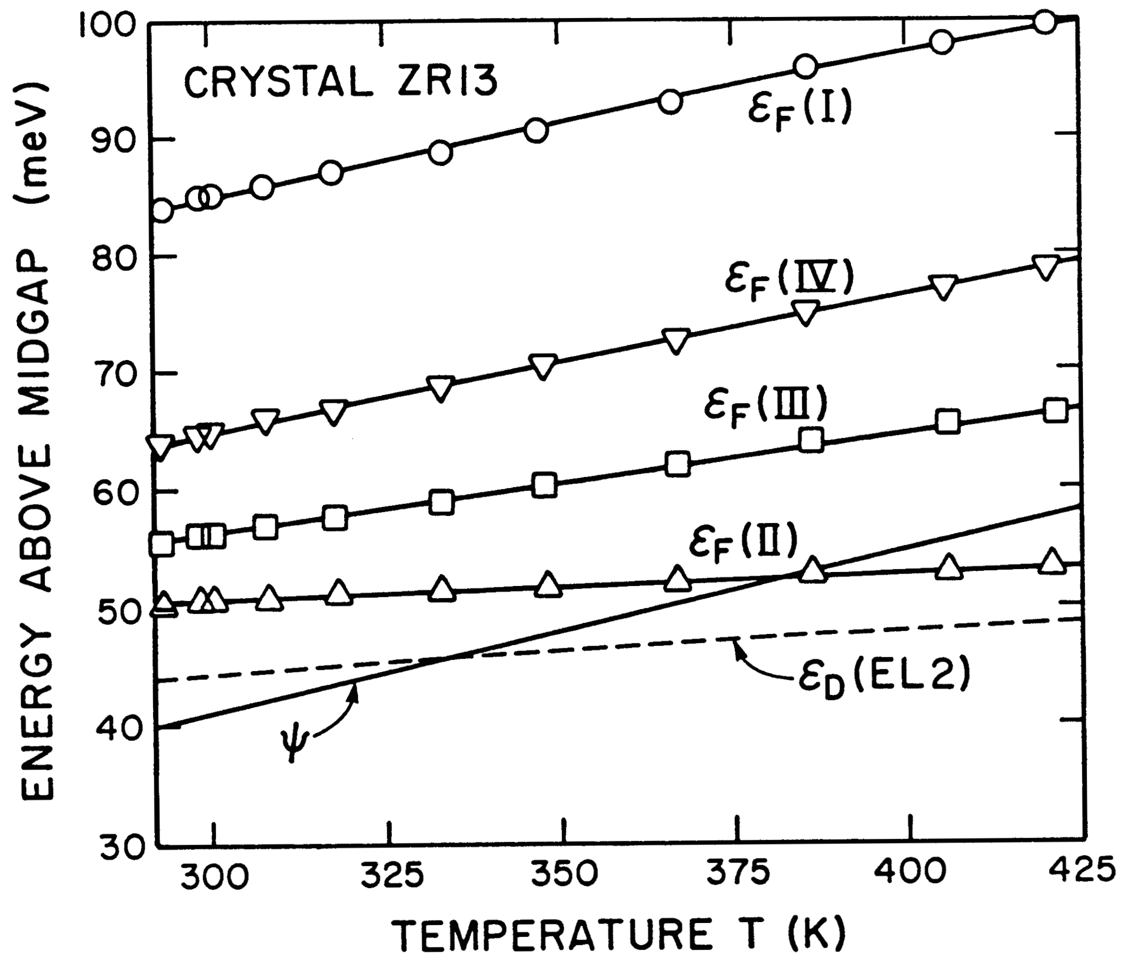


Figure 4-22 Fermi energy $\varepsilon_F(T)$ vs temperature for samples from the first four sections of Crystal ZR13. Midgap is used as the zero reference energy. Also, as before, shows the EL2 energy $\varepsilon_D$, and the intrinsic Fermi energy $\psi$.

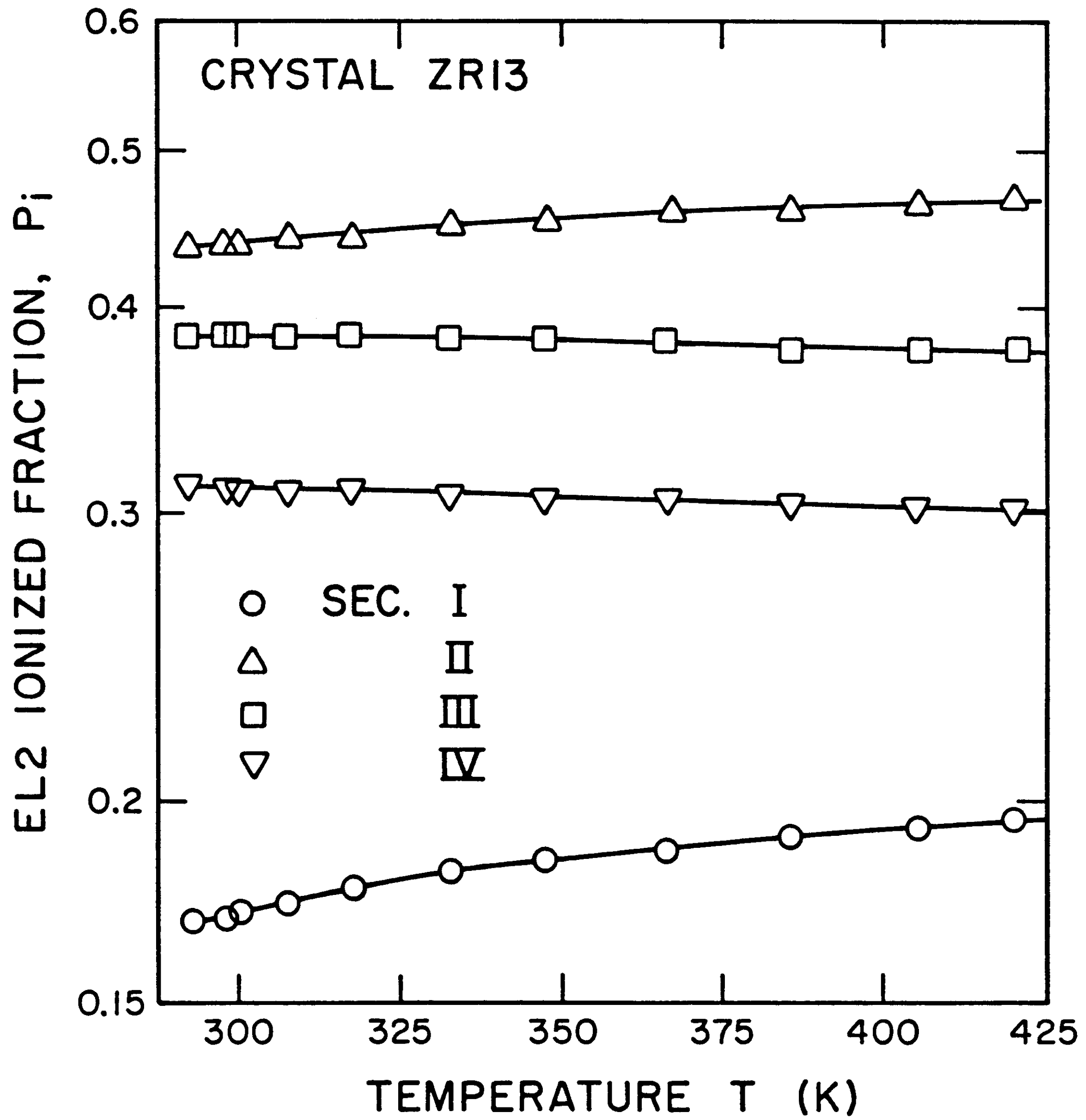


Figure 4-23 The EL2 ionized fraction $P_i$ for samples from the first four sections of Crystal ZR 13.

shows, of course, that $\varepsilon_F(T)$ of section II crosses over the intrinsic Fermi level $\Psi$, clinging parallel to the free energy $\varepsilon_D(T)$ of EL2. Since carbon will be rejected from the following zone during refining, section-I should have the highest $N_{Carb}$. That expectation was confirmed by LVM absorption measurements, for which spectral traces are shown in Fig.4-24. One might expect that most EL2 in section-I will be compensated by the high $N_{Carb}$, but Fig.4-23 shows that section-I has the lowest $P_i$ of the first four sections. The probable reason is that the high concentration of carbon in this seed-cone section was not compensated by the EL2 deep donor alone, but also by some shallow donor impurity dissolved from the seed tip. For one cannot initiate monocrystal growth without melting part of the seed!

Fig.4-25 summarizes the spatial distributions of the optically detectable (essentially neutral) EL2 concentration $N_{EL2^0}$, the *total* EL2 concentration $N_{EL2}$, and the carbon acceptor concentration $N_{Carb}$, along the length of crystal ZR13. Figure 4-25 again shows the effects of zone refining, for instance that carbon has been accumulated in the first few sections. In contrast, EL2 shows fluctuations but not a lengthwise distribution, due to the fact that it is a crystal defect not an impurity. Thus EL2 only reflects the thermal history of the growing process.

As with the single-zone-pass VZM crystals, we have made near-IR absorption maps over sections I to VI in crystal ZR13. None of these reveal any crystallographic significance, just random fluctuations of EL2 content. Again, this is due to a low thermal stress of the zone growth environment, which was also confirmed by a low dislocation density ($N_D \approx 2000$ to 5000

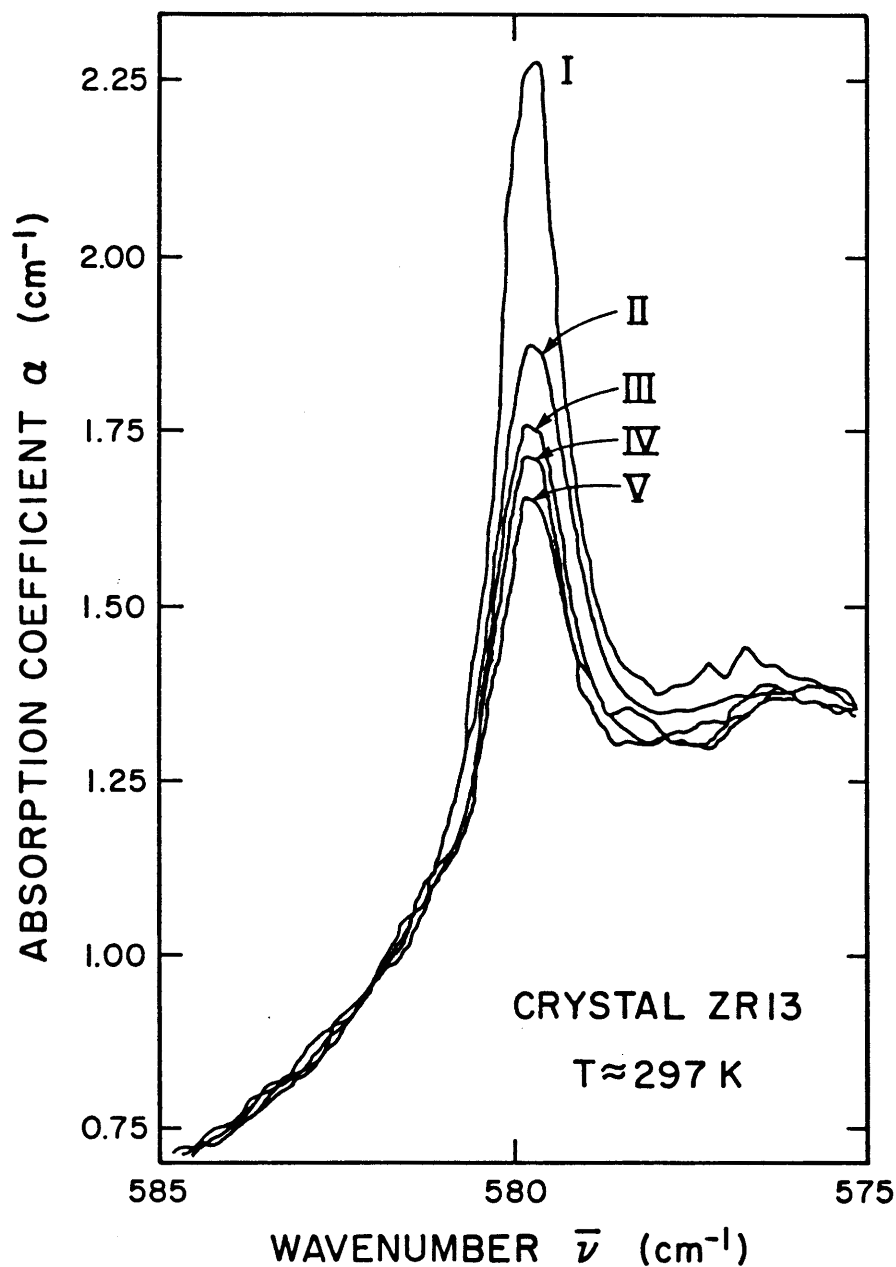


Figure 4-24 FTIR traces of optical absorption for thick samples from the first five sections of Crystal ZR 13, each one taken through the region of the carbon LVM band.

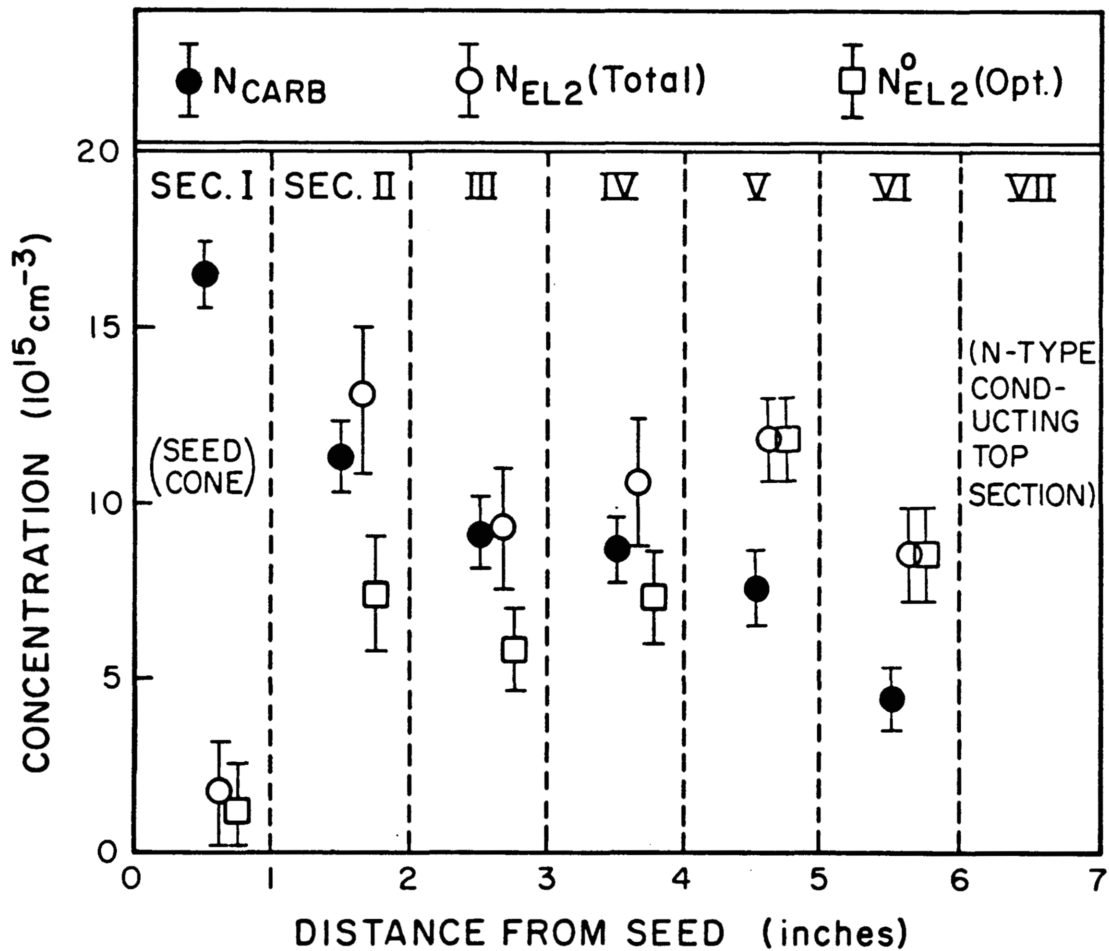


**Figure 4-25** A visual summary, for the various sections of Crystal ZR 13, of the carbon acceptor concentration (from LVM absorption), of the "neutral" EL2 concentration $N^0$ (from 1.0 μm absorption), and of the derived total EL2 concentration $N^0/(1 - P_i)$. The latter of course relies on an electrical determination of $P_i$.

$cm^{-2}$) throughout most of the length of crystal ZR13.

## 4.6 Data for More Recent VZM GaAs

As a footnote to the rather extensive investigation reported in Section 4.5 for two crystals (VZM6 and VZM8) grown by a single-zone-pass vertical zone method, and for one crystal (ZR13) grown with multiple pass zone refining, brief comments are made here on some data for more recently grown VZM GaAs. It is, naturally, a pleasure that those who grow crystals by a new method are able to benefit from data we have provided them, and have produced better material as a result. This has been the case for the VZM program at the US Naval Research Laboratory.

It will have been noted from the results described in Section 4.5 that the early VZM crystals contained more carbon than is necessary or desirable. In preparing the boron nitride boat, and its charge of pre-synthesized GaAs, more recent NRL growth work has had a decrease of contamination (including carbon) as one objective. The thermal conformation of the molten zone has also been adjusted, to achieve a molten zone more nearly a cylindrical section with near-planar lower (solidifying) and upper (melting) surfaces.

Table 4-5 summarizes room temperature results (electrical data converted to the 300.0 K numbers) for samples from two sections of Crystal 25-66N, and for three sections from 25-69N. Significant aspects of the

Table 4-5 300 K properties for Samples from VZM-grown Crystals 25-66N and 25-69N.

| Crystal & Section | 25-66N-II | 25-66N-III | 25-69N-II | 25-69N-III | 25-69N-IV |
|---|---|---|---|---|---|
| Resistivity $\rho$ ($\Omega$ cm) | $7.5 \times 10^7$ | $4.2 \times 10^7$ | $8.6 \times 10^7$ | $4.5 \times 10^7$ | $1.8 \times 10^7$ |
| Hall Mobility $\mu_{Hn} = (R'_H/\rho)$ ($cm^2/V\text{-}s$) | 6035 | 6250 | 6350 | 4920 | 3540 |
| Electron Concentration $n_0$ ($cm^{-3}$) | $1.6 \times 10^7$ | $2.8 \times 10^7$ | $1.35 \times 10^7$ | $3.3 \times 10^7$ | $1.2 \times 10^8$ |
| EL2 Ionized Fraction $P_i$ | 0.137 | 0.086 | 0.163 | 0.073 | 0.022 |
| Optically Detected EL2 Concentration $N_{EL2}^o$ ($cm^{-3}$) | $7.0 \times 10^{15}$ | $7.0 \times 10^{15}$ | $6.5 \times 10^{15}$ | $8.3 \times 10^{15}$ | ---- |

results so tabulated are as follows:

(1) The compensation of EL2 is now relatively small, even starting at Section II of each crystal. The total amount of EL2 is slightly smaller than hitherto, indicating a somewhat changed thermal history from the earlier crystals, but is still perfectly adequate for the role EL2 is called upon to play in SI GaAs [9,10]. (2) The reduction of carbon contamination, through making $P_i$ smaller, provides GaAs which, while still comfortably semi-insulating, has $\rho_{300}$ down below $10^8$ ohm-cm. For our work, this means that an ambipolar correction is not necessary. For any user, the reduced carbon content permits a gratifying improvement of electron Hall mobility - to more than 6,000 $cm^2/V$ s for three of these samples.

Of these five samples, the poorest Hall mobility occurred for the sample from Section IV of Crystal 25-69N. Our temperature-dependent resistivity and Hall data for that sample showed that $P_i$ was not *quite* large enough here for EL2 to *control* the Fermi energy, a situation analogous to that of Sample ZVM8-III (see Fig.4-14). Note that because of the poor mobility, Sample 25-69N-IV would be judged - on the basis of resistivity alone - to meet the "SI specification". One really needs Hall data (versus temperature) to show that (a) $n_0$ at any temperature is larger than proper for SI GaAs, that (b) the activation energy (enthalpy) for $n_0(T)$ is smaller than proper for EL2, and (c) concomitantly that $\varepsilon_F$ and $P_i$ vary with temperature in a manner incompatible with control by EL2.

The values for $P_i$ in Table 4-5 (each derived from the temperature-dependent electrical data) all show $P_i$ to be relatively small, so that one can

expect a spectral trace of near-infrared absorption to be *dominated* by the photoionization of neutral EL2 (cf. the $N^o\sigma_n^o$ curve in Figs. 2-6 and 4-17). This did indeed prove to be the case. As an example, Fig. 4-26 shows absorption coefficient $\alpha$ versus wavelength for a thick sample ($t \sim 3$ mm) of Crystal 25-66N, Section III, as measured at room temperature. Data for this figure were taken of the relative transmittance ($I_t/I_o$) at 0.5 nm intervals over the range 950 - 1500 nm (a total of 1100 points, each recorded digitally) and the data were then converted into $\alpha$ by means of Eq.(2-4), making correction for reflectance and for multiple reflections. Despite the substantial thickness of this sample, multiple reflections are significant at the longer wavelengths, where $(\alpha t) \ll 1$.

These same data for Sample 25-66N-III were then converted into the corresponding plot of $\alpha$ versus $h\nu$, with the result shown in Fig. 4-27. The dashed line superimposed is the $N^o\sigma_n^o$ behavior for EL2 photoionization alone, scaled according to Martin's room temperature scale [8] for $N_{EL2^o} \approx 7 \times 10^{15}$ cm$^{-3}$. By means of this near-IR absorption analysis, values for $N_{EL2^o}$ were thus obtained for four of the five sample regions listed in Table 4-5, and account for the numbers listed in that final row of the table.

This chapter can thus conclude with words of encouragement for the quality of SI GaAs as produced by both the VB method (Section 4.3), and the VZM method (Sections 4.5 and 4.6). Neither of these methods is likely, in the near future, to *replace* the well-known and widely used LEC method, but both show promise. The VB method (and also the VGF method of AT&T Bell Laboratories and of AXT) has recently been shown able to produce 3"

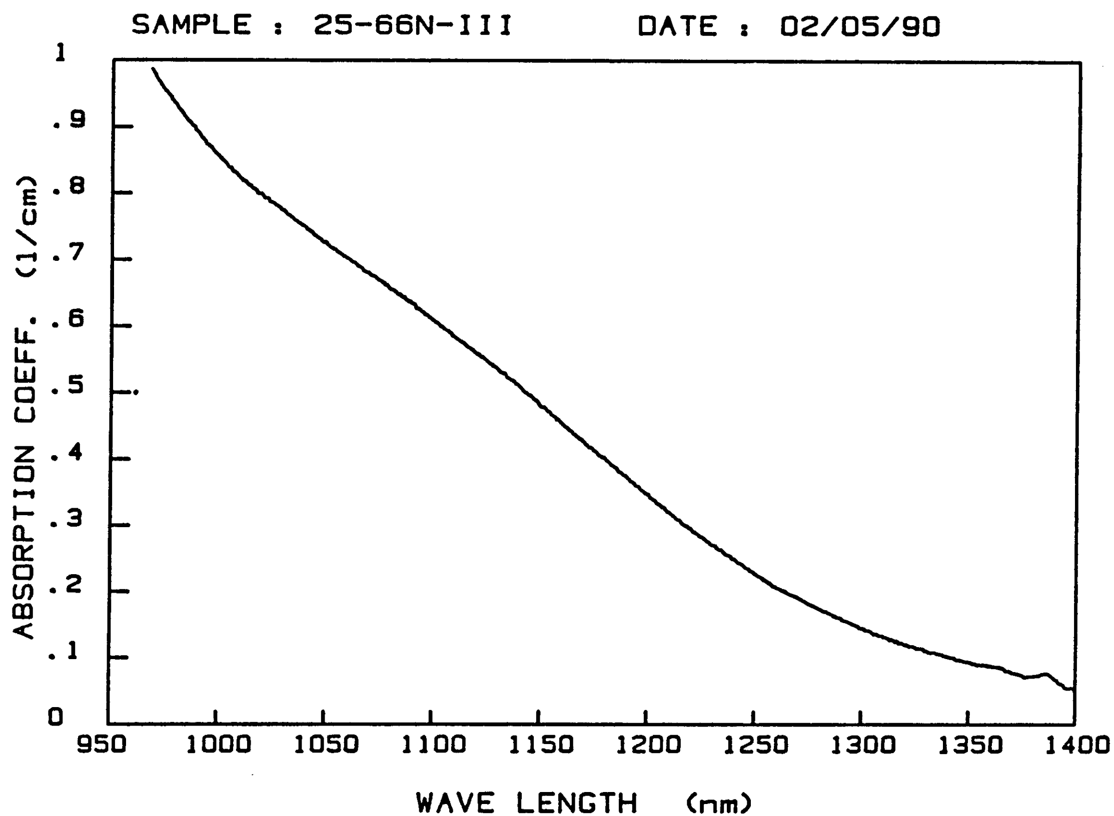


Figure 4-26 Room temperature optical absorption vs wavelength, for a sample from VZM-grown Crystal 25-66N. See also Fig. 4-27.

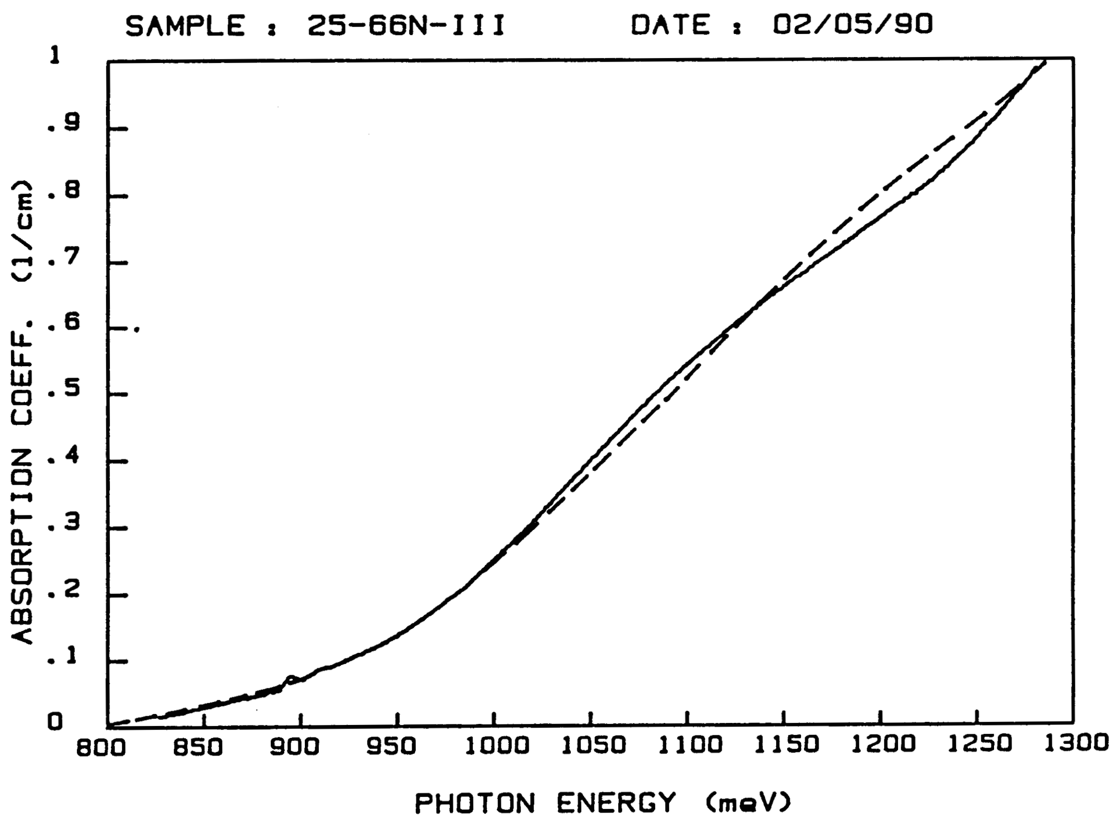


Figure 4-27 The absorption data from Fig. 4-26, converted into a plot of $\alpha$ vs $h\nu$. The dashed curve shows the behavior predicted for EL2 photoionization alone, with $N^0 = 7 \times 10^{15}$ $cm^{-3}$ if the scaling of Martin [8] is used.

diameter SI monocrystals, and an extension to 4" growth in the future seems almost inevitable. The VZM growth at NRL has used a small-scale furnace, with the crystal diameter constrained to ~30 mm, and that small-scale work has shown the method capable of producing SI material with consistency, and of pleasing quality. Whether the VZM method for GaAs will in the future be adapted to a much larger diameter (as has happened with silicon float-zone growth over the years) will be interesting to watch.

One reason why several methods for SI GaAs growth should be kept viable is that "SI GaAs" is not just one commodity. In a recent invited paper at the 1990 Semi-Insulating III-V Materials conference, Sylvie Martin [22] of the Philips LEP GaAs foundry in France pointed out that the qualification processes of SI GaAs for digital applications and microwave analog applications are quite different; one depending on MESFET $V_{th}$ consistency, the other on microwave noise level. She noted that a crystal which fails the digital qualification procedure may be admirable for analog use, and *vice versa*. The matter of dislocations - unimportant for MESFETs but of grave import for laser substrates - is a further reason why less conventional growth methods that can provide near-dislocation-free SI GaAs merit further consideration.

## REFERENCES: CH.4


1. J. L. Robert, B. Pistoulet, A. Raymond, J. M. Dusseau, and G. M. Martin, J. Appl. Phys. **50**, 349 (1979)
2. B. Pistoulet, P. Girard, and G. Hamamdjian, J. Appl. Phys. **56**, 2268 (1984)
3. J. S. Blakemore, J. Phys. Chem. Solids 49, 627 (1988)
4. G. M. Martin, A. Mitonneau, and A. Mircea, Electronics Letters, **13**, 191 (1977)
5. M. Taniguchi and T. Ikoma, Inst. Phys. Conf. Ser. **65**, 65 (1982)
6. M. L. Gray, L. Sargent, J. S. Blakemore, J. M. Parsey, and J. E. Clemans, J. Appl. Phys. **63**, 5689 (1988)
7. D. Rumsby, I. Grant, M. R. Brozel, E. J. Foulkes, and R. M. Ware, in *Semi-Insulating III-V Materials: Kah-nee-ta1984*, edited by D. C. Look and J. S. Blakemore, (Shiva, Nantwich, UK, 1984), p. 165
8. G. M. Martin, Appl. Phys. Lett. **39**, 747 (1981)
9. R. A. Morrow, J. Appl. Phys. **62**, 3671 (1987)
10. R. Anholt and T. W. Sigmon, J. Appl. Phys. **62**, 3995 (1987)
11. W. G. Pfann, Trans. AIME **194**, 747 (1952)
12. P. H. Keck and M. J. E. Golay, Phys. Rev. **89**, 1297 (1953)
13. E. M. Swiggard, J. Electrochem. Soc. **114**, 976 (1967)
14. E. S. Johnson, J. Crystal Growth **30**, 249 (1975)
15. E. M. Swiggard, J. Crystal Growth **94**, 556 (1989)
16. L. Sargent and J. S. Blakemore, Appl. Phys. Lett. **54**, 1013 (1989)

17. J. S. Blakemore, L. Sargent, R-S. Tang, and E. M. Swiggard, Appl. Phys. Lett. **54**, 2106 (1989)

18. P. Dobrilla and J. S. Blakemore, J. Appl. Phys. **58**, 208 (1985)

19. P. Dobrilla and J. S. Blakemore, J. Appl. Phys. **60**, 169 (1986)

20. P. Dobrilla and J. S. Blakemore, Appl. Phys. Lett. **48**, 1303 (1986)

21. L. Sargent, P. Dobrilla, R.-S Tang, and J. S. Blakemore, in *Defect Recognition and Image Processing in III-V Compounds ; Monterey, 1987*, edited by E. R. Weber (Elsevier, Amsterdam, Netherlands, 1987), p.55

22. S. Martin, Invited paper C.1. at Sixth Conference on Semi-insulating III-V Materials (Toronto, May 1990)

# CHAPTER 5

# RESULTS FOR DOPED GaAs CRYSTALS

## 5.1 Dopants for High-Resistivity GaAs

A semi-insulating material can be defined as a high-resistivity semiconductor crystal with the Fermi level located in a position near midgap. Due to the non-zero residual impurity and defect concentrations in a real GaAs crystal, the near-midgap Fermi level can not be expected to arise from a genuinely intrinsic condition, but is actually a result of suitable compensation. Therefore, even so-called "undoped" (or more practically the "unintentionally doped") SI GaAs still depends on a small amount of carbon dopant to compensate the residual shallow donors, and also to compensate part of the deep donor EL2. That allows the Fermi level to be pinned by this dominant deep level defect. However, control of $\varepsilon_F$ near midgap in "undoped" GaAs was historically only an occasional accident during the years of growth from silica boats and crucibles: the pre-PBN era.

As we mentioned before, Cr was the first successful dopant to make GaAs consistently semi-insulating [1]. In such a crystal, Cr acceptors are able to compensate the shallow Si donors with concentration from $\sim 10^{15}$ to $\sim 10^{17}$

$cm^{-3}$ which come from a silica crucible during a melt growth process. If the concentration of Cr is high enough to make $N_{Cr} > (N_{Si} - N_a)$ (where $N_a$ adds over all residual shallow acceptors), then the Fermi level will be firmly locked at the $Cr^{+3}/Cr^{+2}$ level which is located close to the band gap center [2]. In fact, Cr is not the only deep level in a GaAs crystal, since the native defect deep donor EL2 is also present in a melt-grown crystal. Because the energy level of $EL2^{o}/EL2^{+}$ is slightly lower than that of $Cr^{+3}/Cr^{+2}$ for T < 450 K [2,3], there are two kind of SI conditions which can exist. Firstly, when

$$N_a > N_d \qquad (5\text{-}1)$$

(shallow residual acceptors outnumber all types of shallow donors including silicon), and also

$$N_{EL2} > (N_a - N_d) \qquad (5\text{-}2)$$

then EL2 are partially ionized, and the Fermi level is locked near to the $EL2^{o}/EL2^{+}$ level. In this case, most (but not all) Cr are still neutral (unoccupied $Cr^{+3}$ state) since the Fermi level is slightly below the $Cr^{+3}/Cr^{+2}$ level.

A second possible condition is for the Fermi level to be locked at the $Cr^{+3}/Cr^{+2}$ level when

$$N_d > N_a \qquad (5\text{-}3)$$

and

$$N_{Cr} > (N_d - N_a). \qquad (5\text{-}4)$$

In this case, the $Cr^{+3}/Cr^{+2}$ level is partially ionized, but most of the EL2 are still neutral (occupied $EL2^{o}$ state) because the Fermi level is above them. Other than these two conditions, the Fermi level will sit on one of the

shallower energy levels. The resulting crystal can be failed SI, or just P-type, or even N-type conducting.

Beside C and Cr, there are some other dopants used occasionally in modern semi-insulating crystal growth activity. One such dopant is iron, as the $Fe_{Ga}$ acceptor. This is not a "new" dopant at all, but it has never received much attention before, because the highest (P-type) resistivity a Fe-doped crystal can achieve is only about $10^5$ Ω-cm at room temperature [4]. In this case, the Fermi level is pinned at the $Fe^{3+}/Fe^{2+}$ level, which we shall call $\varepsilon_A$. Then $(\varepsilon_A - \varepsilon_v) \approx 0.5$ eV [5,6].

Consider now a crystal containing some EL2, small amounts of residual shallow donors and acceptors, no chromium, and a modest amount of iron. If the dose of iron is properly reduced, it allows one to grow a SI Fe-doped GaAs crystal. In this situation, the Fermi energy is actually controlled by the $EL2^o/EL2^+$ level instead of the $Fe^{3+}/Fe^{2+}$ level. Unlike Cr, this $Fe^{3+}/Fe^{2+}$ level lies well below the $EL2^o/EL2^+$ level. This allows each Fe acceptor to ionize an EL2 donor. When Eq.(5-1) is obeyed, the Fermi level in Fe-doped GaAs can be located at three possible positions:

(a) If $(N_a - N_d) < (N_{EL2} - N_{Fe})$, all iron acceptors (approximately) are ionized (occupied as the $Fe^{2+}$ state) and the EL2 are partially ionized with $N_{EL2^+} \approx N_{Fe} + (N_a - N_d)$. In this case, $\varepsilon_F$ is pinned at the $EL2^o/EL2^+$ level, and the crystal is highly semi-insulating.

(b) If $(N_a - N_d) > (N_{EL2} - N_{Fe})$, approximately all EL2 are empty (ionized), and the iron centers are partially ionized with $N_{Fe^{2+}} \approx N_{EL2} - (N_a - N_d)$. In this case, $\varepsilon_F$ is pinned at the $Fe^{3+}/Fe^{2+}$ level, and the crystal is P-type but of

high resistivity.

(c) If $N_{EL2} < (N_a - N_d)$, all EL2 and Fe states are empty, $\varepsilon_F$ falls to a shallower acceptor level, and the crystal is just P-type conducting.

On the other hand, when Eq.(5-3) is obeyed, the Fermi level can also be located at three possible positions:

(d) If $(N_d - N_a) < (N_{Fe} - N_{EL2})$, almost all EL2 are empty (ionized to $EL2^+$), while iron centers are partially ionized to the $Fe^{2+}$ ionized (or occupied) state. Then $N_{Fe^{2+}} \approx N_{EL2} + (N_d - N_a)$, $\varepsilon_F$ is pinned at the $Fe^{3+}/Fe^{2+}$ level, and the crystal is P-type high-resistivity.

(e) If $(N_d - N_a) > (N_{Fe} - N_{EL2})$, almost all Fe are empty (ionized to $Fe^{2+}$), and the EL2 are partially ionized with $N_{EL2^+} \approx N_{Fe} - (N_d - N_a)$. Then $\varepsilon_F$ is pinned at the $EL2^0/EL2^+$ level, and the crystal is highly semi-insulating.

(f) If $N_{Fe} < (N_d - N_a)$, all EL2 and Fe states contain electrons (i.e., the charge states $EL2^0$ and $Fe^{2+}$), $\varepsilon_F$ is just floated around a shallower donor level, and the crystal is N-type conducting.

### 5.1.1 Some Contrasts Between Carbon and Iron as Acceptors

Carbon is a Group-IV element, present predominantly as the $C_{As}$ monovalent shallow acceptor, with the outer electron shell occupancy giving the acceptor nature. In contrast, iron is a 3d transition element, and as $Fe_{Ga}$ it is partial occupancy of the 3d subshell which provides dopant impurity character. When Fe as $Fe_{Ga}$ provides three electrons (the same as

Ga) for bonding, its "lattice-neutral" charge state in GaAs is $Fe^{3+}$ ($3d^5$). Due to Coulomb barriers, Fe prefers to substitute for a Group-III Ga atom rather than the Group-V As atom, and there is no definitive evidence of any interstitial Fe impurity existing in GaAs crystals [6].

The solid solubility for transition metals in III-V materials is usually low compared with that of shallow impurities [7]. The "limit" is around $10^{17}$ $cm^{-3}$ for Fe compared with $10^{18}$ $cm^{-3}$ for C in GaAs. Therefore, there is less chance for iron doping to overpower EL2 than in a deliberately carbon-doped crystal. Nevertheless, results to be shown in Section 5.2 show that iron doping *can* make GaAs high resistivity P-type, the scenario just described as (b), with $N_{Fe^{2+}} \approx (N_{EL2} + N_d - N_a) > 0$.

Note also that iron is not a hydrogen-like impurity, so the wave function is more localized than for a shallow acceptor in GaAs. Therefore, the electronic cross-section is smaller and thus the mobility is less impaired by Fe impurities than by (for example) carbon impurities in GaAs.

From Chapter 4, we learned that (in contrast to the residual shallow donor impurities) carbon has a larger than unity segregation coefficient. Carbon is thus rejected from the melt during a growing process. Therefore, the carbon concentration decreases along the crystal growth direction, while other residual shallow donor concentrations increase. Because of this, only the first portion of a crystal can get properly compensated for C-doped GaAs. However, the segregation coefficient of Fe is less than unity [4]. And so the iron concentration has the same variant tendency from seed to tail as other impurities in a GaAs crystal. There is thus more of a chance for

compensation to remain under control for an appreciable part of the length of a Fe-doped crystal. It is still not possible for this to be achieved over *most* of the length, since that compensation depends on the iron itself (sub-unity segregation coefficient), EL2 (not subject to segregation rules), and shallow impurities of which some have a sub-unity segregation coefficient but carbon does not!

Having described - but hopefully not obscured - the range of phenomena that deep-level doping may achieve, some data for Fe-doped and Cr-doped GaAs are now presented and discussed in Section 5.2.

## 5.2 Electrical and Optical Data for Doped High-Resistivity GaAs

Let us begin with resistivity and Hall data, taken versus temperature. The first data shown are for a Fe-doped crystal which was grown at AT&T by the VGF method. Possibly by accident, this crystal (denoted Fe-A) contained enough iron dopant to come out not semi-insulating but high-resistivity P-type ($\rho_{300} = 3.6 \times 10^4\ \Omega$-cm). That is to say, the relative proportions of shallow dopants, iron, and EL2 met the criteria listed as (b) in Section 5.1, with $N_{Fe^{2+}} \approx (N_{EL2} + N_d - N_a) > 0$. Such material also contains a finite concentration $N_{Fe^{3+}} = (N_{Fe} - N_{Fe^{2+}}) > 0$ of $Fe_{Ga}$ acceptors in the lattice-neutral charge state.

Fig.5-1 shows the resistivity, and the free hole concentration, in the same reciprocal temperature plot. The resistivity varies quite linearly with

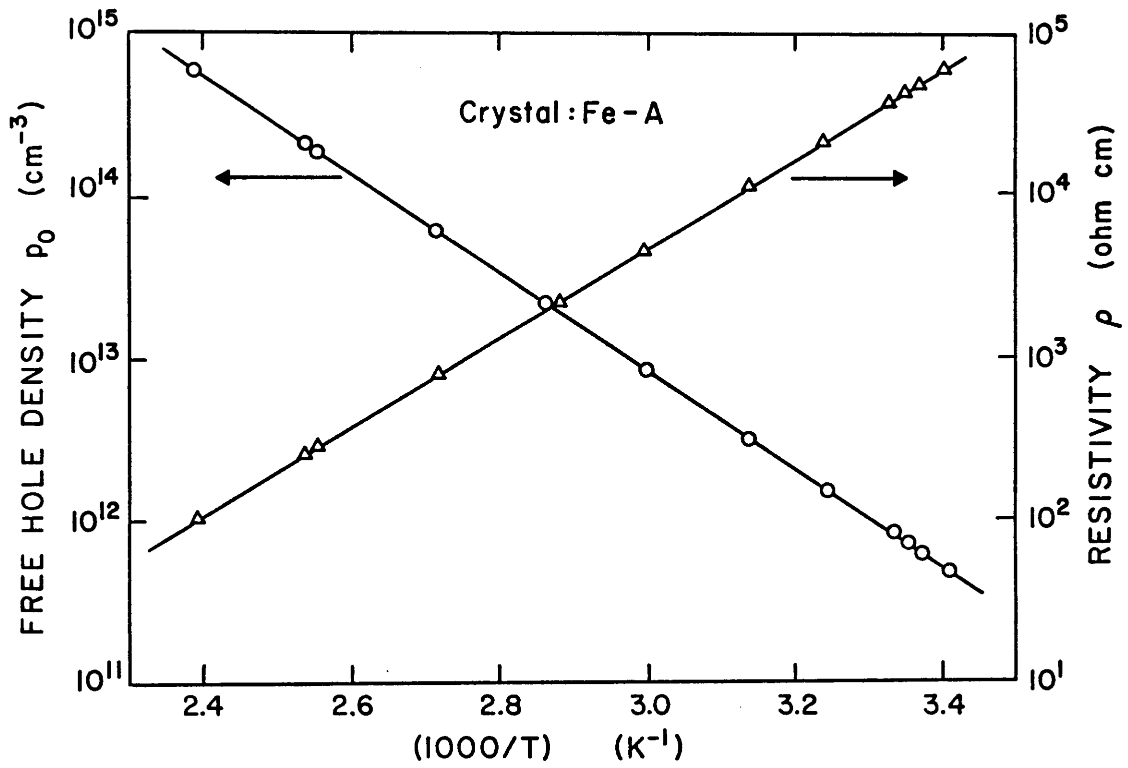


**Figure 5-1** Hole density and resistivity vs reciprocal temperature for Crystal Fe-A.

this semi-logarithmic scale and can be fitted as

$$\rho = 3.15 \times 10^{-5} \exp(0.54\ \mathrm{eV}/kT) \quad \Omega\text{-cm}. \qquad (5\text{-}5)$$

For the hole concentration, we can adopt the form used in Chapter 4, and model $p_0$ as

$$p_0 = 3.3 \times 10^{17}\, T^{3/2} \exp(-0.555\ \mathrm{eV}/kT) \quad \mathrm{cm}^{-3} \qquad (5\text{-}6)$$

with an enthalpy slope of $\Delta H = 0.555$ eV. This value is slightly higher than the activation energy (0.52 eV) quoted by Haisty and Cronin [1]. We know that the activation enthalpy $\Delta H$ is a quantity which usually over-estimates the free energy difference between $\varepsilon_A$ and $\varepsilon_v$.

The 300 K Hall mobility is around 300 cm$^2$/v-sec, which is a standard value for P-type GaAs. Fig.5-2 shows the temperature dependent Hall mobility data for crystal Fe-A. The Fermi level for a non-degenerated P-type semiconductor can be expressed as

$$\varepsilon_F(T) = \psi - kT \ln(p_0/n_i) \qquad (5\text{-}7)$$

or

$$\varepsilon_F(T) = \varepsilon_v + kT \ln(N_V/p_0) \qquad (5\text{-}8)$$

If one chooses the valence band edge $\varepsilon_v$ as zero energy reference, then one can plot the Fermi level and other energies of interest, versus temperature, as shown in Fig.5-3. The $\varepsilon_F$ data show clearly that the $Fe^{+3}/Fe^{+2}$ level is in control, with the Fermi energy "pinned" almost 0.3 eV below midgap.

Having established the P-type high resistivity nature of Crystal Fe-A from the electrical measurements versus temperature, it then became of interest to learn about the optical characteristics of this $Fe^{+3}/Fe^{+2}$ controlled material. Accordingly, the optical transmittance of a polished sample was

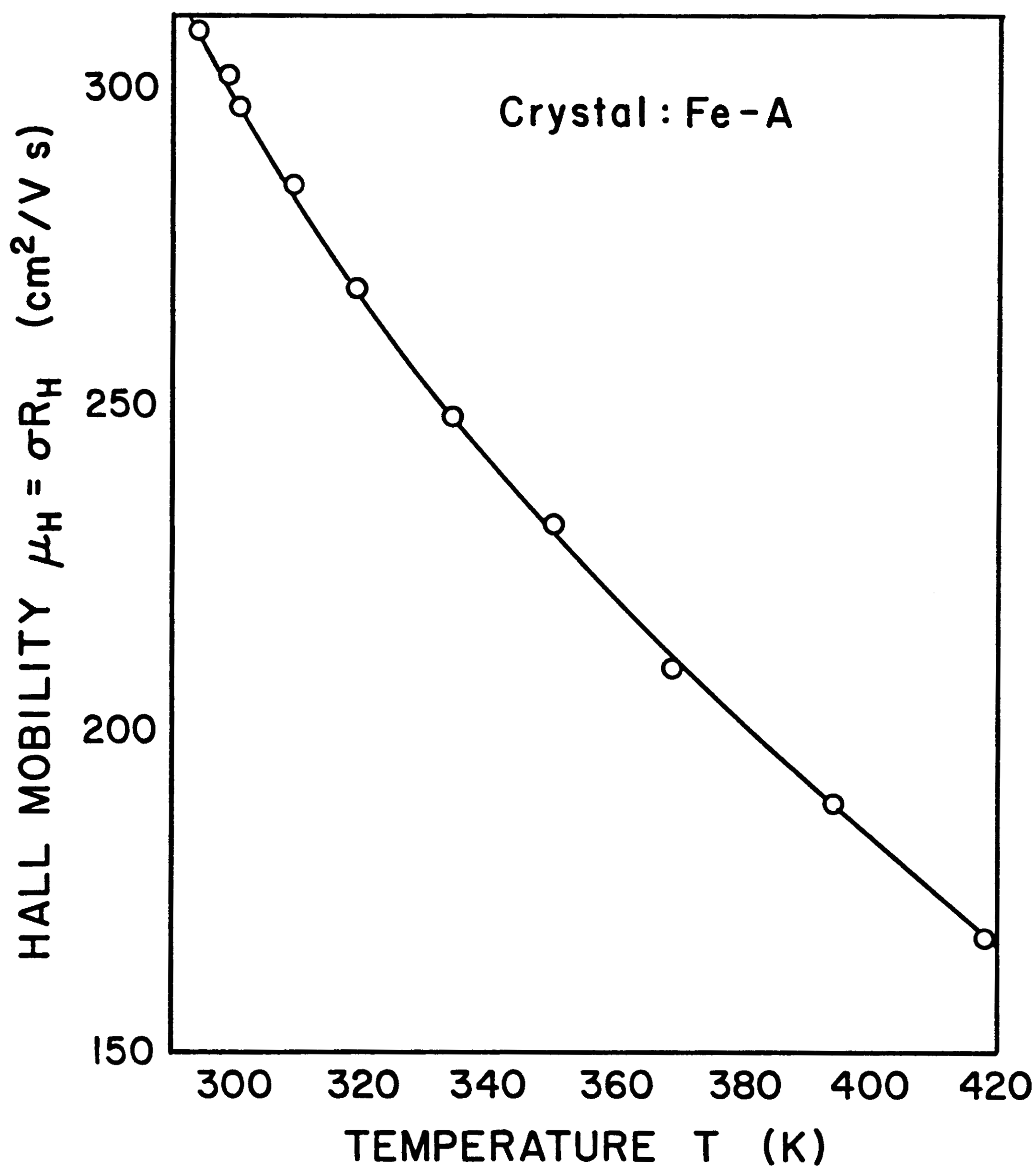


Figure 5-2 Hole Hall mobility vs temperature for Crystal Fe-A.

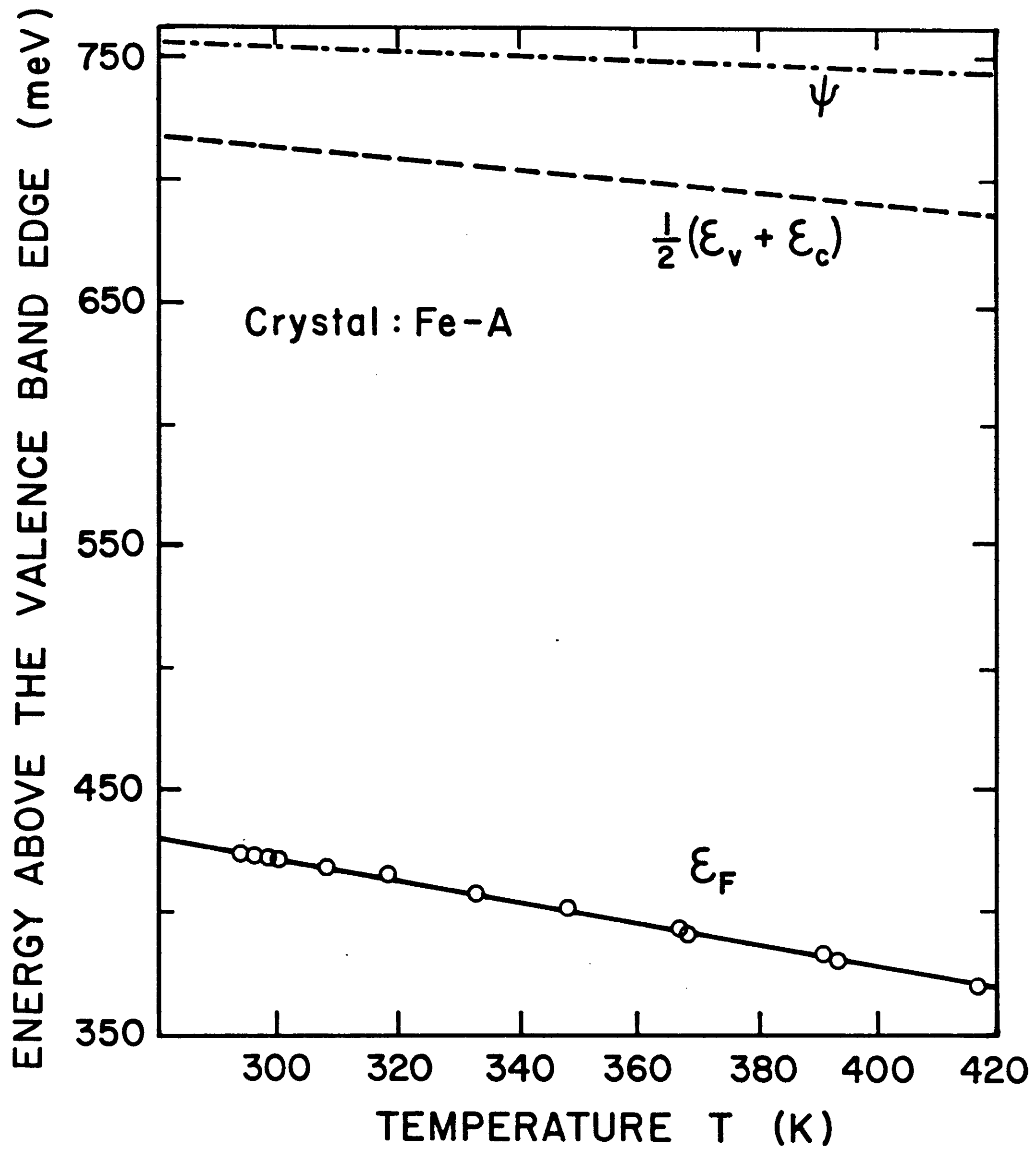


Figure 5-3 Fermi energy $\varepsilon_F$ for Crystal Fe-A, the intrinsic Fermi level $\psi$, and the midgap level $(\varepsilon_c + \varepsilon_v)/2$ vs temperature with valence band edge $\varepsilon_v$ used as the zero for the ordinate scale.

measured at room temperature over the range $0.9 < \lambda < 2.0\ \mu m$ ($0.62 < h\nu < 1.38$ eV). These data were converted using a multiple reflection correction to the bulk absorption coefficient $\alpha$, for this near-IR range. The results are shown as the set of open circles in Fig.5-4.

Also shown in Fig. 5-4 are three lines, two of them dashed and marked $\alpha_1(\mathrm{Fe})$ and $\alpha_2(\mathrm{EL2})$ respectively, while the solid curve is their sum:

$$\alpha = \alpha_1(\mathrm{Fe}) + \alpha_2(\mathrm{EL2}) \qquad (5\text{-}9)$$

The intent has been that the solid curve of $\alpha(h\nu)$ should fit the experimental data, which it appears to do quite well over most of the spectral range. The rapid rise of the data for $h\nu > 1.3$ eV signals the beginning of the intrinsic threshold, not seen in the $\alpha_1(\mathrm{Fe})$ dashed curve, since that is based on lower-temperature (50 K and 130 K) data of iron absorption by Kleverman *et al.* [8].

The above remarks make it clear that the absorption spectrum for the sample from Crystal Fe-A is to be fitted by a superposition of iron-related and EL2-related absorption. Since we know that this material must contain $Fe_{Ga}$ in both the $Fe^{3+}$ (lattice neutral) and $Fe^{2+}$ (ionized acceptor) states of charge, one could well expect absorption arising from a photoionization process

$$Fe^{3+} + h\nu \rightarrow Fe^{2+} + h^+ \qquad [h\nu > (\varepsilon_A - \varepsilon_v)] \qquad (5\text{-}10)$$

with optical cross-section $\sigma_I(h\nu)$; and also from a photoneutralization process

$$Fe^{2+} + h\nu \rightarrow Fe^{3+} + e^- \qquad [h\nu > (\varepsilon_c - \varepsilon_A)] \qquad (5\text{-}11)$$

with a spectrally-dependent optical cross-section $\sigma_N(h\nu)$. One could easily surmise from the 2-threshold form of the Fe-related curve in Fig. 5-4 that

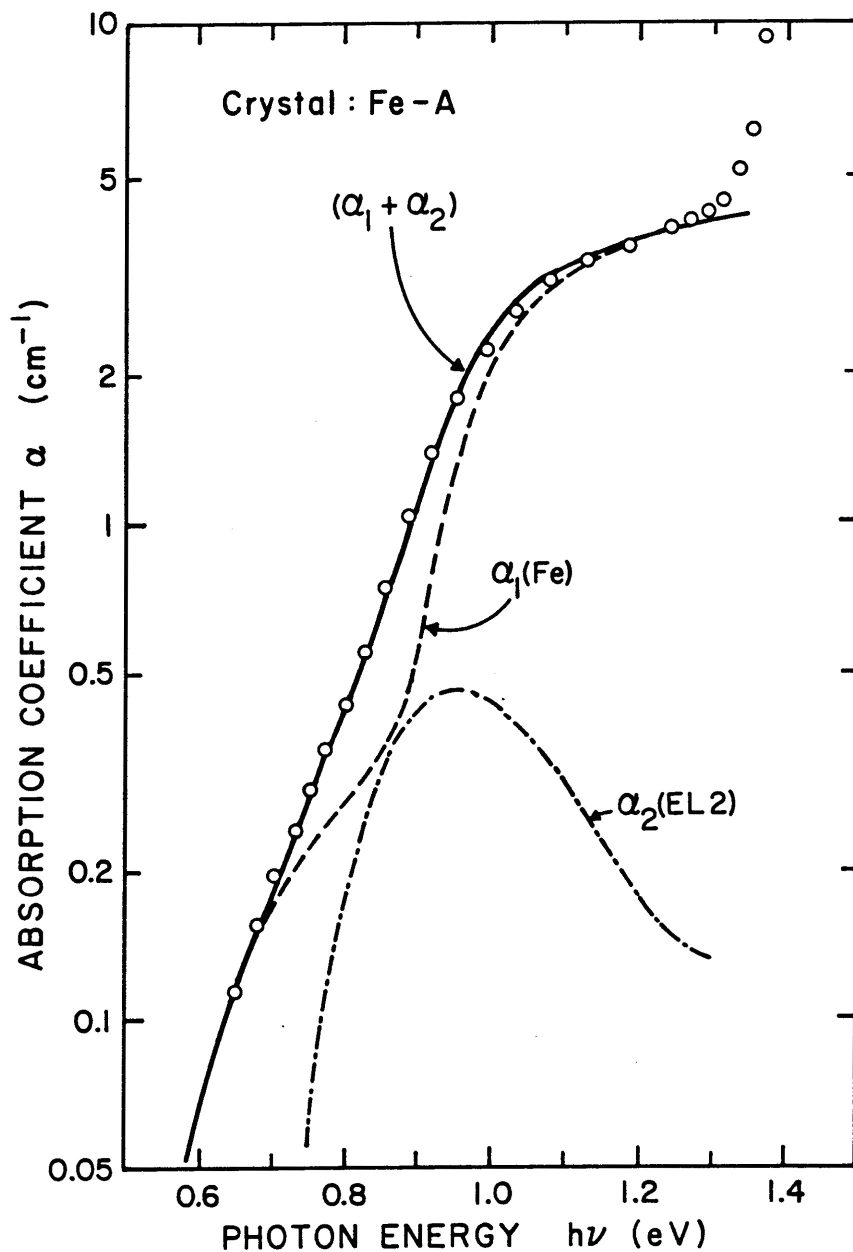


Figure 5-4 Near-infrared optical absorption for a sample from Crystal Fe-A, plotted as circles. The solid curve is a plausible fit, and is the sum of contributions from the two dashed curves. Those dashed curves are for iron photoionization, and $EL2^+$ photoneutralization, respectively.

the first threshold belongs to Eq. (5-10) and the second to Eq. (5-11), but we are assured by Kleverman *et al* [8] that this is not the case. Those workers actually found $\sigma_N$ to be much smaller than $\sigma_I$, having a negligible effect on the absorption spectrum for a Fe-doped sample containing any finite $Fe^{3+}$ population.

Instead, the dual-rise character of the $\alpha_1(Fe)$ curve arises from the opportunities for an electron to be lifted optically into a hitherto $Fe^{3+}$ center without internal excitation ($h\nu > 0.46$ eV) or in causing the new $Fe^{2+}$ center to be internally excited ($h\nu > 0.83$ eV). An iron center so excited will subsequently decay to $Fe^{2+}$ (ground state) by multiphonon emission. The optical transition to the excited state shows up well since evidently that process has an optical matrix element some six times larger.

The two threshold energies for Eq. (5-10) reported by Kleverman *et al.* do of course reflect their low temperature measurements; at 50 K and 130 K. However, they found *no* thermal shift over that 80 K range. One can expect the $Fe^{2+}/Fe^{3+}$ level to be "pinned" primarily by the valence band, and thus any decrease of $(\varepsilon_A - \varepsilon_v)$ between 130 K and 300 K is probably fairly small. It was thus decided to use Kleverman's $\sigma_I(h\nu)$ curve without any thermal correction in generating a curve of

$$\alpha_1(Fe) = \sigma_I N_{Fe^{3+}} \qquad (5\text{-}12)$$

for comparison with the Fe-A absorption data in Fig. 5-4. The vertical placement of the $\alpha_1(Fe)$ dashed curve in Fig. 5-4 uses Kleverman *et al.*'s reported strength for $\sigma_I(h\nu)$, together with $N_{Fe^{3+}} = 2 \times 10^{16}$ cm$^{-3}$. This matches the data for $h\nu < 0.7$ eV, and for $h\nu \approx 1.2$ eV.

Another absorption mechanism must be invoked for the spectral region $0.7 < h\nu < 1.2$ eV. A likely candidate that can create such absorption in this spectral range is EL2. Since for Crystal Fe-A the Fermi level is far below the $EL2^0/EL2^+$ free energy $\varepsilon_D$, we know that all EL2 centers are in the $EL2^+$ charge state. Hence the manner in which Eq. (5-9) is expressed, with absorption arising only from iron photo*ionization* and EL2 photo*neutralization*

$$\alpha = (\sigma_I N_{Fe^{3+}}) + (\sigma_p N_{EL2^+}) \qquad (5\text{-}13)$$

In Fig. 5-4, the dashed curve for $\alpha_2(EL2) = (\sigma_p N_{EL2^+})$ is placed using the $\sigma_p(h\nu)$ by Silverberg *et al* [9], and on the assumption that $N_{EL2^+} = 8 \times 10^{15}$ $cm^{-3}$. This would be a fairly typical EL2 concentration for a VGF-grown GaAs crystal.

The result of the superposition in the manner of Eqs. (5-9) and (5-13), shown as the solid curve in Fig. 5-4, agrees well with the measured room temperature absorption data over almost the entire spectral range. (The reason for the different room temperature behavior above 1.3 eV has already been noted.) Thus we can have confidence that $N_{Fe^{3+}} \approx 2 \times 10^{16}$ $cm^{-3}$ in this material; and may expect (from the amount of ionized EL2) that $N_{Fe^{2+}} \approx 8 \times 10^{15}$ $cm^{-3}$, for a total $N_{Fe} \approx 3 \times 10^{16}$ $cm^{-3}$.

We now turn to three other very high-resistivity doped-GaAs samples. The first one is from a Cr-doped HB crystal. Because a quartz boat was used, we can safely presume that this crystal has enough Si to overpower all the various shallow acceptors and make the Fermi level pinned at the $Cr^{+3}/Cr^{+2}$ level. The other two samples, Fe-B3 and Fe-B12, were cut from different

parts of another Fe-doped VGF crystal. Since crystal Fe-B was carefully doped with a small amount of Fe, we can expect that the semi-insulating property is due to the Fermi energy pinned by the $EL2^o/EL2^+$ level, not by the $Fe^{+3}/Fe^{+2}$ level. The situation could be either (i) $N_d > N_a$ and

$$N_{EL2} > N_{Fe} - (N_d - N_a) \qquad (5\text{-}14)$$

or (ii) $N_a > N_d$ and

$$N_{EL2} > N_{Fe} + (N_a - N_d) \qquad (5\text{-}15)$$

The temperature dependent resistivities and the free electron concentrations of these three samples are plotted in Figs. 5-5 and 5-6. The data are almost identical for the two Fe-doped samples. The slopes of Cr-doped and Fe-doped samples are quite close in Figs.5-5 and 5-6, but the Fermi levels are clearly separated in a $\varepsilon_F(T)$ plot. Fig.5-7 shows that the Cr-sample has a higher Fermi level than the Fe-samples. Fig 5-8 shows Hall mobility data for these three samples. All have a healthy $\mu_{Hn}(T)$ behavior, with more than 4500 $cm^2/V$-s room temperature mobility.

## 5.3 Conducting GaAs

For contrast and completeness, included here are some results for conducting GaAs controlled by shallow impurities. Some data are from a Zn-doped P-type crystal, and other data are from two Si-doped N-type crystals.

From the temperature-dependent Hall effect measurement, we plot the free electron concentrations in Fig.5-9 and the electron Hall mobilities in

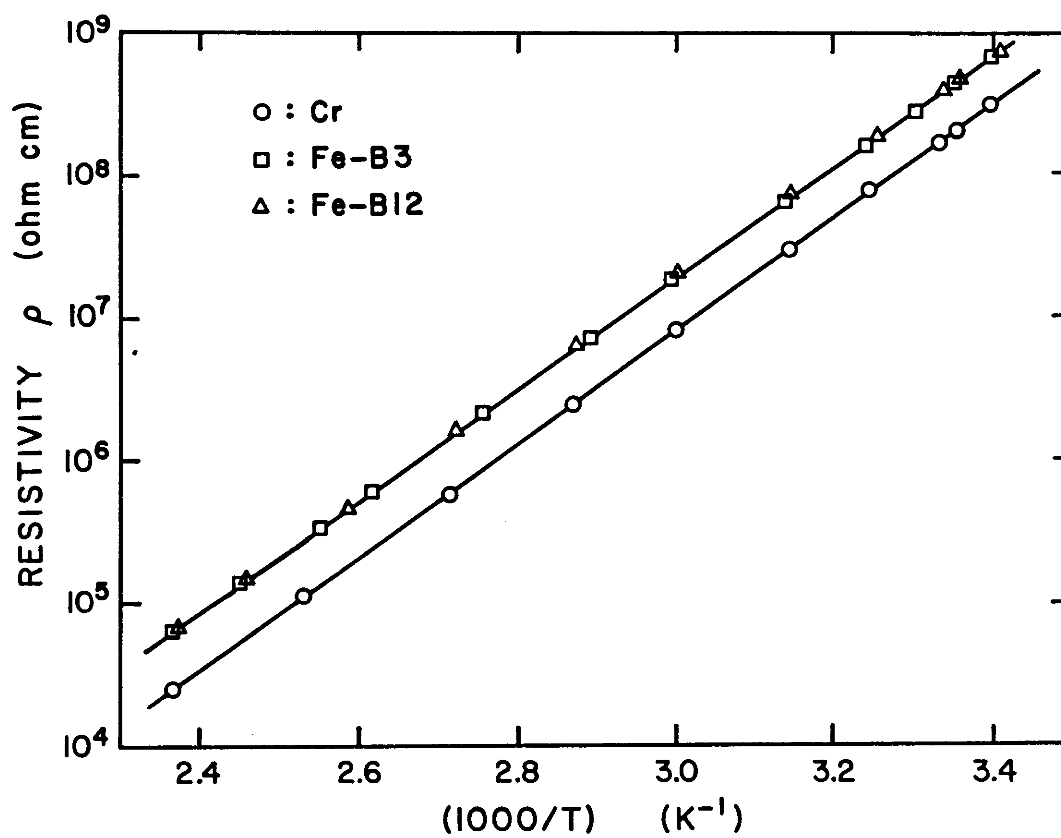


Figure 5-5 Resistivity vs reciprocal temperature for a Cr-doped and two Fe-doped samples.

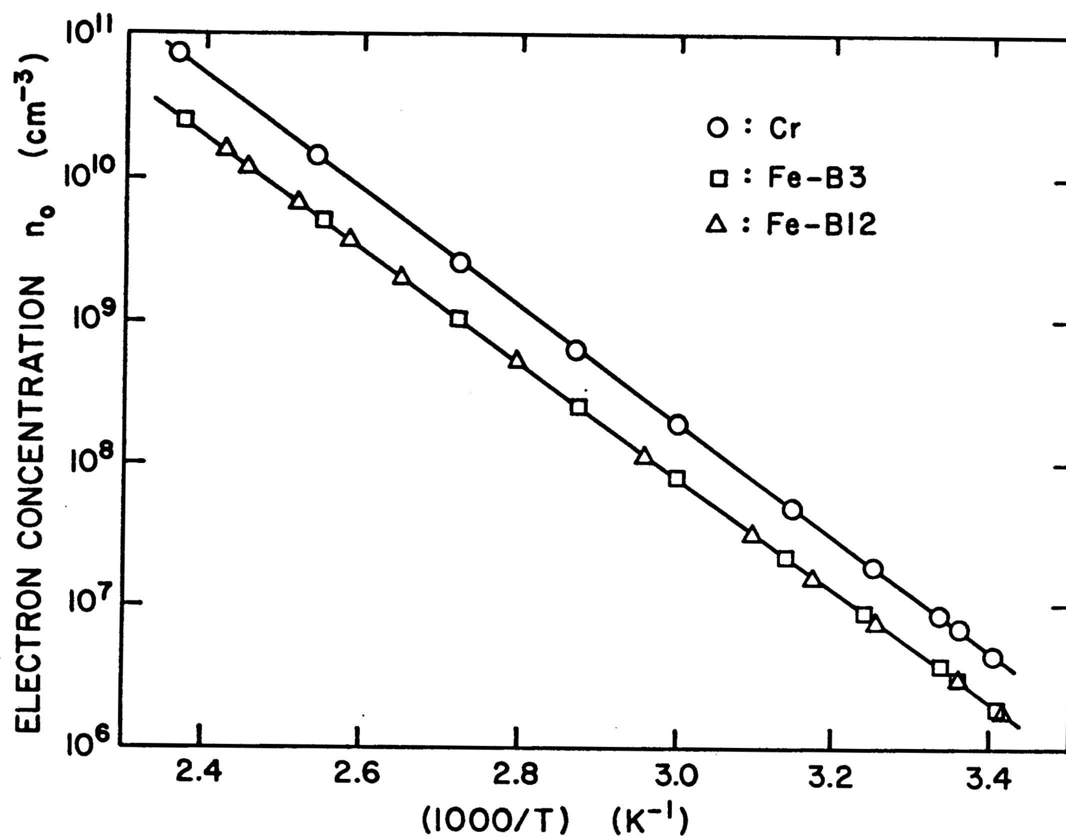


Figure 5-6 Electron concentration vs reciprocal temperature for a Cr-doped and two Fe-doped samples.

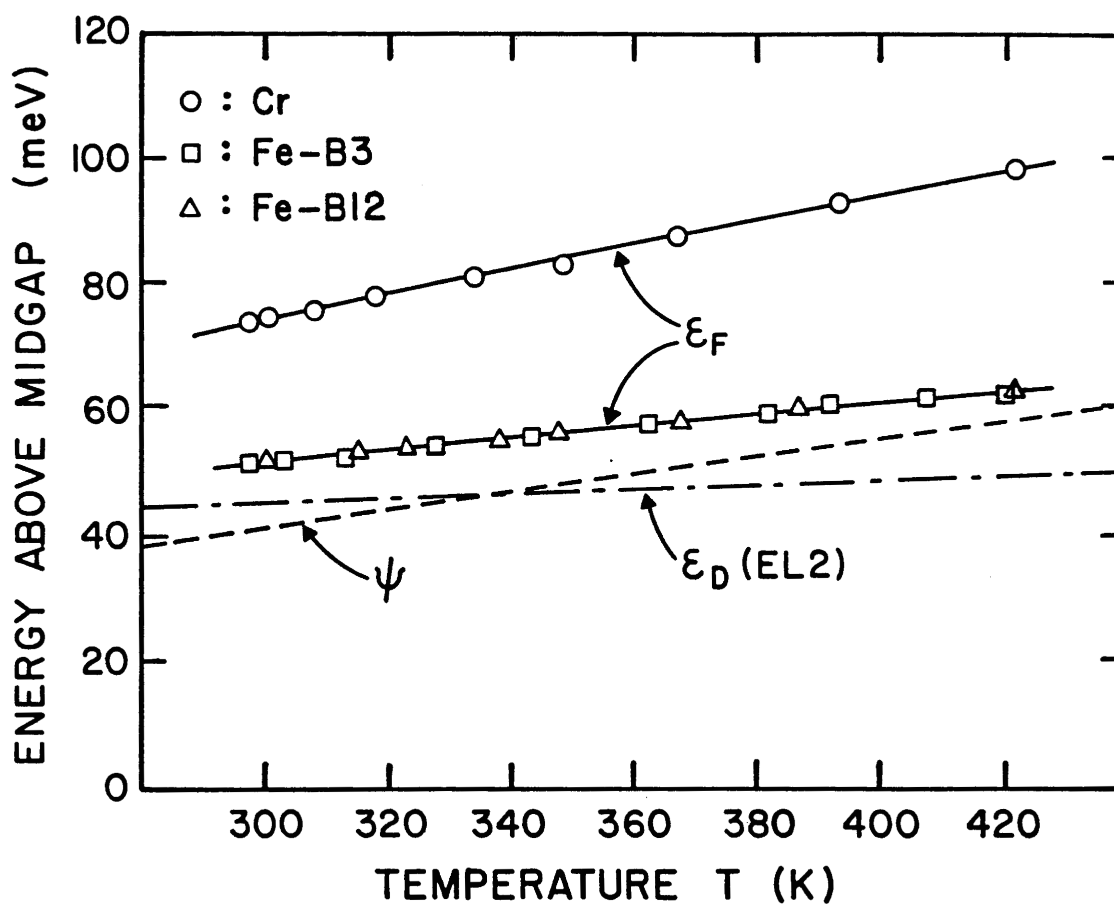


Figure 5-7 Fermi energy (relative to midgap) vs temperature, for the Cr-doped and two weakly Fe-doped samples. (The latter two are essentially indistinguishable.) Also shows EL2 $\varepsilon_D$, and the intrinsic Fermi level $\psi$.

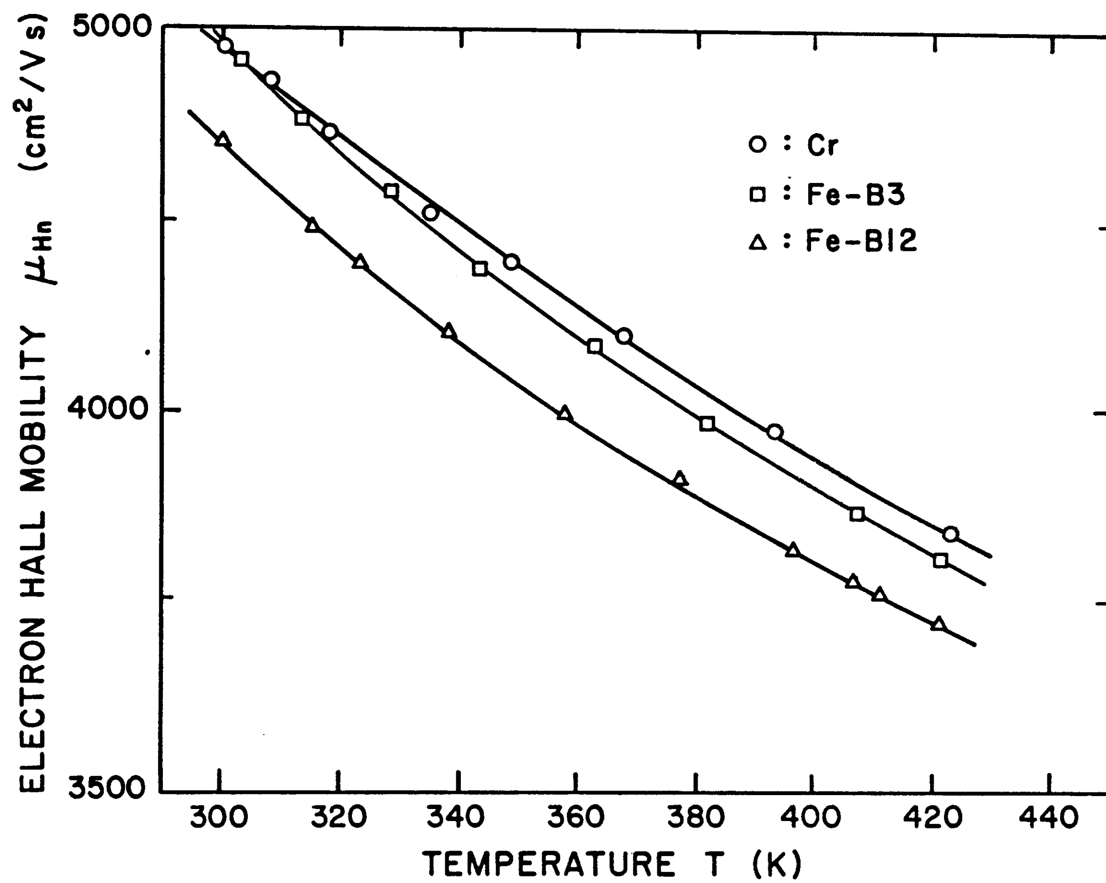


Figure 5-8 Electron Hall mobility vs temperature for a Cr-doped and two Fe-doped samples.

Fig.5-10 for these two Si-doped crystals.

Since the thermal energy kT is larger than the ionization energy of $Si_{Ga}$ in GaAs (5.8 meV [10]) around our measurement temperature (80 - 360 K), all $Si_{Ga}$ donors are ionized and samples are in the so-called "exhaustion" or "saturation" region. The electron concentration derived from $n_0$ = $(-1 / eR_H)$ is quite constant for sample Si-I but slightly increases for sample Si-II during warming up. There are two possible reasons why $n_0$ as expressed and plotted in that way may vary over the 80 - 360 K range.

One reason can be the lack of a suitable Hall correction factor $r_{Hn}$, in deriving the $n_0$ values in Fig. 5-9. No such Hall factor was used, since a good model is not available for $r_{Hn}(T)$ with medium to large shallow doping strength. The "actual" value of $r_{Hn}$ then depends on the ratio $(n_0 / N_c)$, which is $\gg 1$ for a truly degenerate sample, $\ll 1$ for a truly nondegenerate sample, whereas many doped sample fall into the intermediate "semi-degenerate" category. The value of $r_{Hn}$ is also affected by doping in the way that this affects the mix of lattice and impurity scattering. Thus for Fig. 5-9 the over-simplification $r_{Hn} = 1.00$ was used.

Now for Sample Si-I, since $n_0 \approx 1.15 \times 10^{18}$ $cm^{-3}$, and $N_c(300) = 4.2 \times 10^{17}$ $cm^{-3}$, then $(n_0 / N_c) \approx 2.75$ at room temperature, perceptibly inside the degenerate range; this sample becomes progressively more degenerate upon cooling, since $N_c(T)$ varies as $T^{3/2}$. We can be reasonably safe in assuming $r_{Hn} \approx 1.00$ for sample Si-I throughout the temperature range.

That assumption of degeneracy is not justified for sample Si-II, where $(-1 / eR_H) < 10^{17}$ $cm^{-3}$. Does the rise of $(-1 / eR_H)$ with temperature reflect

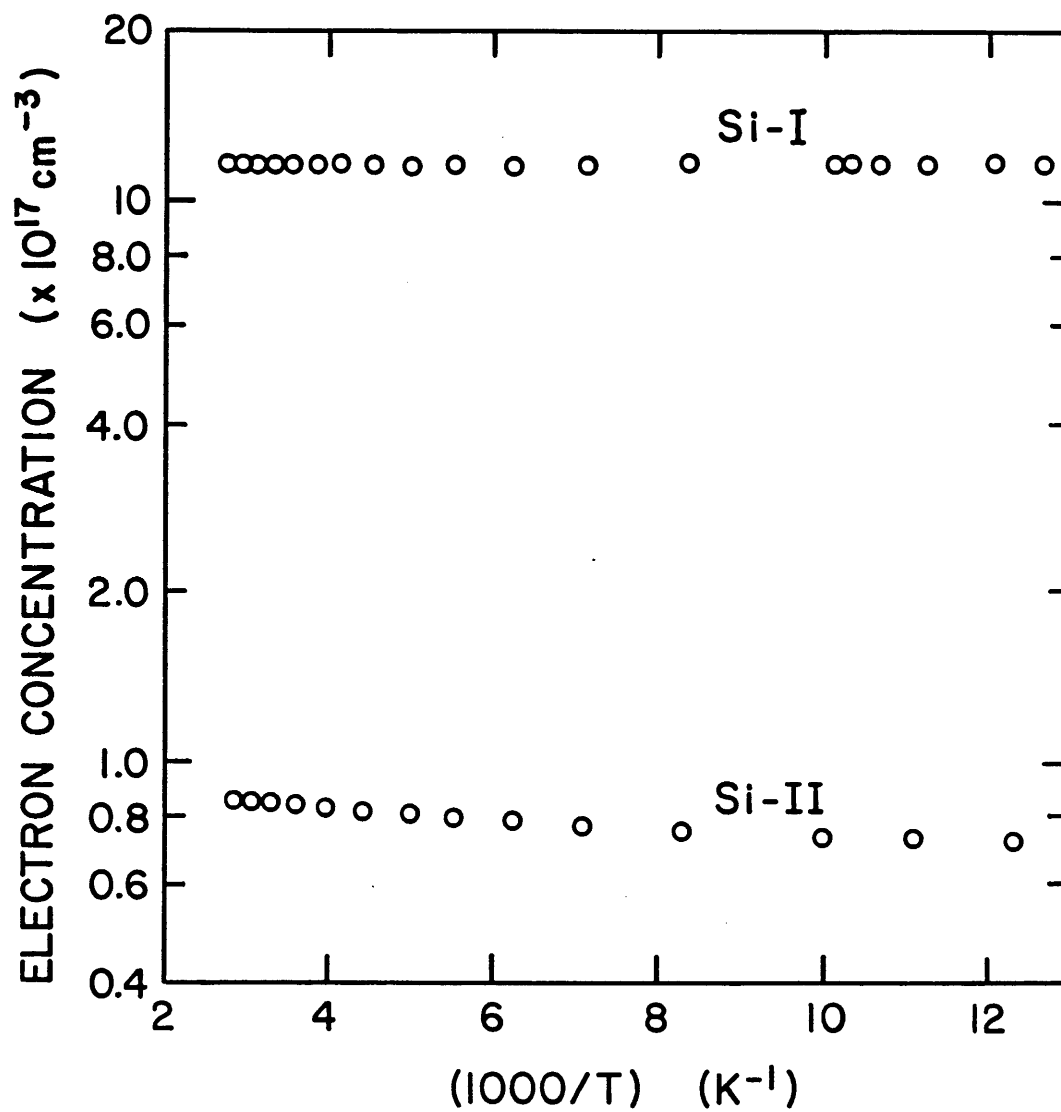


**Figure 5-9 Electron concentration vs reciprocal temperature for Samples Si-I and Si-II.**

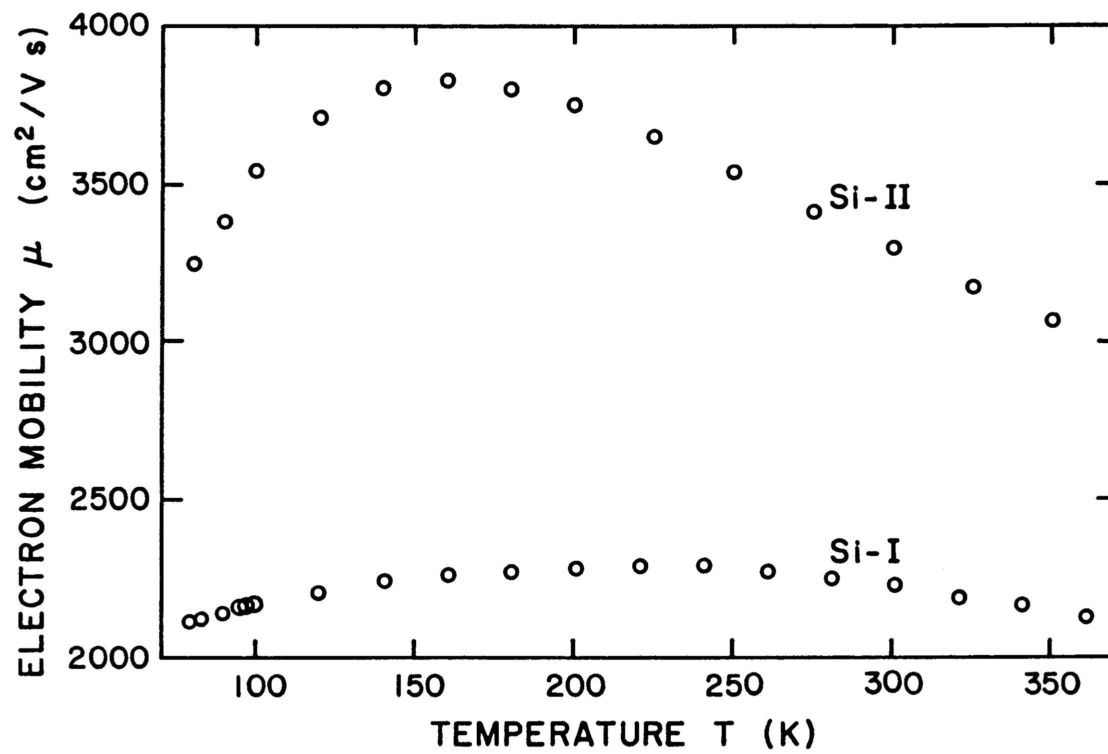


Figure 5-10 Electron mobility vs temperature for Samples Si-I and Si-II.

*only* a temperature dependence of the "true" $r_{Hn}$, with the actual $n_0$ independent of temperature? It does not seem very likely that this could account for the trend of the Si-II data in Fig. 5-9, since the $r_{Hn}(T)$ curve of Rode [11] for *weakly* doped N-type GaAs shows $r_{Hn}$ rising in the range 100 - 200 K, falling again above 200 K. Are thing so different with $N_d \sim 10^{17}$ cm$^{-3}$? Another possible contributor to the rise of $n_0$ for Sample Si-II above 200 K could be progressive partial ionization of some donor (impurity-related complex, or native defect) of slightly larger donor ionization energy, since $(\varepsilon_c - \varepsilon_F) \approx 25$ meV for this sample by room temperature. Any such slightly deeper-lying defect or impurity (complex) would need to have a concentration ~ $10^{16}$ cm$^{-3}$, i.e., some 10% of the $Si_{Ga}$ shallow donor content. This *is* possible for some cases in melt-grown GaAs (the material of Sample Si-II was grown by the HB method) but caution is necessary. We can have more confidence about this assumption after checking with the results of photoluminescence spectral scans.

Because of the scattering by $1.2 \times 10^{18}$ cm$^{-3}$ of $Si_{Ga}$ centers, the electron mobility for sample Si-I is generally low through the range 80 - 360 K. However, the mobility is depressed to an extent which implies more scattering centers than just ionized shallow silicon donors. If one compares the Si-I mobility data with the family of curves by Rode [11] for $\mu_n$ versus electron density at 77 K and 300 K, one would have to acknowledge that Si-I is 50% compensated. For uncompensated N-type GaAs with $n_0 \sim 10^{18}$ cm$^{-3}$, Rode indicates that one should expect $\mu_n \sim 3000$ at 300 K, and 5000 to 6000 cm$^2$/V-s at 77K. We know that Si-doping tends to produce *frosting* if one

pushes the silicon content too high in the $10^{18}$ $cm^{-3}$ range [12]. Therefore, we wonder whether some of the added silicon went to places other than Ga substitutional sites in the Si-I crystal. This in fact could be connected with the PL results shown shortly. For sample Si-II, the Hall mobility versus T shows that mobility falls off below 150 K. That is not surprising with ~ $10^{17}$ $cm^{-3}$ of ionized Si donors - plus whatever else may be contributing to the scattering in Si-II. Here again, PL results give a more complete view of the consequence of doping.

For a Zn-doped P-type sample, we call Zn-C, the quantity $(-1 / eR_H) \approx p_0$ is about $1.25 \times 10^{19}$ $cm^{-3}$ and with less than 3.5% fluctuation throughout 80 - 350 K temperature range. Sample Zn-C is modestly degenerate, with $(p_0 / N_v) \approx 1.3$ at 300 K. The hole mobility $\mu_p$ decreases from 102 to 69 $cm^2/V$-s in that temperature range, and thus the resistivity increases from $4.84 \times 10^{-3}$ to $7.04 \times 10^{-3}$ $\Omega$-cm as the sample temperature is raised from 80 K to 350 K.

Since transport data alone can not supply much detailed information for a conducting GaAs sample in this temperature range (80 to 350 K), optical measurements can be a good complement in such a case. Fig. 5-11 shows photoluminescence spectra for the P-type sample Zn-C and the N-type sample Si-I. Both samples were cooled with a MMR cryostat to 80 K, and the signal was detected by a liquid nitrogen cooled Ge photovoltaic detector. Note that these two samples both represent reasonably degenerate conditions, since at T = 80 K,

$$(n_0 / N_c) \approx 20 \qquad \text{for Sample Si-I} \qquad (5\text{-}16)$$

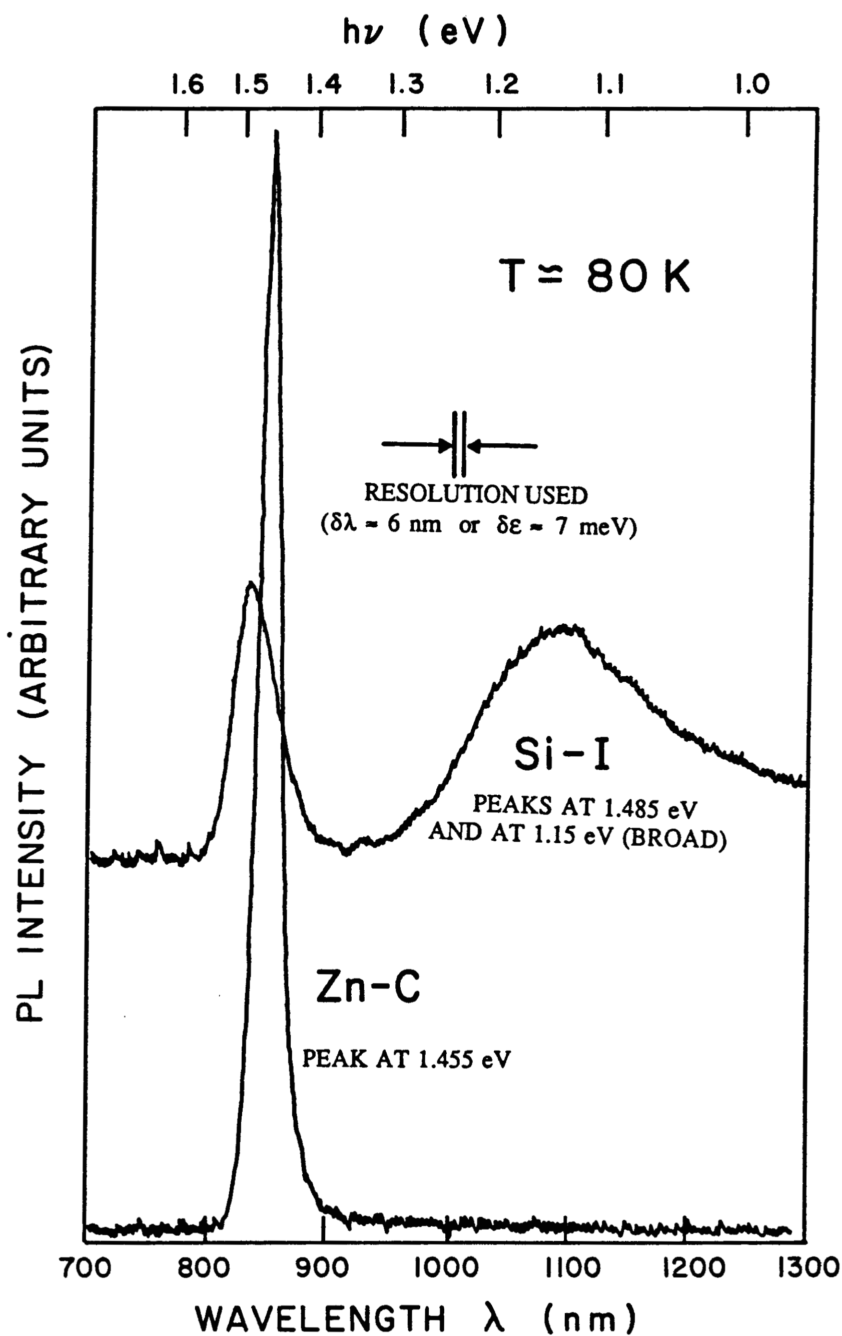


Figure 5-11 80 K photoluminescence spectra for N-type sample Si-I peak at 1.455 eV, and P-type sample Zn-C peaks at 1.485 ev and at 1.15 eV (broad).

$$(p_0 / N_V) \approx 10 \qquad \text{for Sample Zn-C} \qquad (5\text{-}17)$$

The corresponding 80 K PL data for the less strongly silicon doped sample (Si-II) will be shown shortly.

Because the sample temperature (80 K) is not very low, and the monochromator we used does not have high resolution (0.27 m focus length), we can not expect to see any fine structure from free exciton or bounded exciton lines in such PL spectra. Fig.5-11 is therefore just a combination of band-to-band and impurity-to-band luminescence. The luminescence peak of the Zn-doped sample does appear at an energy some 0.03 eV lower than for the Si-doped sample. That arises in part from the larger binding energy of a Zn acceptor contrasted with a Si donor[10], but is affected also.by the incorporation of all those Zn acceptors into a massive bandtail, which extends above the top of the "pure" valence band when $p_0$ is high as $1.25 \times 10^{19}$ $cm^{-3}$. No PL signal was detectable at longer wavelengths for Sample Zn-C. On the other hand, sample Si-I shows a well-known broad PL band, with a peak around 1.15 eV and a FWHM of ~0.2 eV. This has been seen in some N-type conducting GaAs for many years, and was studied by the late Ed Williams in the late 1960s, for Si and for various other shallow donor dopants [13]. He assigned this broadband PL emission to complexes involving the donor impurity atoms plus gallium vacancies. Evidentially, the sample Si-I does contain more than $1.2 \times 10^{18}$ $cm^{-3}$ of silicon, some of this present in complex form (not just the simple $Si_{Ga}$ substitutional donor). The PL data thus confirm the low mobility result.

Fig. 5-12 shows two PL spectra taken at 80 K for sample Si-II. The

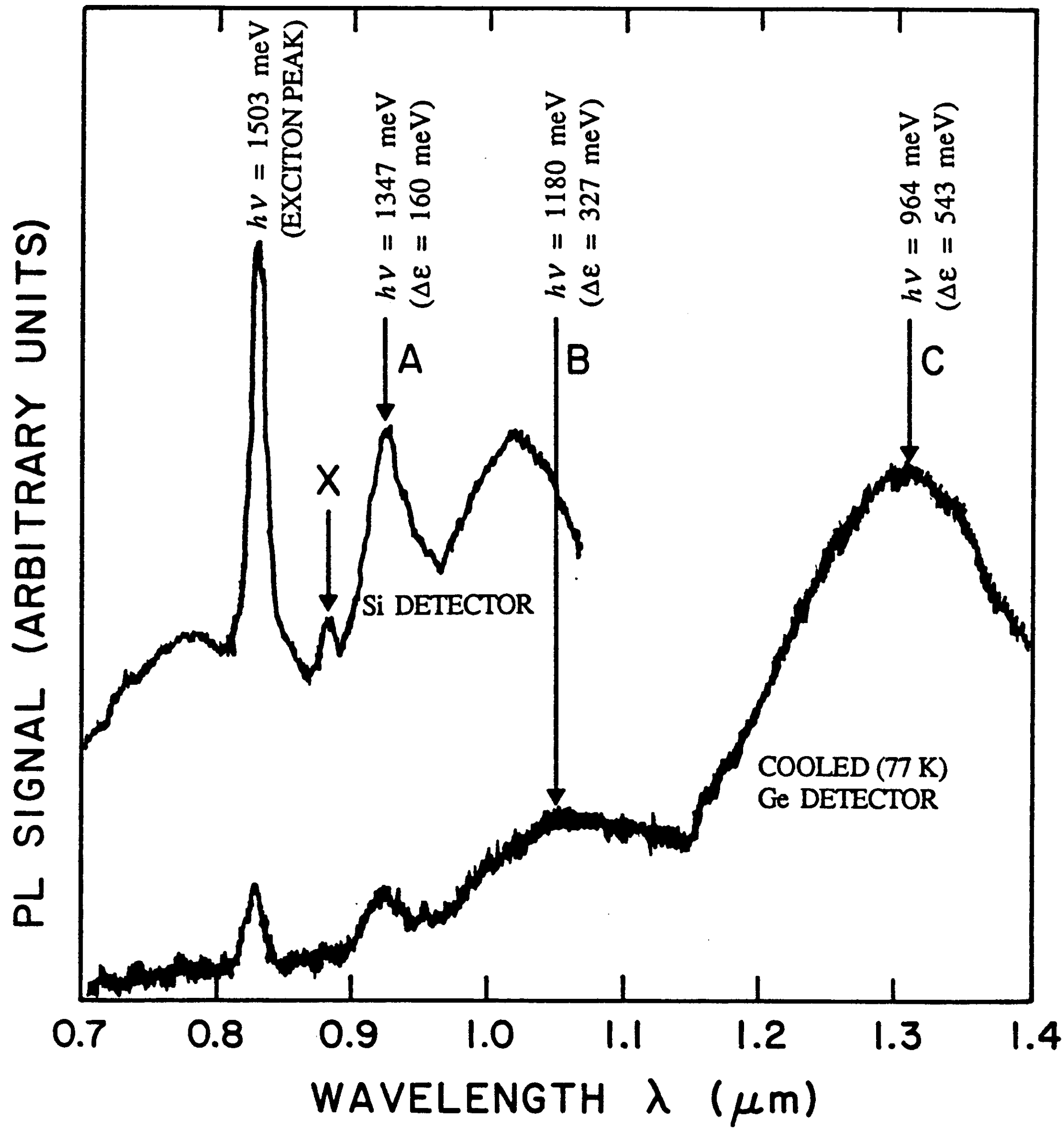


Figure 5-12 80 K photoluminescence traces for Sample Si-II, using either a silicon detector (upper curve), or a 77 K cooled germanium detector (low curve).

lower trace, with range covered from 0.7 to 1.4 µm, was taken using a cooled (77 K) germanium photovoltaic detector, and the upper trace was taken using a room temperature silicon detector. Since the Si-detector has better sensitivity at shorter wavelengths, we can have an optimized signal to noise ratio for that range. However, the Si-detector responsivity starts to collapse beyond 1 µm, and we can thus make better use of the Ge-detector at longer wavelengths.

The intrinsic gapwidth of GaAs is some 1507 meV at 80 K, and subtracting the 4 meV exciton binding energy gives us 1503 meV ($\lambda$ - 825 nm) as the location of the free exciton PL peak. That is (within 2 meV or so) the same spectral location as for Si-donor to V.B. transitions. We can see the combined and broadened "near-bandgap" emission, but can never see the two separate phenomena with our typical observation conditions, at a resolution of $\delta\lambda \sim 9$ nm; i.e., $\delta\varepsilon \sim 10$ meV.

Besides the near-bandgap emission and a weak peak X next to it, we can see clearly that there are three other peaks located at A - 1.347 eV, B - 1.180 eV, and C - 0.964 eV. The broad band and low energy characteristic of Peaks B and C implies that each one is associated with a localized deep level. The narrow band A is an emission from a level which is not *very* deep, but ~ 0.1 eV deeper than $Si_{Ga}$ donors. This result could explain part of the story for Si-II: why is $n_0$ temperature dependent in Fig. 5-9?

The Zn-doped sample Zn-C is totally opaque in the mid-IR range, and has less than 0.1% transmittance in the near-IR range because of the tremendous free carrier absorption. Fig. 5-13 shows a near-IR transmission

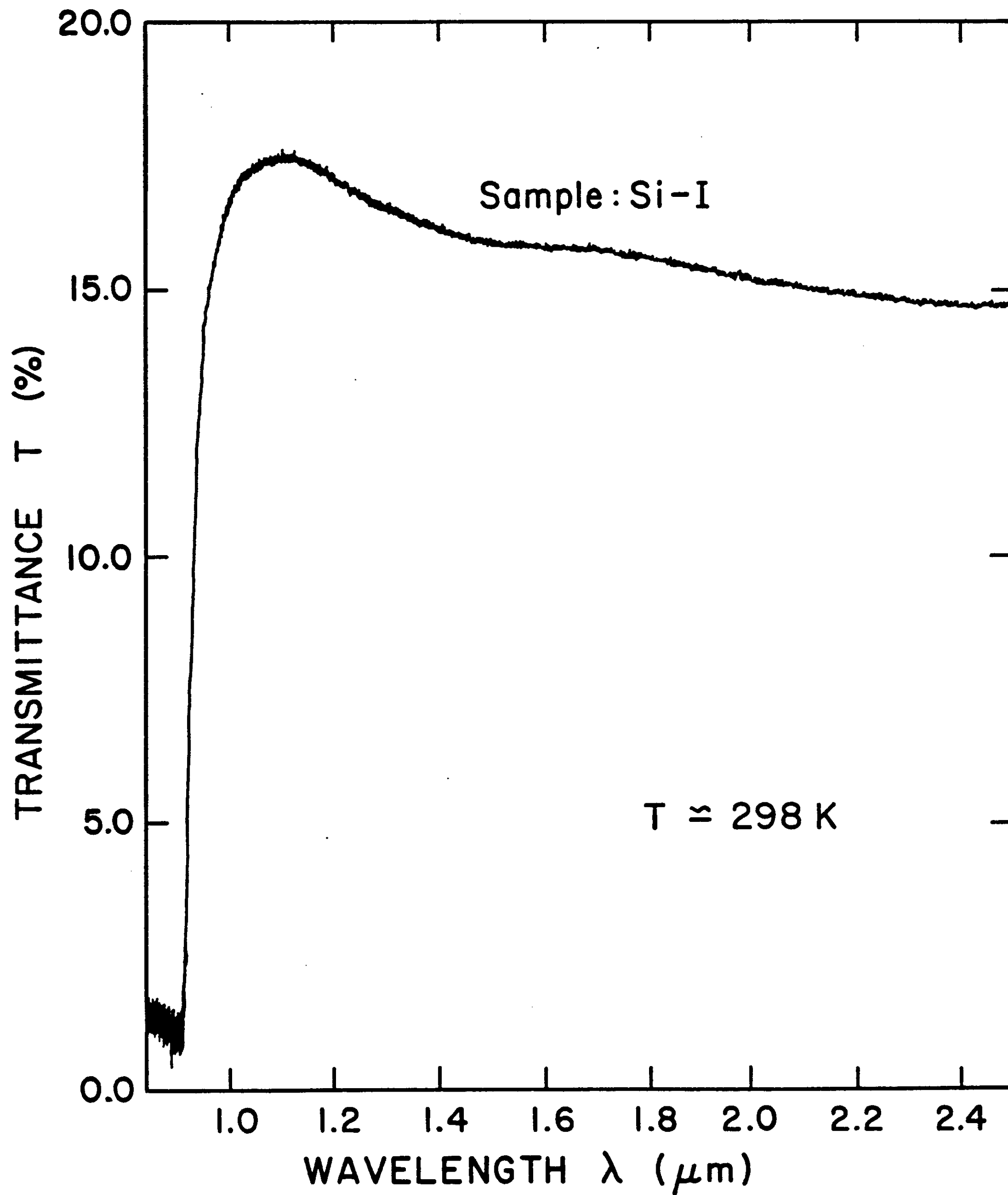


Figure 5-13 Near-infrared transmittance spectrum (at ~298 K) for Sample Si-I. The maximum transmittance is quite small (absorption quite large - see Table 5-1) because of the large electron concentration, $n_0 > 10^{18}$ cm$^{-3}$.

spectrum for sample Si-I at room temperature. The maximum transmittance ($T_{max}$ = 17.5%) occurs at 1.1 μm.

It would be pointless to check the transmittance of Si-I beyond the near-IR range, because any longer-wavelength incident radiation would be blocked by the strong free carrier absorption, a process which increases approximately as $\lambda^3$ after ~4 μm. The absorption coefficient $\alpha$ for sample Si-I is converted from the Fig. 5-13 transmittance, and listed in Tab.5-1. Comparing the value of free carrier absorption at $\lambda$ = 2.0 μm with the classic work done by Spitzer and Whelan [14] (later reconfirmed and quoted by Pfeffer *et. al* [15]), the absorption coefficient $\alpha \approx 5$ cm$^{-1}$ for sample Si-I would correspond to an electron concentration of $n_0 \approx 1.1 \times 10^{18}$ cm$^{-3}$. This is in excellent agreement with our Hall measurement result for the sample.

We measured the transmittance at room temperature for sample Si-II over the range from 2.5 to 17.5 μm. This was converted to absorption coefficient $\alpha$ and plotted in Fig. 5-14 using a log-log scale which is convenient for comparison with free carrier absorption. For comparison and contrast is shown in Fig. 5-14 also the Spitzer and Whelan curve for their Sample #2, nominally of $n_0 = 1.3 \times 10^{17}$ cm$^{-3}$. One can thus see that at long wavelengths, our Si-II is less absorbing, consistent with $n_0$ being slightly less than $10^{17}$ cm$^{-3}$. However, Si-II shows an absorption up to ten times larger at shorter wavelengths. There must be some extra absorption mechanisms at work, which are capable of producing a contribution to $\alpha$ of several cm$^{-1}$ in the near-IR. This question is in fact again answered by the PL data in Fig. 5-12. Photoluminescence shows the energy an electron loses

Table 5-1 The absorption coefficient and related parameters for sample Si-I

| wavelength $\lambda$ ($\mu$m) | photon Energy $h\nu$ (eV) | Refractive Index n | Reflectivity R | Absorption Coefficient $\alpha$ ($cm^{-1}$) | Transmittance T (%) |
|---|---|---|---|---|---|
| 1.0 | 1.2399 | 3.511 | 0.3098 | 4.28 | 16.9 |
| 1.1 | 1.1272 | 3.464 | 0.3047 | 4.20 | 17.5 |
| 1.2 | 1.0333 | 3.432 | 0.3011 | 4.35 | 17.0 |
| 1.3 | 0.9538 | 3.409 | 0.2985 | 4.50 | 16.5 |
| 1.4 | 0.8857 | 3.391 | 0.2965 | 4.63 | 16.1 |
| 1.5 | 0.8266 | 3.377 | 0.2950 | 4.70 | 15.9 |
| 1.6 | 0.7749 | 3.367 | 0.2938 | 4.73 | 15.8 |
| 1.7 | 0.7294 | 3.358 | 0.2928 | 4.76 | 15.7 |
| 1.8 | 0.6888 | 3.351 | 0.2920 | 4.82 | 15.5 |
| 1.9 | 0.6526 | 3.345 | 0.2913 | 4.87 | 15.4 |
| 2.0 | 0.6199 | 3.340 | 0.2907 | 4.93 | 15.2 |
| 2.1 | 0.5904 | 3.336 | 0.2902 | 4.98 | 15.0 |
| 2.2 | 0.5636 | 3.332 | 0.2898 | 5.02 | 14.9 |
| 2.3 | 0.5391 | 3.329 | 0.2894 | 5.04 | 14.8 |
| 2.4 | 0.5166 | 3.326 | 0.2891 | 5.07 | 14.7 |

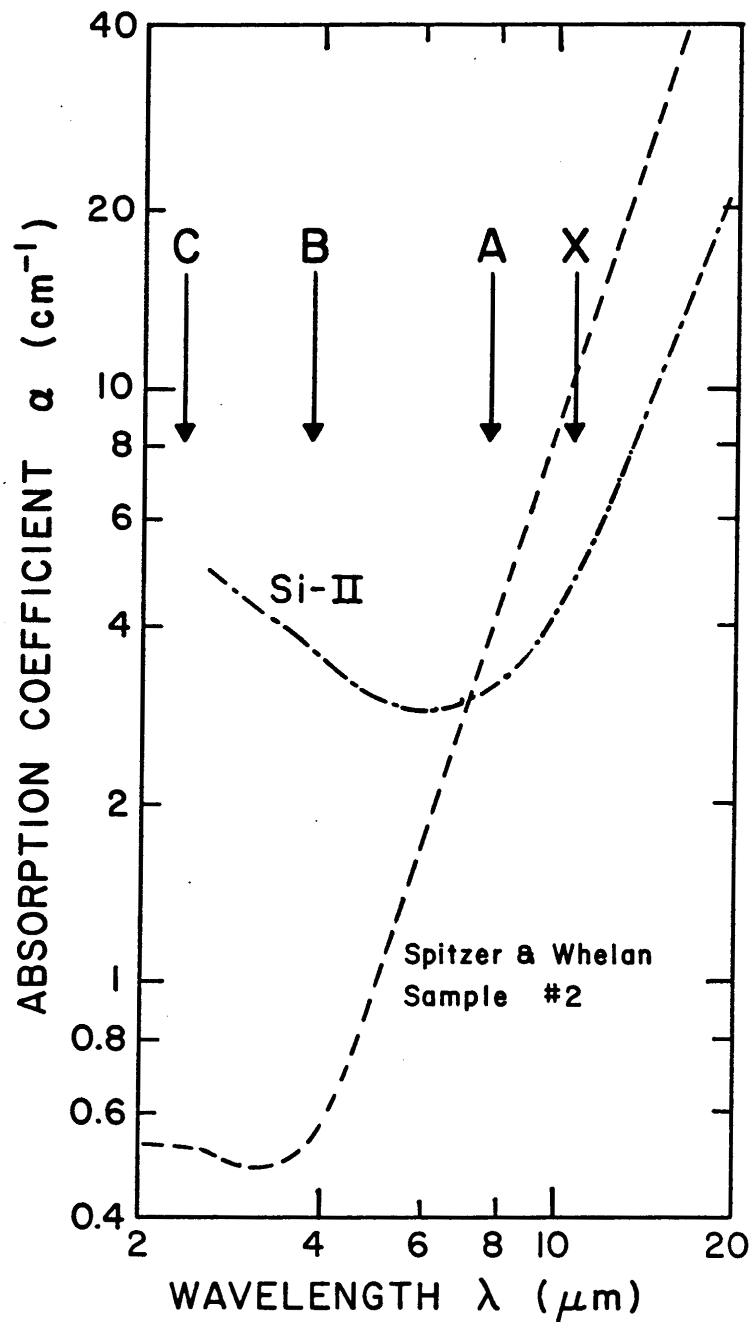


Figure 5-14 Infrared absorption behavior at 300 K for Sample Si-II, compared with the "free carrier absorption" curve for Sample # 2 in the work of Spitzer and Whelan [14].

in falling, to the valence band. However, absorption in this case (as in many other cases) shows the absorption threshold for the complementary upwards transition between the trap and the conduction band. If we superimpose arrows at the four wavelengths corresponding to the complementary photon energies: $\Delta\varepsilon = (\varepsilon_i - h\nu) = h\nu'$, for the four PL bands X, A, B, and C, we can see why sample Si-II has more absorption (extending out to beyond 6 μm) than provided by free carrier absorption alone.

## REFERENCES: CH.5


1. R. W. Haisty and G. R. Cronin, in *Physics of Semiconductors*, (Dunod, Paris, 1964), p. 1161
2. J. S. Blakemore, in *Semi-Insulating III-V Materials: Hakone 1986*, edited by H. Kukimoto and S. Miyazawa, (Ohmasa,Toyko, 1986), p. 389
3. G. M. Martin, J. P. Farges, G. Jacob, J. P. Hallais, and G. Poiblaud, J. Appl. Phys. **51**, 2840 (1980)
4. A. G. Milnes, *Deep Impurities in Semiconductors*, (John Wiley & Sons, New York 1973), p. 61
5. A. G. Milnes, in *Advances in Electronics and Electron Physics* Vol. **61**, (Academic Press, 1983), p. 100
6. B. Clerjaud, J. Phys. C: Solid State Phys. **18**, 3615 (1985)
7. U. Kaufmann and J. Schneider, in *Advances in Electronics and Electron Physics*, Vol. **58**, (Academic Press, 1982), p. 109
8. M. Kleverman, P. Omling, L-A. Ledebo, and H. G. Grimmeiss, J. Appl. Phys. 54, 814 (1983)
9. P. Silverberg, P. Omling, and L. Samuelson, Appl. Phys. Lett. **52**, 1689 (1988)
10. S. M. Sze and J. C. Irvin, Solid State Electronics **11**, 599 (1968)
11. R. L. Rode, in *Semiconductors and Semimetals Vol. 10*, Ch.1 (1975)
12. Measurement Report to Crystal Specialties, Inc. We examined the *frosted* part of Si-doped ($N_{Si}$ = 2 to 7 x $10^{18}$ $cm^{-3}$) GaAs samples by SEM and EDX. This indicated that *frosting* is associated with the

presence of micro-precipitates, comprising silicon or some refractory intermetallic silicide compound.

13. E. W. Williams and H. B. Bebb, in *Semiconductors and Semimetals Vol. 8*, Ch.5 (1972)
14. W. G. Spitzer and J. M. Whelan, Phys. Rev. **114**, 59 (1959)
15. P. Pfeffer, I. Gorczyca, and W. Zawadzki, Solid State Comm. **51**, 179 (1984)

# CHAPTER 6

## CONCLUSIONS CONCERNING SEMI-INSULATING GaAs

Any study such as this one, which attempts to monitor the properties and the overall "quality" of a material such as SI GaAs, has to observe a moving target. For the quality of SI GaAs, especially of "undoped" SI GaAs, has progressed significantly during the 1980s, and can reasonably be expected to show further advances during the 1990s. It has been interesting to play a part in the assessment of this material, especially that grown by the less-conventional non-LEC processes.

For that reason, results reported in this dissertation, while including some LEC-grown GaAs, have tended to concentrate on crystals grown (mostly without intentional doping) by several other methods. The horizontal Bridgman (HB) method has been used for melt-growth of highly conducting doped GaAs for many years (and some examples of that for Si-doped GaAs were included, for completeness, in Chapter 5), but was not attempted for "undoped SI" growth in a PBN boat until the 1980's. Indeed, that method has already become passé, since the automatically circular (100) wafers which result from a *vertical* Bridgman (VB) arrangement show considerable promise for device SI substrates. The combination of good electrical properties, low dislocation density (significant for optoelectronic

substrate uses), and a scaling-up of size already to a 3" diameter, makes VB-grown SI GaAs a viable material for use as the 1990s unfold.

Related in some respects to the VB method is the vertical gradient freeze (VGF) method of crystal growth. AT&T Bell Laboratories have made a major study of how to grow GaAs, GaP, and InP by the VGF technique, in which there are no moving parts. This method also has been able to produce 3" diameter wafers, and VGF could probably go larger still. The properties of VGF GaAs appear generally similar to that attainable by the VB method, thus economic factors will probably determine whether both, either or neither of those two methods survives in the long run. There are some small companies in the GaAs growth business (AXT Inc. being one example of a commercial VGF supplier), yet it seems inevitable that the long-term future of the GaAs materials industry will be dominated by a few solidly-based companies. The departure during 1989 of both Morgan Semiconductor and Spectrum Technology Inc., and the withdrawal of Varian Instruments from GaAs activities in 1990 is part of that trend.

Thus VB and VGF GaAs (whether doped and conducting, doped yet high resistivity, or undoped SI) must compete economically with GaAs grown by any other method-of which LEC is favored for SI, and HB has been traditional for conducting. As a refreshing change from those economic considerations, it has been a pleasure to collaborate with NRL on assessment of "undoped" GaAs grown by a vertical zone melt (VZM) method, or by multiple-pass zone refining (ZR). It can be concluded that these processes, while still far from commercial production status, have shown excellent

promise. A comparison with Ge and Si is appropriate. Horizontal zone refining of Ge went from the first small trial stage to a commercially useful size in very few years. (Of course, for Ge one can use a quartz boat!) The initial demonstration of float-zone (FZ) silicon occurred during the 1950s, and there has been more than 30 years of steady development of FZ-Si to the present very large and high quality FZ crystals. A corresponding development of the VZM method for GaAs remained elusive for several decades, but has now come to pass. Can there be any major scale-up of size in future years? This can not so far be safely predicted. However, the first two years of GaAs VZM and ZR growth at NRL have been an excellent story of scientific success.

As a summary of this writer's contributions to the GaAs assessment subject, it may be noted that a versatile Hall and conductivity measurement system has been developed, for reliable measurements over a temperature range (to above room temperature for SI material, and to cryogenic temperatures for conducting samples). The value of such temperature-dependent analysis for SI samples in particular has been demonstrated. The system can give reliable data for samples with a conductance exceeding $10^3$ S, and also for those with a resistance approaching $10^{10}$ Ω.

For any such near-intrinsic SI GaAs sample, the measured Hall coefficient and conductance are affected by ambipolar conduction (holes as well as electrons), and a simple method for making an ambipolar correction has been demonstrated. The software program for analysis of Hall/conductivity data incorporates that ambipolar correction program. One

can thereby obtain reliable numbers for the Fermi energy versus temperature, and learn whether or not the EL2 defect controls the Fermi energy.

Complementary to the electrical evaluation of GaAs (whether doped or undoped), a variety of optical assessment techniques have been brought to bear. Use of carbon LVM absorption made it possible, for example, to monitor the decrease of $C_{As}$ acceptor concentration as one moves further from the seed region of a VGF or ZR crystal. The contributions to the compensation balance (charge balance) equation for a nominally "undoped" GaAs sample could be assessed by use of mid-IR LVM absorption for carbon, while using near-IR absorption for the neutral and ionized components of the EL2 population. For some deliberately Fe-doped GaAs, near-IR absorption could also elucidate the contribution of iron photoionization processes. Photoluminescence was not a major technique in the work leading to this dissertation, but some simple PL scans with Si-doped GaAs did indicate that part of the silicon ended up as a component of deep-level complexes.

# APPENDIX

## SAMPLE PREPARATION AND OHMIC CONTACT APPLICATION

1. Cut the sample into a square slab from $0.5 \times 0.5\ cm^2$ to $1 \times 1\ cm^2$ in area, using a low speed diamond saw, or a diamond tip pen.
2. Lap the sample into a parallel-sided slab of suitable thickness, desirably less than 1/10 of the width. Optical grade fine polish is not necessary, but at least 600 grit sand pad lapping is required to get smooth surfaces.
3. Clean the sample with organic solvents to remove finger print or any grease contamination on the surface. Our conventional cleaning process.uses TCE (trichloroethylene) agitated in an ultrasonic vibrator for three minutes. This is followed by agitating with ACE (acetone) for two minutes, and then MET (methanol) for two minutes. Then rinse in deionized water six or more times.
4. Etch the sample to remove surface damage and to expose fresh GaAs for ohmic contact. A suitable etching solution is $H_2SO_4 : H_2O_2(30\%) : H_2O$ = 4 : 1 : 1 contained in a water bath heated to 40° C. Lower the sample into the etching solution, and shake for 3 minutes, then rinse thoroughly in DI-water and dry with an air gun.
5. For a sample of 300 K resistivity higher than $10^7\ \Omega$-cm, making ohmic contact is simple: just use pure indium solder with an ultrasonic iron.